

University of New Orleans

ScholarWorks@UNO

University of New Orleans Theses and
Dissertations

Dissertations and Theses

12-19-2008

Applications of Mass Spectrometry to Analysis of Prodiginines, Bioactivated Methylenedianiline Intermediates, and Hypoxia Induced Changes in the Zebrafish Skeletal Muscle Proteome

Kan Chen

University of New Orleans

Follow this and additional works at: <https://scholarworks.uno.edu/td>

Recommended Citation

Chen, Kan, "Applications of Mass Spectrometry to Analysis of Prodiginines, Bioactivated Methylenedianiline Intermediates, and Hypoxia Induced Changes in the Zebrafish Skeletal Muscle Proteome" (2008). *University of New Orleans Theses and Dissertations*. 899.

<https://scholarworks.uno.edu/td/899>

This Dissertation is protected by copyright and/or related rights. It has been brought to you by ScholarWorks@UNO with permission from the rights-holder(s). You are free to use this Dissertation in any way that is permitted by the copyright and related rights legislation that applies to your use. For other uses you need to obtain permission from the rights-holder(s) directly, unless additional rights are indicated by a Creative Commons license in the record and/or on the work itself.

This Dissertation has been accepted for inclusion in University of New Orleans Theses and Dissertations by an authorized administrator of ScholarWorks@UNO. For more information, please contact scholarworks@uno.edu.

Applications of Mass Spectrometry to Analysis of Prodiginines,
Bioactivated Methylenedianiline Intermediates, and Hypoxia Induced
Changes in the Zebrafish Skeletal Muscle Proteome

A Dissertation

Submitted to the Graduate Faculty of the
University of New Orleans
in partial fulfillment of the
requirements for the degree of

Doctor of Philosophy
in
the Department of Chemistry
Analytical Chemistry

by

Kan Chen

B.Eng., Nanjing University of Chemical Technology, 1996
M.S., Shanghai Jiaotong University Medical School, 2001

December 2008

Acknowledgements

So many encouraged me during my stay at the University of New Orleans and along this journey in writing the dissertation. There are many thanks. First and the foremost I want to thank Dr. Richard B Cole, my research Advisor for his guidance, encouragement and consistent support. His broad academic knowledge and insight proved to be invaluable to my graduate career and beyond.

I would like to express my sincere gratitude to Dr. Tammy R. Dugas and her group members, in particular: Dr. Bo Jiang and VY Hebert, for their earnest help in the time of need after the devastation brought by hurricane Katrina in New Orleans. Dr. Dugas helped me in the studies of metabolism and toxicity of methylenedianiline with her strong background, encouragement and kindness. It was a great pleasure to work in her lab.

I wish to thank Dr. Bernard B Rees. He trained me from the basic to the advanced level in proteomics research, and the majority of my work would not be otherwise possible without his kind help. His willingness to take a chance with me shall never be forgotten, when I came up with some “adventurous” ideas.

I also thank Dr. Yang Cai for providing us a good environment and instruments in Children’s Hospital of New Orleans after hurricane Katrina. His expertise in mass spectrometry and proteomics helped me in this dissertation.

I just felt so lucky to work with so many knowledgeable and kind people during my exploration in the scientific world. My work has also benefited from conversation with colleagues and the friends. I am grateful to Drs. Chau-Wen Chou, Mr. Qiang Zhang and Dr. Guangdi Wang for their assistance in instrumentation setup.

Last but most importantly, I thank my wife, Wenkun Mo (莫雯坤) for her understanding and love, and my parents, Wenguo Chen (陈文国) and Cong Xu (许琮) for their dedication and supports during these years.

Table of Contents

Acknowledgements	ii
List of Figures	v
List of Tables	viii
Abstract	ix
Chapter 1	1
Introduction	
Introduction to Mass Spectrometry.....	2
Electrospray Ionization (ESI)	3
Matrix Assisted Laser Desorption Ionization (MALDI).....	4
Different Types of Mass Analyzers.....	4
Quadrupole Ion Trap.....	5
Two-dimensional Linear Ion Trap (2D LIT).....	5
Triple Quadrupole.....	6
TOF and TOF/TOF	7
Separation Tools (on-line or off-line) coupled with Mass Spectrometry.....	8
High Performance Liquid Chromatography (HPLC)	9
Two Dimensional Polyacrylamide Gel Electrophoresis (2D-PAGE)	9
Applications of Mass Spectrometry.....	11
Identification and Characterization of Metabolites.....	11
Proteomics.....	13
References.....	16
Chapter 2	20
Identification of Metabolites of 4,4'-Methylenedianiline in Vascular Smooth Muscle Cells by Liquid Chromatography-Electrospray Tandem Mass Spectrometry	
Abstract.....	21
Introduction.....	22
Experimental.....	25
Chemical and Reagents.....	25
Sample Preparation and Handling	25
LC/MS/MS.....	25
Results and Discussion	26
LC/UV Chromatograms of the Sample and the Control Sample.....	27
LC/MS Chromatograms of the Sample and the Control Sample.....	30
Conclusion	36
References.....	37
Chapter 3	38
Liquid Chromatography-Electrospray Tandem Mass Spectrometry Investigations of Fragmentation Pathways of Biliary 4,4'-Methylenedianiline Conjugates Produced in Rats	
Abstract.....	39
Introduction.....	40
Experimental Details.....	42
Animals.....	42
Liquid Chromatography/Mass Spectrometry.....	42
Results and Discussion	43

Metabolite M2.....	43
Metabolite M7.....	47
Conclusion	48
References.....	52
Chapter 4	53
Unusual Odd-electron Fragments from Even-electron Protonated Prodiginine Precursors using Positive Ion Electrospray Tandem Mass Spectrometry	
Abstract.....	54
Introduction.....	55
Experimental.....	58
Chemicals and Sample Preparation	58
Mass Spectrometry.....	58
Computational Methods.....	59
Results and Discussion	60
Interpretation of the Detailed Fragmentation Pathways of Prodigiosin.....	60
Computational Studies of the Fragmentation Pathways of Prodiginine	65
Comparison of Apparent Thresholds and Activation Energies for the Two Competing Mechanisms.....	67
New Strategy for Prodiginine Identification.....	70
Conclusion	74
References.....	75
Chapter 5	77
Hypoxia-Induced Changes in the Zebrafish Skeletal Muscle Proteome	
Abstract	78
Introduction	79
Experimental.....	80
Chemical and Reagents.....	80
Animals.....	81
Preparation of Protein Extracts	81
Two-dimensional Polyacrylamide Gel Electrophoresis.....	81
Protein Visualization and 2D-DIGE Gel Image Analysis.....	82
Preparative 2D-PAGE and in-gel Digestion	84
Mass Spectrometry.....	84
Results.....	85
Optimization of 2D-PAGE Separation.....	85
2D-DIGE Analysis	85
Protein Identification	86
Discussion.....	93
Conclusion	96
References.....	97
Appendix	99
VITA.....	108

List of Figures

Figure 2.1 Structure of DAPM.....	23
Figure 2.2 Illustration of the column switching technique for pre-column sample concentration and separation.....	28
Figure 2.3 LC/UV chromatogram of sample derived from vascular smooth muscle cells that have been exposed to DAPM for 24 hr and the control medium (no VSMC contact)	29
Figure 2.4 LC-ES-MS of vascular smooth muscle cells sample that has been exposed to DAPM	32
Figure 2.5 LC-ES-MS of the control sample with the same amount of DAPM (but no vascular cell contact).....	33
Figure 2.6 LC-ES-MS/MS product ion spectrum of protonated DAPM precursor at m/z 199.....	34
Figure 2.7 LC-ES-MS/MS product ion spectrum of m/z 241 precursor, protonated Metabolite II	35
Figure 3.1 LC/MS total ion chromatogram (TIC) of biliary metabolites in a rat dosed with methylenedianiline (DAPM); LC/MS reconstructed ion chromatogram of M2 at m/z 532 and M3 at m/x 478	41
Figure 3.2 MS/MS spectrum of protonated M2 at m/z 532 and MS ³ spectrum of m/z 300; proposed fragmentation pathways of protonated M2 and m/z 300	44
Figure 3.3 MS ³ spectra of the precursor ions at: m/z 225; and m/z 199 derived from protonated M2 present in bile of a rat dosed with DAPM; corresponding fragmentation pathways	46
Figure 3.4 MS ³ spectra of the precursor ions at: m/z 225; and m/z 199 derived from protonated M2 present in bile of a rat dosed with DAPM; corresponding fragmentation pathways	49
Figure 3.5 MS ³ spectra of: m/z 302 and m/z 285; MS ⁴ spectra of: m/z 241; and m/z 267; proposed fragmentation pathways of m/z 285 leading to the fragment ions at m/z 136 and 150.....	50
Figure 3.6 Proposed fragmentation pathways leading to the MS ³ product ions at m/z 241 and 267, and the MS ⁴ product ions at m/z 106, 132 and 148	51
Figure 4.1 ES-CID-MS ⁿ spectra for prodigiosin and the proposed major fragmentation pathways: MS/MS spectrum of [M+H] ⁺ precursor at m/z 324; MS ³ spectrum of m/z 309 (324→309); MS ³ spectrum of m/z 149 (324→149).....	62
Figure 4.2 ES-CID-MS ⁿ spectra for undecylprodiginine and the proposed principal fragmentation pathways: (A) MS/MS spectrum of [M+H] ⁺ precursor at m/z 394; MS ³ spectrum of m/z 377 (394→379)	63
Figure 4.3 ES-CID-MS ⁿ spectra for streptorubin B and the proposed major fragmentation pathways: MS/MS spectrum of [M+H] ⁺ precursor at m/z 392; MS ³ spectrum of m/z 377 (392→377); MS ³ spectrum	

of m/z 295 (392→295)..... 64

Figure 4.4 Structures of neutral prodiginine model system showing the preferred site for the proton attachment during electrospray ionization process. (I) the energetically optimized geometry at the B3PW91/6-31G* level; (II) chemical structure; (III) electron density map (sequence of electron density listed as followings: purple > blue > green > yellow > red) indicating highest electron density at the central nitrogen bearing no proton. The optimized prodiginine conformations and the relative energies calculated by density function theory (DFT) 71

Figure 4.5 Breakdown curves showing ion abundance vs. collision energy for MS/MS of prodigiosin. The plots show the evolution of precursor and fragment ions representing two competing pathways (m/z 324 = precursor; m/z 309 and 252 represent the formation of OE⁺ by methyl radical loss and methyl radical loss plus consecutive butyl radical loss, respectively; m/z 292 represents the formation of EE⁺ after the loss of methanol).The MS/MS spectra of the m/z 324 prodigiosin precursor with collision energies of 5, 10 and 12.5 eV performed under single collision conditions 71

Figure 4.6 Positive ion ES-MS spectrum of the extract from *H. chejuensis* showing [M+H]⁺ of m/z 324 from prodigiosin, and m/z 352 from the analog; positive ion neutral loss (15 Da) spectrum, showing both prodigiosin and its analog at m/z 324 and 352, respectively; positive ion neutral loss spectrum of 32 Da mass loss, showing both prodigiosin and its analog at m/z 324 and 352; Positive ion ES-MS/MS spectrum of protonated prodigiosin analog at m/z 352; and MS3 spectrum of m/z 337; the proposed fragmentation pathways of protonated prodigiosin analog at m/z 352 73

Scheme 4.1 Traditional structural representation of three investigated prodiginines: prodigiosin, streptorubin B, and undecylprodiginine..... 56

Scheme 4.2 Two competing fragmentation pathways of the protonated prodiginine model system leading either to OE⁺ after homolytic cleavage to lose a methyl radical, or to EE⁺ after heterolytic bond dissociation to lose a methanol molecule..... 69

Figure 5.1 Experimental design of 2D-DIGE, preparative gel electrophoresis, and identification of zebrafish skeletal muscle proteins..... 83

Figure 5.2 The Cy 2 images of representative 2D-DIGE gels between pH 4-7 (A) and 7-11(B) intervals. Proteins from the hypoxic or normoxic samples were labeled with either Cy 3 or Cy 5 dye. A pooled internal standard combining all extracts, labeled with Cy 2 dye, was included in all gels. Spots that differed between hypoxia and normoxia are indicated with spot number. These spots were selected for mass spectrometric analysis..... 87

Figure 5.3 2D-DIGE gel Images showing spots identified as zebrafish hemoglobin variants (spots 0904 (A) and 0909 (B)) with quantitative comparison between hypoxia and normoxia shown below. The error bars represent one standard deviation for n = 7 fish 90

Figure 5.4 CLUSTAL 2.0.8 multiple sequence alignment of the two identified hemoglobin variants (CAE48980 and CAE48986), with hemoglobin α adult-1 (NP_571332), hemoglobin β (NP_571095), cytoglobin (NP_694484), myoglobin (NP_956880), neuroglobin (NP_571928) and globin X (NP_001012261). All sequences are from zebrafish (*Danio reio*). The peptides identified by mass spectrometry are shown in bold type. The highlighted residues (in yellow) indicate the amino acid differences among the three Hb α sequences..... 91

List of Tables

Table 5.1 Identification of differentially expressed spots corresponding to putative intact protein..	89
Table 5.2 Identification of differentially expressed spots corresponding to putative protein fragments	92
Table A-1 pI, molecular weight, and the matched sequence to putative intact proteins.....	99
Table A-2 pI, molecular weight, and the matched sequence to putative protein fragments	104

Abstract

Mass spectrometry coupled with liquid chromatography and gel electrophoresis enables separation and detection of components in a complex mixture. During the last two decades, its applications were dramatically extended and remarkable progress has been made in many fields, in particular, environmental and biological analyses. This dissertation focuses on identification and characterization of biologically active compounds and comparative analysis of protein expression changes.

The first two projects (**Chapters 2 and 3**) focus on the application of LC/MS approach to profile the bioactivated intermediates of 4,4'-methylenedianiline (DAPM) from rat vascular smooth muscle cells (VSMCs) and bile. In our study, several DAPM metabolites were detected and characterized in detail by liquid chromatography-electrospray tandem mass spectrometry. The structural assignments of these metabolites from VSMCs and rat bile significantly improve our understanding of DAPM biotransformations and toxicity.

The third project described in **Chapter 4** focuses on using electrospray tandem mass spectrometry (ES-MS/MS) and theoretical calculation (GAUSSIAN 03 program) to investigate the unusual methyl radical loss and consecutive fragment ions that dominate the low-energy collision induced dissociation (CID) mass spectra of prodiginine compounds. Structures of the fragment ions are proposed and explanations are given to rationalize the observed competition between the formation of even-electron ions and radical ions. Our study shows that the lower apparent threshold associated with methyl radical loss points to a lower kinetic barrier.

In **Chapter 5**, hypoxia-induced changes of zebrafish skeletal muscle were studied using two-dimensional difference in-gel electrophoresis (2D-DIGE) *in vivo* after 48 h in hypoxia vs. normoxia. The results showed that proteins involved in mitochondrial oxidative metabolism are down-regulated, whereas

glycolytic enzymes are up-regulated to compensate for the loss of ATP synthesis in aerobic metabolism. The up-regulation of two spots identified as hemoglobin variants was also observed. These protein expression changes are consistent with a hypoxic response that enhances anaerobic metabolism or O₂ transport to tissues.

Key words: Mass Spectrometry, NMR spectroscopy, Liquid Chromatography, Two-dimensional Polyacrylamide Gel Electrophoresis, Metabolite Profiling, Proteomics, Methylenedianiline, Prodiginine, Hypoxia, Zebrafish

Chapter 1

Introduction

Introduction to Mass Spectrometry

During the last decade, mass spectrometry has played an important role in life science particularly for protein characterization and identification. Advances in ionization of biological molecules and complementary fragmentation techniques such as collision induced dissociation (CID),^{1,2} electron capture dissociation (ECD),^{3,4} and electron transfer dissociation (ETD)^{5,6} for peptides and proteins contribute to structural elucidation and sequence determination. Advances in ionization source configuration and electronic lenses in a new generation of mass spectrometry instruments led to significant improvements in detection.

The principle of mass spectrometry is to ionize molecules, separate the gas-phase ions and detect them according to their mass to charge ratios (m/z). There are different types of ionization sources, mass analyzers and detectors. Magnetic deflection, quadrupole filter, ion trap, time of flight and ion cyclotron resonance are the most commonly used techniques for mass analysis. Various types of mass spectrometry coupled with liquid chromatography or electrophoresis are suitable for different purposes of analyses. Presently, two ionization methods, matrix assisted laser desorption⁷ (MALDI) and electrospray⁸ (ES) ionization, have led the main stream in ionization of biomolecules, providing sensitive and soft-ionization. After nonvolatile biomolecules are ionized via protonation/deprotonation, the ions are sent and mass resolved in different types of mass analyzers, for example a magnetic sector, quadrupole, time-of-flight (TOF), quadrupole ion trap, linear ion trap, fourier transform ion cyclotron resonance⁹ (FTICR) mass spectrometer.¹⁰ Finally the ions are detected by a dynode/electron multiplier for quadrupole, ion trap and magnetic sector instruments, and by a multi-channel plate for TOF instruments, or image current for FTICR and Orbitrap¹¹ instruments. The performance of mass spectrometers is dependent upon ionization efficiency of the target compounds, ion transmission through ion optics, collision processes and sensitivity of detection. In the work that leads to this dissertation, several different types of mass spectrometers were utilized to obtain the data.

Mass spectrometry has conventionally been used with gas chromatography (GC) to study the vaporized

organic components eluted from GC column. In the combined GC-MS technique, molecular weight, plus the identity could be obtained from the fragmentation pattern of the component, and the approach also served as a basis to construct a library of compounds for structural identification. GC separation of the sample is essential because tandem mass spectrometry isn't widely applicable to GC-EI-MS, and without it, the fragments from co-eluting compounds will interfere with identifications. However, many polar compounds can't be vaporized in GC, thus limiting the application of the technique.

During the last two decades, a great deal of progress has been made towards the analysis of biological macromolecules when soft ionization techniques, especially ES and MALDI sources, were introduced as new interfaces for mass spectrometers. The nondestructive nature of soft ionization has proven advantages for the characterization of complex and polar substances that might be found in organic matter. To apply the technology more effectively, it is important to understand the ionization process and instrument configurations.

Electrospray ionization (ESI)

Several excellent reviews about the technology have been published.^{12, 13} In the electrospary process, high voltage is applied between the solution and counter electrode to transform the solution into an electrified mist, and form a shape of the spraying liquid named as the Taylor cone. Consequently, electrospary was referred to as a neublization process instead of an ionization process. The mist consists of tiny droplets containing solvent and analytes moving towards the counter electrode. Evaporation of solvent facilitates a decrease in the size of droplets and an increase in charge repulsion on the droplet surface. High charge density results in "columbic repulsion", and further shrinks the droplets, and finally ejects the ions from the droplets. The removal of solvent from the droplets could be assisted by a combination of heating and/or gas flow. Desolvated ions are transferred into mass analyzer via ion optics. Although ES is already a mature technique for ionization, there are still debates about the mechanism of ion formation.¹²

Matrix assisted laser desorption ionization (MALDI)

In the MALDI process, sample is co-crystallized with a low molecular weight, UV-absorbing matrix that enhances intact desorption and soft ionization of the analytes.¹⁴ A pulsed laser at a specific wavelength absorbed by matrix is used to induce both desorption and ionization of the analytes. Meanwhile, ions arising from the co-crystallized solid carry charges and even form dimers or multimers of the compounds and tolerate a relatively high concentration of salts or buffers brought from biological experiments.¹⁴ Studies involving the energy transfer indirectly from a matrix to ionize the sample can be dated back to the middle of 1980 by a beam of neutral atoms and molecules in fast atom bombardment (FAB-MS)¹⁵ or by a flux of high energy photons in MALDI¹⁴. IR and UV laser sources have been used to ionize samples. In MALDI, there are two observations obtained from different studies.^{7, 16, 17} In order to insure highly efficient and well-controlled energy transfer to the sample, a resonance adsorption is required at the laser wavelength. Secondly, to avoid the thermal decomposition of thermally labile compounds, each laser shot should take place in a very short time interval. The recent development of atmospheric pressure MALDI (AP-MALDI) doesn't require a vacuum source, thus significantly increasing the throughput of analysis.¹⁸

Different Types of Mass Analyzers

In order to separate the complicated and limited amount of samples from biological sources, liquid chromatography was coupled with electrospray mass spectrometer to obtain information about target compounds. Three types of mass analyzers (quadrupole, quadrupole 3D ion trap, hybrid quadrupole/linear ion trap) with ESI source have been mainly employed in metabolite profiling of the samples from rat biliary effluent and vacular smooth muscle cells exposed to a low dosage of methylenedianiline, as well as in the quadrupole ion trap protein identification using "bottom-up" strategy. The quadrupole ion trap uses a combination of radio frequency and constant potential to store the ions in a potential well.¹⁹ Selected ions are either stored or ejected from the trap by changing the potentials depending on their different m/z values. To obtain structural information, the stored ions can be analyzed to determine the m/z value or further fragmented to form small fragments by ion-molecule collisions. Increasing the fill

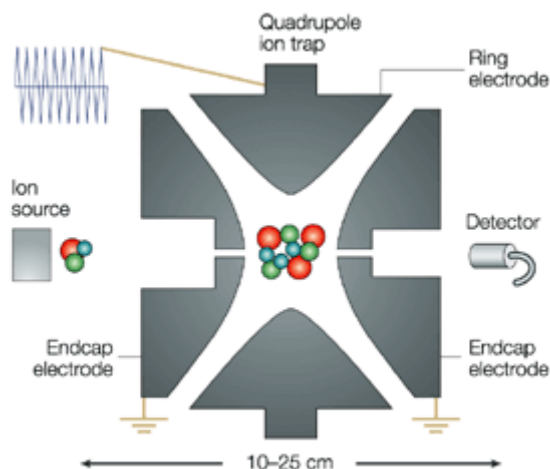
time for the ion trap can enhance the sensitivity and resolution of mass peaks, however, space charge effects are observed when high concentrations of ions are loaded into the trap, inducing ion repulsions and limiting the mass accuracy and resolution.¹⁹ Auto gain control (AGC) was introduced to limit the number of ions present in the trap by estimating the ion concentration with a rapid and “dirty” scan, and then determining the fill time to maintain a certain amount of ions in the trap. The strategy not only improved the sensitivity but also avoided space charge effects.^{20, 21} Up to now, it has been widely employed in most commercial quadrupole ion trap mass spectrometry instruments.

Quadrupole Ion Trap

The quadrupole ion trap has two configurations: the two dimensional linear ion trap (2D LIT)²² and the three dimensional ion trap (3D QIT)¹⁹, also named as “Paul Trap”. The former generally consists of two hyperbolic cap electrodes facing towards each other and one hyperbolic ring electrode halfway between them. A combination of AC and DC voltage on the trap can create a saddle-shaped field to trap the ions in a complex motion. If ion excitation is desired, a sweep voltage is applied onto the two end cap electrodes to empty the trap except for the selected ions. Then, an on-resonance radio-frequency voltage oscillates between the two electrodes to increase the collisions between the ions and inert gas molecules to induce fragmentation.¹⁹

Two-dimensional Linear Ion Trap (2D LIT)

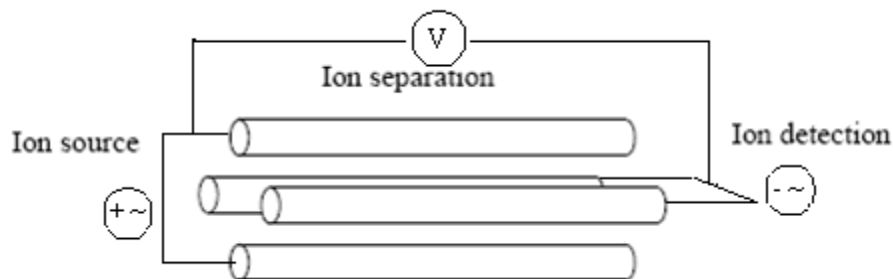
The linear form of the ion trap can be used as a mass selective filter by creating a trapping potential well along the axial electrodes.²² Advantages of the LIT includes a simple configuration, a fast scanning rate and a larger trapping capacity than the 3D QIT. Although the trapping capacity of LIT has been improved compared with that of QIT, the dynamic range of measurement is still the biggest limitation of ion trap based mass spectrometry.²²



Schematic drawings of 3D quadrupole ion trap²³

Triple Quadrupole

Another type of mass analyzer was built on three series of quadrupole mass analyzer, i.e. the triple quadrupole. A quadrupole consists of four parallel rods on which a combination of rf and DC voltage was applied. Scanning both rf and DC on the rods allows the quadrupole to act as a mass filter that allows only certain m/z ions to be transmitted through the rods, and simultaneously other m/z ions will collide with the rods. Based on this configuration, the triple quadrupole doesn't trap the ions in a certain space, thus avoiding the space charge effects occurring on the ion trap. The dynamic range of measurement is much higher than both QIT and LIT. It has been widely used in quantitative analysis, however, because no time is spent trapping the ions, the duty cycle of measurement is comparatively lower than that of the ion trap. Thus, the sensitivity and mass accuracy of the triple quadrupole mass spectrometry are lower than those of QIT and LIT. Triple quadrupole mass spectrometry is a typical space-based tandem MS in which it selects the precursor ions in the Q1 and fragments them in the Q2 collision cell, and finally mass separate the fragments in the Q3 mass analyzer.



Schematic drawing of a single quadrupole mass filter

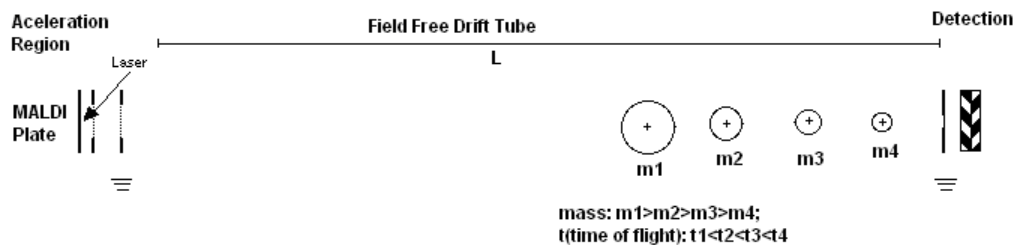
The electron multiplier is the last step in signal production. Transmitted ions are converted by multiplier to a measurable current. Too low settings on multiplier will reduce the signal. In contrast, too high settings will saturate the signal and reduce the lifetime of the detector, as well as give a poor quantitative result.

TOF and TOF/TOF

In this dissertation, we used an ABI 4800 MALDI-TOF/TOF mass spectrometer to identify the proteins regulated by hypoxia. In the TOF analyzer, ions formed in the pulsed ionization source are accelerated with the same potential from a fixed starting line and at a fixed initial time and allowed to drift in a field-free tube, the ions separate according to their m/z values. The time (t) that is required for the ions to travel through the region is dependent of the m/z described in the equation below.

$$t = L \left(\frac{m}{2zV} \right)^{\frac{1}{2}}$$

L is the length of the drift tube or the travel distance to reach the detector. To increase the resolving power of the TOF mass analyzer, a reflectron TOF mass analyzer allows for energy focusing of the ions. In the equation above, “ L ” represents the length of the drift tube, “ m ” the mass of the ions, “ z ” the charge of the ions and “ V ” the potential applied to accelerate the ions into the drift tube. Lighter ions drift more quickly to the detector, heavier ions drift more slowly.



Schematic drawing of linear TOF mass spectrometry

Separation Tools (on-line or off-line) coupled with Mass Spectrometry

After over more than one century of development, separation science plays an active role in many fields: organic synthesis for measuring purity and performing structural characterization of products; molecular biology for sequencing the genome of human and other species; forensic science for analyzing the blood and hair for criminal activities. Benefiting from the invention of capillary electrophoresis, the Human Genome Project completed work much faster than was expected. The next challenging project demanding the contribution of separation scientists is the analysis of the proteome, i.e., the complement of the genome. Since the proteome is defined by a combination of the genome, the environment at the moment and even cell history, cells do not have a fixed proteome. Instead, proteins are expressed with broad dynamic range depending upon the particular characteristics of the cell. The combination of separation science and mass spectrometry offers a promising future and resolution to these difficulties in proteomics research. This dissertation focuses on the exploration of two most popular separation methods that were readily available for on-line or off-line coupling with different mass spectrometers employed in my studies. Additionally, the merits of LC/MS coupling are widely recognized for universality, high sensitivity and outstanding selectivity in metabolite characterization. We used several LC/MS instruments for determining the biotransformations of methylenedianiline in rat liver and vascular smooth muscle cells.

High Performance Liquid Chromatography (HPLC)

The combination of gas chromatography and electron ionization mass spectrometry still remains unsurpassed for rapid separation and structural determination.²⁴ However, not all the compounds can be vaporized and ionized in GC/MS. The application of LC/MS allows the analysis of non-volatile samples. However, this method has gone through some practical difficulties because of inefficient sample delivery into the mass spectrometry before electrospray was introduced as a interface between LC and MS.

Among the forces driving the development of HPLC coupled with mass spectrometry, was the demand for miniaturization of column size to improve the sensitivity and reduce sample consumption.^{25, 26} Increased chromatographic resolving power and faster analysis by utilizing low volumes of stationary phase and development of new chemical modified stationary phase to reduce “column bleeding” that primarily produced the background noise were also primary concerns. Although most popular reports of LC-MS use the ES source interface, off-line MALDI-ToF/ToF coupled with HPLC has continued to be improved for proteomics work.^{27, 28}

Two-Dimensional Polyacrylamide Gel Electrophoresis (2D-PAGE)

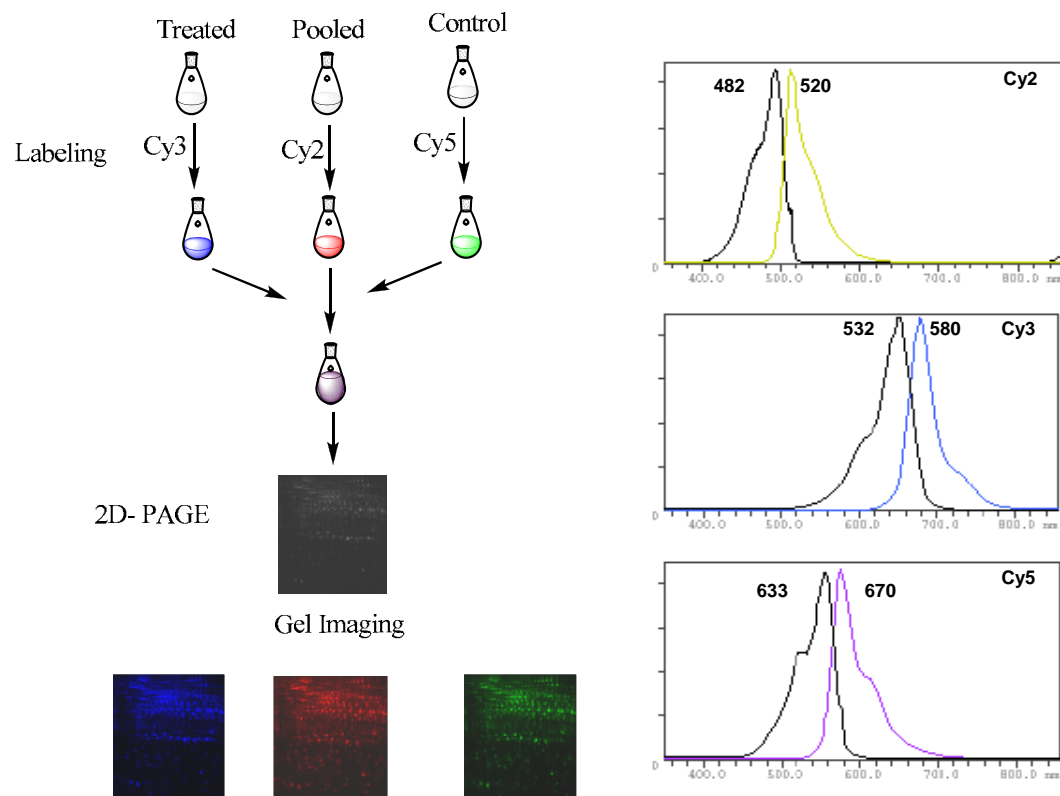
Two-dimensional gel electrophoresis combines isoelectric focusing and mass separation steps to generate a global view of the proteome in cells or tissue at a particular moment.²⁹⁻³¹ With the utilization of different visualization techniques such as radioactive labeling of protein, fluorescent dye labeling (CyDye), fluorescent dye staining (commercial available products like Sypro Ruby, Deep Purple and Flamingo) and non-fluorescence staining (silver or coomassie blue staining), one can visualize and quantify the protein spots.

This technique enables identification of major proteins in tissue or sub-cellular fractions when it is coupled off-line with mass spectrometry.³² In addition, 2D-PAGE have been used to quantitatively determine the protein expression changes between two samples, such as a treated sample and the control. However, quantitation was hampered by several factors. Low sensitivity and narrow dynamic range limits the detection of the response of certain low abundance proteins that are critical in cellular functions.

Another technical issue is gel-to-gel variation. Practically speaking, there are no two gels that are superimposable, which is required to overlay and compare them especially when significant proteome expression changes occur or subtle proteome expression differences are under investigation.

2D Difference in-Gel Electrophoresis (2D-DIGE)³³

2D-DIGE circumvents some these problems associated with traditional 2D-PAGE methodology. It utilizes pre-electrophoretic labeled protein samples with one of three spectrally resolvable fluorescent CyDye reagents (Cy2, 3 and 5), and Cy2 labeled protein as internal standard. These three CyDyes have similar structures but distinct spectral properties. The samples can be imaged separately, and overlaid and compared without warping since they come from the same gel.



Schematic diagram of 2D-DIGE procedure and excitation and emission spectra of Cy2 , Cy3 and Cy5

(Adapted from GE health Science 2D-DIGE manual).

The technique has a dynamic range that covers 5 orders of magnitude and nanogram level detection limits that allow one to differentiate subtle, low abundance protein expression changes. DIGE does not require modifications of the sample preparation protocol that is used in the conventional 2D-PAGE technique.

Applications of Mass Spectrometry

Identification and Characterization of Metabolites

All organisms are exposed to foreign compounds, i.e., to xenobiotics. The absorption routes could be through the skin, lungs, or gastrointestinal tract. Elimination of these potential toxins usually relies on biotransformations into non-toxic and hydrophilic chemicals that are readily for excretion. Without biotransformation, lipophilic xenobiotics would only be eliminated very slowly out of the body. Studies of the biotransformations of certain xenobiotics can assist the understanding of their toxicity upon exposure.

Biotransforming reactions are divided into two groups, named as phase I and phase II.³⁴ Phase I includes hydrolysis, reduction and oxidation; during the process some functional groups can be introduced including -OH, -NH₂, -SH or -COOH.³⁴ Phase II reactions involve conjugations with the functional groups previously introduced during phase I reactions such as glucuronidation, sulfonation, acetylation, methylation, fatty acid, glutathione and amino acid conjugation.³⁴ Most of phase II biotransformations increase the hydrophilicity, thus greatly promoting the excretion of xenobiotics. Some exceptions to this rule like fatty acid conjugation were found to significantly increase the lipophilicity that plagued the elimination of toxins like aniline.³⁵

Glucuronidation is one of the major phase II biotransformations where glucuronic acid is attached to a hydroxyl or carboxylic group (defined as O-glucuronidation); as well as N-glucuronidation is also possible.³⁴ The product of O-glucuronidation with phenols or alcohols is an ether glucuronide, while that formed with carboxylic acid is an ester glucuronide. Gluronides are polar and water soluble conjugates that are readily eliminated from the body in bile or urine. The substrates for N-glucuronidation include primary and secondary aromatic and aliphatic amines. To quickly identify the glucuronides of xenobiotics,

some characteristic neutral fragments (e.s. neutral loss of 176 Da, consecutive water losses from the precursor ions) may appear in tandem mass spectra.

The substrates for **acetylation** are the xenobiotics containing an aromatic amine or a hydrazine group, which form aromatic amides and hydrazides, respectively.³⁶ However, acetylation replaces the amine with a nonionizable group, which decreases the solubility of the metabolites. This process is catalyzed by N-acetyltransferase and also requires the cofactor acetyl-coenzyme A.³⁶ Thus, the conjugates may be more toxic than their precursor, and conjugation does not improve the excretion of phase I metabolites. In the mass spectra of acetyl conjugates, protonated or deprotonated molecular ions showed 42 Da increase as compared to their non-conjugated metabolites. During the fragmentation, acetyl-ketene loss (42 Da) is observed in CID-MS/MS spectra. For example, biotransformations of glutathione adducts lead to cysteine conjugates that are followed by N-acetylation,³⁶ which typically show 42 Da loss in MS/MS spectra.

Amino acid conjugations are also observed, which results in a further increase in the solubility of phase I metabolites. There are two possible pathways for the conjugation with either the xenobiotics containing a carboxylic acid functionality or phase I metabolites including the hydroxylamine group. Amide bond cleavage is dominant in the tandem mass spectra of the conjugates while other consecutive losses of water (18 Da) and/or CO (28 Da) are present in lower abundance. We reported that a metabolite resulting from glycine conjugation with DAPM hydroxylamine intermediate lost CO₂ (44 Da) following the loss of NH₃ (17 Da). This characteristic loss of CO₂ (44 Da) can be used to identify amino acid conjugation with an activated intermediate containing a hydroxylamine group.

The tripeptide **glutathione** containing nucleophilic cysteinyl thiol group is present in millimolar concentration in cells of most animals, which allows formation of glutathione adducts with the electrophilic reactive intermediates of xenobiotics. The process significantly increases the solubility of the phase I metabolites, and affords detoxification. The glutathione conjugates are usually followed by subsequent biotransformation, thus leading to either loss of glycine to form γ -glutamylcysteinyl conjugates³⁷ or loss of glutamic acid to form glycinylcysteinyl conjugates³⁸.

Thus, identification and structural characterization of these metabolites are essentially critical to

understanding the potential toxicity of drug candidates and other contaminating toxins. Detailed structural characterization of metabolites, produced *in vivo* or *in vitro*, can be performed using a variety of spectroscopic techniques. The combination of chromatographic techniques with mass spectrometry is presently the most efficient and powerful tool to provide structural information of the metabolites in biological fluids. However, mass spectrometry can not differentiate some configurational or conformational isomers. Other spectroscopic tools like NMR or IR are still needed to determine these structures.

Proteomics

In the 1970s and 1980s, most biologists placed their attention on Genomics and Genetic Engineering.^{39,40} During the past two decades, however, there has been a renaissance in protein biochemistry because of accumulation of genome sequence data housed in accessible databases. It is obvious that the sequencing of the entire genome is less meaningful if the functions of the gene can't be clarified; this pursuit is named "functional genomics".³⁷ Determination of the functions of gene products (genome complement, proteome) was thought to be an efficient way of finding prognostic markers (biomarkers) of diseases.⁴¹ Proteins are the ultimate determinant in cellular function; however, it also embodies high order of complexity. There are several factors that determine the protein function, such as the primary amino acid sequence, post-translational modifications (PTMs), three dimensional structures, and the formation of protein complexes for certain cellular function. Accordingly, proteomics research aims to determine protein structure, modifications, localization, protein expression changes upon environmental stimulation or drug treatment, and protein-protein interactions.^{42,43}

The challenges of proteomics research currently lies on several aspects: (1) limited sample quantities and lacking of a amplification tool comparable to PCR in genome studies, thus creating an urgent need for high sensitivity tools for protein identification and characterization; (2) broad dynamic range of protein abundance in cells, that requires analytical tools with comparable dynamic range for detection and quantification; (3) more complex information than that of the genome built upon four-base units (A, G, C

and T), thus demanding methods to provide quantitative and structurally informative output.

With the development of soft ionization methods like ESI⁸ and MALDI,^{44, 45} mass spectrometry earned the reputation for its high sensitivity, broad dynamic range of measurements, rich information obtained from complementary fragmentation techniques like CID,^{45, 46} infrared multiphoton dissociation (IRMPD)⁴⁷, electron capture dissociation (ECD)⁴⁸ and electron transfer dissociation (ETD)⁵. MS for protein identification and quantitation relies on the digestion by sequence-specific proteases. Short sequence peptide is more suitable for MS analysis and they fragment more readily to provide sequence information. The application of nano-size HPLC columns and on-line coupling with mass spectrometry enables the proteomic analysis of complex protein mixtures. However, after the proteins are digested, some peptides are either lost during the sample preparation, or their response is suppressed by other easily ionizable peptides. In order to fully characterize the protein of specific interest, the concept of “top-down” proteomics was proposed^{48, 49}. The application of electron capture dissociation allows fragmentation of the whole protein with low-energy electrons in FT-ICR mass spectrometry,⁵⁰ thus revealing the labile modifications on the whole protein. Thus it has attracted much attention for labile PTM characterization. It also can be used to investigate protein-protein interactions because non-covalent bonds often remain intact after backbone dissociation.⁵¹ Low-energy electron capture dissociation provides extensive sequence coverage,⁵² while high energy electrons give *w* or *z* ions from polypeptides, thus allowing one to distinguish isoleucine and leucine.⁵³

Until recently, 2D-PAGE or 2D-DGIE had been widely used in the investigation of global protein levels and differences in protein composition between two related samples.⁴¹ This enables the display of hundreds or thousands of protein spots in a 2D-PAGE; however, hydrophobic, extremely basic or acidic proteins are difficult to analyze. MS provides a large amount of information on a small sample size in an automated manner. However, the ion abundance of peptides relies on the ionization efficiency that is related to ionic strength in sample, source temperature, nebulizing and drying gas flow rate and other factors. Thus, relative quantitation using hydrogen/deuterium (H/D) isotope tag labeling has been developed to compare the protein expression levels. There are two approaches for peptide stable isotope

labeling to compare differential expression of proteins between the samples: chemically tagging the cysteine residue or N-terminal amino group of the proteins using ICAT⁵⁴ or iTRAQ⁵⁵ reagents; metabolic incorporation, in which protein tagging is achieved by culturing the cells in the medium containing stable isotope enriched amino acids like SILAC.⁵⁶ Tissue culture cells are grown in a medium that is short of certain essential amino acids, and then the amino acid is supplied in two forms: one containing the natural abundance of isotopes and the other containing the stable labeling isotope. After several cell cycles, all the proteins are tagged with the provided amino acids. After selection of candidate tryptic peptides for quantitative measurements, further MS/MS experiment on these precursors can identify the protein using either *de novo* peptide sequencing⁵⁷ or searching against the available database⁵⁸.

The activity of proteins is modulated through post-translational modification (PTM) such as phosphorylation and ubiquitinylation or through proteolytic cleavage. These PTMs result in a change in the molecular mass of the amino acid residues, or constant neutral loss in tandem mass spectra.⁵⁹ All these properties allow efficient characterization of PTMs in the proteins using the LC-MS/MS approach.

Proteomics research will impose significant changes to scientific world, especially in the pharmaceutical industry. Because most drugs inhibit the function of specific proteins, several strategies were successfully developed that incorporate the drug candidate screens with proteomic readout. For example, activity-based profiling identifies and quantifies the active proteases in a complex proteome (cells or tissue) using a small chemical probe to covalently attach to the active site of proteases.⁶⁰ Another approach is to elute the proteins from an immobilized drug, making them available for proteomic study.⁶¹

⁶² All the methodologies were developed in the last decade to successfully link many endogenous proteins with drug candidates, rather than the current single drug-single target model.

References of Chapter 1

1. Hunt, D. F.; Yates, J. R.; Shabanowitz, J.; Winston, S.; Hauer, C. R., Protein Sequencing By Tandem Mass-Spectrometry. *Proceedings Of The National Academy Of Sciences Of The United States Of America* **1986**, 83, (17), 6233-6237.
2. Biemann, K.; Scoble, H. A., Characterization By Tandem Mass-Spectrometry Of Structural Modifications In Proteins. *Science* **1987**, 237, (4818), 992-998.
3. Kelleher, R. L.; Zubarev, R. A.; Bush, K.; Furie, B.; Furie, B. C.; McLafferty, F. W.; Walsh, C. T., Localization of labile posttranslational modifications by electron capture dissociation: The case of gamma-carboxyglutamic acid. *Analytical Chemistry* **1999**, 71, (19), 4250-4253.
4. Mirgorodskaya, E.; Roepstorff, P.; Zubarev, R. A., Localization of O-glycosylation sites in peptides by electron capture dissociation in a fourier transform mass spectrometer. *Analytical Chemistry* **1999**, 71, (20), 4431-4436.
5. Syka, J. E. P.; Coon, J. J.; Schroeder, M. J.; Shabanowitz, J.; Hunt, D. F., Peptide and protein sequence analysis by electron transfer dissociation mass spectrometry. *Proceedings Of The National Academy Of Sciences Of The United States Of America* **2004**, 101, (26), 9528-9533.
6. Pitteri, S. J.; Chrisman, P. A.; McLuckey, S. A., Electron-transfer ion/ion reactions of doubly protonated peptides: Effect of elevated bath gas temperature. *Analytical Chemistry* **2005**, 77, (17), 5662-5669.
7. Karas, M.; Hillenkamp, F., Laser Desorption Ionization of Proteins with Molecular Masses Exceeding 10,000 Daltons. *Analytical Chemistry* **1988**, 60, 2299-2301.
8. Fenn, J. B.; Mann, M.; Meng, C. K.; Wong, S. F.; Whitehouse, C. M., Electrospray Ionization For Mass-Spectrometry Of Large Biomolecules. *Science* **1989**, 246, (4926), 64-71.
9. Amster, I. J., Fourier transform mass spectrometry. *Journal Of Mass Spectrometry* **1996**, 31, (12), 1325-1337.
10. Yeboah, F. K.; Konishi, Y., Mass Spectrometry of biomolecules: Functional foods, nutraceuticals, and natural health products. *Analytical Letters* **2003**, 36, (15), 3271-3307.
11. Hu, Q. Z.; Noll, R. J.; Li, H. Y.; Makarov, A.; Hardman, M.; Cooks, R. G., The Orbitrap: a new mass spectrometer. *Journal Of Mass Spectrometry* **2005**, 40, (4), 430-443.
12. Cole, R. B., Some tenets pertaining to electrospray ionization mass spectrometry. *J Mass Spectrom* **2000**, 35, (7), 763-72.
13. Van Berkel, G. J., An overview of some recent developments in ionization methods for mass spectrometry. *European Journal Of Mass Spectrometry* **2003**, 9, (6), 539-562.
14. Cotter, R. J., *Time-of-Flight Mass Spectrometry: Instrumentation and Applications in Biological Research* American Chemical Society Columbus, OH, 1994.
15. Caprioli, R. M., *Continuous Flow Fast Atom Bombardment Mass Spectrometry*. John Wiley & Sons Inc 1990.
16. Karas, M.; Bachmann, D.; Hillenkamp, F., Influence of the Wavelength in High-Irradiance Ultraviolet Laser Desorption Mass Spectrometry of Organic Molecules. *Analytical Chemistry* **1985**, 57, 2935-2939.
17. Stahl, B.; Steup, M.; Karas, M.; Hillenkamp, F., Analysis of Neutral Oligosaccharides by Matrix-Assisted Laser Desorption/Ionization Mass Spectrometry. *Analytical Chemistry* **1991**, 63, 1463-1466.
18. Laiko, V.; Baldwin, M.; Burlingame, A., Atmospheric pressure matrix-assisted laser desorption/ionization mass spectrometry. *Analytical Chemistry* **2000**, 72, (4), 652-657.
19. Stafford, G. C.; Kelley, P. E.; Syka, J. E. P.; Reynolds, W. E.; Todd, J. F. J., Recent improvements in and analytical applications of advanced ion trap technology. *International Journal of Mass Spectrometry and Ion Processes* **1984**, 60, (1), 85-98.
20. Belov, M. E.; Zhang, R.; Strittmatter, E. F.; Prior, D. C.; Tang, K.; Smith, R. D., Automated Gain Control and Internal Calibration with External Ion Accumulation Capillary Liquid Chromatography-Electrospray Ionization-Fourier Transform Ion Cyclotron Resonance. *Analytical Chemistry* **2003**, 75, 4195-4205.
21. Belov, M. E.; Rakov, V. S.; Nikolaev, E. N.; Goshe, M. B.; Anderson, G. A.; Smith, R. D., Initial implementation, of external accumulation liquid chromatography/electrospray ionization Fourier transform ion cyclotron resonance with automated gain control. *Rapid Communications In Mass Spectrometry* **2003**, 17, (7), 627-636.
22. Douglas, D. J.; Frank, A. J.; Mao, D. M., Linear ion traps in mass spectrometry. *Mass Spectrometry Reviews* **2005**, 24, (1), 1-29.
23. Glish, G.; Vachet, R., The basics of mass spectrometry in the twenty-first century. *Nature Reviews Drug Discovery* **2003**, 2.
24. Eugene, F. B.; Grob, R. L., *Modern practice of gas chromatography*. Wiley-Interscience: New York, 2004.
25. Jorgenson, J. W.; Guthrie, E. J., *Liquid-Chromatography In Open-Tubular Columns - Theory Of Column Optimization With Limited Pressure And Analysis Time, And Fabrication Of Chemically Bonded Reversed-Phase*

- Columns On Etched Borosilicate Glass-Capillaries. *Journal Of Chromatography* **1983**, 255, (JAN), 335-348.
- 26.Knox, J. H., Band dispersion in chromatography - a new view of A-term dispersion. *Journal Of Chromatography A* **1999**, 831, (1), 3-15.
- 27.Peter, J. F.; Otto, A. M.; Szabados, I.; Wolf, B., The use of magnetic microparticles and mass spectrometry (LC-MALDI-TOF-MS) for the enrichment and detection of molecules secreted by tumor cells. *European Journal Of Cell Biology* **2007**, 86, 43-43.
- 28.Connolly, J. B.; Burniston, J. G., LC-MALDI investigation of membrane-enriched protein fraction of rat heart muscle. *Molecular & Cellular Proteomics* **2006**, 5, (10), S12-S12.
- 29.Hoving, S.; Voshol, H.; van Oostrum, J., Towards high performance two-dimensional gel electrophoresis using ultrazoom gels. *Electrophoresis* **2000**, 21, (13), 2617-2621.
- 30.Bjellqvist, B.; Ek, K.; Righetti, P. G.; Gianazza, E.; Gorg, A.; Westermeier, R.; Postel, W., Isoelectric-Focusing In Immobilized Ph Gradients - Principle, Methodology And Some Applications. *Journal Of Biochemical And Biophysical Methods* **1982**, 6, (4), 317-339.
- 31.Ofarrell, P. H., High-Resolution 2-Dimensional Electrophoresis Of Proteins. *Journal Of Biological Chemistry* **1975**, 250, (10), 4007-4021.
- 32.Pappin, D. J. C.; Hojrup, P.; Bleasby, A. J., Rapid Identification Of Proteins By Peptide-Mass Fingerprinting. *Current Biology* **1993**, 3, (6), 327-332.
- 33.Focking, M.; Boersema, P. J.; O'Donoghue, N.; Lubec, G.; Pennington, S. R.; Cotter, D. R.; Dunn, M. J., 2-D DIGE as a quantitative tool for investigating the HUPO Brain Proteome Project mouse series. *Proteomics* **2006**, 6, (18), 4914-4931.
- 34.Gibson, G. G.; Skett, P., *Introduction to Drug Metabolism*. 2nd ed.; Stanley Thornes Publishers, Ltd: London, 1994.
- 35.Ansari, G. A. S.; Kaphalia, B. S.; Khan, M. F., Fatty-Acid Conjugates Of Xenobiotics. *Toxicology Letters* **1995**, 75, (1-3), 1-17.
- 36.Klaassen, C. D., *Casarett & Doull's Toxicology: The Basic Science of Poisons* 6th ed.; McGraw-Hill Professional: 2001.
- 37.Reboul, C.; Tanguy, S.; Gibault, A.; Dauzat, M.; Obert, P., Chronic hypoxia exposure depresses aortic endothelium-dependent vasorelaxation in both sedentary and trained rats: involvement of L-arginine. *J Appl Physiol* **2005**, 99, (3), 1029-35.
- 38.Polhuijs, M.; Gasinska, I.; Cherry, W. F.; J., M. G.; Pang, K. S., Stereoselectivity in glutathione conjugation and amidase-catalyzed hydrolysis of the 2-bromoisovalerylurea enantiomers in the single-pass perfused rat liver. *Journal of Pharmacology* **1993**, 265, (3), 1406-1412.
- 39.Lander, E. S.; Linton, L. M.; Birren, B.; Nusbaum, C.; Zody, M. C.; Baldwin, J.; Devon, K.; Dewar, K.; Doyle, M.; FitzHugh, W.; Funke, R.; Gage, D.; Harris, K.; Heaford, A.; Howland, J.; Kann, L.; Lehoczky, J.; LeVine, R.; McEwan, P.; McKernan, K.; Meldrim, J.; Mesirov, J. P.; Miranda, C.; Morris, W.; Naylor, J.; Raymond, C.; Rosetti, M.; Santos, R.; Sheridan, A.; Sougnez, C.; Stange-Thomann, N.; Stojanovic, N.; Subramanian, A.; Wyman, D.; Rogers, J.; Sulston, J.; Ainscough, R.; Beck, S.; Bentley, D.; Burton, J.; Clee, C.; Carter, N.; Coulson, A.; Deadman, R.; Deloukas, P.; Dunham, A.; Dunham, I.; Durbin, R.; French, L.; Grafham, D.; Gregory, S.; Hubbard, T.; Humphray, S.; Hunt, A.; Jones, M.; Lloyd, C.; McMurray, A.; Matthews, L.; Mercer, S.; Milne, S.; Mullikin, J. C.; Mungall, A.; Plumb, R.; Ross, M.; Shownkeen, R.; Sims, S.; Waterston, R. H.; Wilson, R. K.; Hillier, L. W.; McPherson, J. D.; Marra, M. A.; Mardis, E. R.; Fulton, L. A.; Chinwalla, A. T.; Pepin, K. H.; Gish, W. R.; Chissoe, S. L.; Wendl, M. C.; Delehaunty, K. D.; Miner, T. L.; Delehaunty, A.; Kramer, J. B.; Cook, L. L.; Fulton, R. S.; Johnson, D. L.; Minx, P. J.; Clifton, S. W.; Hawkins, T.; Branscomb, E.; Predki, P.; Richardson, P.; Wenning, S.; Slezak, T.; Doggett, N.; Cheng, J. F.; Olsen, A.; Lucas, S.; Elkin, C.; Uberbacher, E.; Frazier, M.; Gibbs, R. A.; Muzny, D. M.; Scherer, S. E.; Bouck, J. B.; Sodergren, E. J.; Worley, K. C.; Rives, C. M.; Gorrell, J. H.; Metzker, M. L.; Naylor, S. L.; Kucherlapati, R. S.; Nelson, D. L.; Weinstock, G. M.; Sakaki, Y.; Fujiiyama, A.; Hattori, M.; Yada, T.; Toyoda, A.; Itoh, T.; Kawagoe, C.; Watanabe, H.; Totoki, Y.; Taylor, T.; Weissenbach, J.; Heilig, R.; Saurin, W.; Artiguenave, F.; Brottier, P.; Bruls, T.; Pelletier, E.; Robert, C.; Wincker, P.; Rosenthal, A.; Platzer, M.; Nyakatura, G.; Taudien, S.; Rump, A.; Yang, H. M.; Yu, J.; Wang, J.; Huang, G. Y.; Gu, J.; Hood, L.; Rowen, L.; Madan, A.; Qin, S. Z.; Davis, R. W.; Federspiel, N. A.; Abola, A. P.; Proctor, M. J.; Myers, R. M.; Schmutz, J.; Dickson, M.; Grimwood, J.; Cox, D. R.; Olson, M. V.; Kaul, R.; Raymond, C.; Shimizu, N.; Kawasaki, K.; Minoshima, S.; Evans, G. A.; Athanasiou, M.; Schultz, R.; Roe, B. A.; Chen, F.; Pan, H. Q.; Ramser, J.; Lehrach, H.; Reinhardt, R.; McCombie, W. R.; de la Bastide, M.; Dedhia, N.; Blocker, H.; Hornischer, K.; Nordsiek, G.; Agarwala, R.; Aravind, L.; Bailey, J. A.; Bateman, A.; Batzoglou, S.; Birney, E.; Bork, P.; Brown, D. G.; Burge, C. B.; Cerutti, L.; Chen, H. C.; Church, D.; Clamp, M.; Copley, R. R.; Doerks, T.; Eddy, S. R.; Eichler, E. E.; Furey, T. S.; Galagan, J.; Gilbert, J. G. R.; Harmon, C.; Hayashizaki, Y.; Haussler, D.; Hermjakob, H.; Hokamp, K.; Jang, W. H.; Johnson, L. S.; Jones, T. A.; Kasif, S.;

Kasprzyk, A.; Kennedy, S.; Kent, W. J.; Kitts, P.; Koonin, E. V.; Korf, I.; Kulp, D.; Lancet, D.; Lowe, T. M.; McLysaght, A.; Mikkelsen, T.; Moran, J. V.; Mulder, N.; Pollara, V. J.; Ponting, C. P.; Schuler, G.; Schultz, J. R.; Slater, G.; Smit, A. F. A.; Stupka, E.; Szustakowski, J.; Thierry-Mieg, D.; Thierry-Mieg, J.; Wagner, L.; Wallis, J.; Wheeler, R.; Williams, A.; Wolf, Y. I.; Wolfe, K. H.; Yang, S. P.; Yeh, R. F.; Collins, F.; Guyer, M. S.; Peterson, J.; Felsenfeld, A.; Wetterstrand, K. A.; Patrinos, A.; Morgan, M. J., Initial sequencing and analysis of the human genome. *Nature* **2001**, 409, (6822), 860-921.

40. Venter, J. C.; Adams, M. D.; Myers, E. W.; Li, P. W.; Mural, R. J.; Sutton, G. G.; Smith, H. O.; Yandell, M.; Evans, C. A.; Holt, R. A.; Gocayne, J. D.; Amanatides, P.; Ballew, R. M.; Huson, D. H.; Wortman, J. R.; Zhang, Q.; Kodira, C. D.; Zheng, X. Q. H.; Chen, L.; Skupski, M.; Subramanian, G.; Thomas, P. D.; Zhang, J. H.; Miklos, G. L. G.; Nelson, C.; Broder, S.; Clark, A. G.; Nadeau, C.; McKusick, V. A.; Zinder, N.; Levine, A. J.; Roberts, R. J.; Simon, M.; Slayman, C.; Hunkapiller, M.; Bolanos, R.; Delcher, A.; Dew, I.; Fasulo, D.; Flanigan, M.; Florea, L.; Halpern, A.; Hannenhalli, S.; Kravitz, S.; Levy, S.; Mobarry, C.; Reinert, K.; Remington, K.; Abu-Threideh, J.; Beasley, E.; Biddick, K.; Bonazzi, V.; Brandon, R.; Cargill, M.; Chandramouliswaran, I.; Charlab, R.; Chaturvedi, K.; Deng, Z. M.; Di Francesco, V.; Dunn, P.; Eilbeck, K.; Evangelista, C.; Gabrielian, A. E.; Gan, W.; Ge, W. M.; Gong, F. C.; Gu, Z. P.; Guan, P.; Heiman, T. J.; Higgins, M. E.; Ji, R. R.; Ke, Z. X.; Ketchum, K. A.; Lai, Z. W.; Lei, Y. D.; Li, Z. Y.; Li, J. Y.; Liang, Y.; Lin, X. Y.; Lu, F.; Merkulov, G. V.; Milshina, N.; Moore, H. M.; Naik, A. K.; Narayan, V. A.; Neelam, B.; Nuskern, D.; Rusch, D. B.; Salzberg, S.; Shao, W.; Shue, B. X.; Sun, J. T.; Wang, Z. Y.; Wang, A. H.; Wang, X.; Wang, J.; Wei, M. H.; Wides, R.; Xiao, C. L.; Yan, C. H.; Yao, A.; Ye, J.; Zhan, M.; Zhang, W. Q.; Zhang, H. Y.; Zhao, Q.; Zheng, L. S.; Zhong, F.; Zhong, W. Y.; Zhu, S. P. C.; Zhao, S. Y.; Gilbert, D.; Baumhueter, S.; Spier, G.; Carter, C.; Cravchik, A.; Woodage, T.; Ali, F.; An, H. J.; Awe, A.; Baldwin, D.; Baden, H.; Barnstead, M.; Barrow, I.; Beeson, K.; Busam, D.; Carver, A.; Center, A.; Cheng, M. L.; Curry, L.; Danaher, S.; Davenport, L.; Desilets, R.; Dietz, S.; Dodson, K.; Doup, L.; Ferreira, S.; Garg, N.; Gluecksmann, A.; Hart, B.; Haynes, J.; Haynes, C.; Heiner, C.; Hladun, S.; Hostin, D.; Houck, J.; Howland, T.; Ibegwam, C.; Johnson, J.; Kalush, F.; Kline, L.; Koduru, S.; Love, A.; Mann, F.; May, D.; McCawley, S.; McIntosh, T.; McMullen, I.; Moy, M.; Moy, L.; Murphy, B.; Nelson, K.; Pfannkoch, C.; Pratts, E.; Puri, V.; Qureshi, H.; Reardon, M.; Rodriguez, R.; Rogers, Y. H.; Romblad, D.; Ruhfel, B.; Scott, R.; Sitter, C.; Smallwood, M.; Stewart, E.; Strong, R.; Suh, E.; Thomas, R.; Tint, N. N.; Tse, S.; Vech, C.; Wang, G.; Wetter, J.; Williams, S.; Williams, M.; Windsor, S.; Winn-Deen, E.; Wolfe, K.; Zaveri, J.; Zaveri, K.; Abril, J. F.; Guigo, R.; Campbell, M. J.; Sjolander, K. V.; Karlak, B.; Kejariwal, A.; Mi, H. Y.; Lazareva, B.; Hatton, T.; Narechania, A.; Diemer, K.; Muruganujan, A.; Guo, N.; Sato, S.; Bafna, V.; Istrail, S.; Lippert, R.; Schwartz, R.; Walenz, B.; Yooseph, S.; Allen, D.; Basu, A.; Baxendale, J.; Blick, L.; Caminha, M.; Carnes-Stine, J.; Caulk, P.; Chiang, Y. H.; Coyne, M.; Dahlke, C.; Mays, A. D.; Dombroski, M.; Donnelly, M.; Ely, D.; Esparham, S.; Fosler, C.; Gire, H.; Glanowski, S.; Glasser, K.; Glodek, A.; Gorokhov, M.; Graham, K.; Gropman, B.; Harris, M.; Heil, J.; Henderson, S.; Hoover, J.; Jennings, D.; Jordan, C.; Jordan, J.; Kasha, J.; Kagan, L.; Kraft, C.; Levitsky, A.; Lewis, M.; Liu, X. J.; Lopez, J.; Ma, D.; Majoros, W.; McDaniel, J.; Murphy, S.; Newman, M.; Nguyen, T.; Nguyen, N.; Nodell, M.; Pan, S.; Peck, J.; Peterson, M.; Rowe, W.; Sanders, R.; Scott, J.; Simpson, M.; Smith, T.; Sprague, A.; Stockwell, T.; Turner, R.; Venter, E.; Wang, M.; Wen, M. Y.; Wu, D.; Wu, M.; Xia, A.; Zandieh, A.; Zhu, X. H., The sequence of the human genome. *Science* **2001**, 291, (5507), 1304+.

41. Wilkins, M. R.; Pasquali, C.; Appel, R. D.; Ou, K.; Golaz, O.; Sanchez, J. C.; Yan, J. X.; Gooley, A. A.; Hughes, G.; HumpherySmith, I.; Williams, K. L.; Hochstrasser, D. F., From proteins to proteomes: Large scale protein identification by two-dimensional electrophoresis and amino acid analysis. *Bio-Technology* **1996**, 14, (1), 61-65.

42. Pennington, S., *Proteomics: From Protein Sequence to Function* Springer: 2001.

43. Tong, A. H. Y.; Drees, B.; Nardelli, G.; Bader, G. D.; Brannetti, B.; Castagnoli, L.; Evangelista, M.; Ferracuti, S.; Nelson, B.; Paoluzi, S.; Quondam, M.; Zucconi, A.; Hogue, C. W. V.; Fields, S.; Boone, C.; Cesareni, G., A combined experimental and computational strategy to define protein interaction networks for peptide recognition modules. *Science* **2002**, 295, (5553), 321-324.

44. Nelson, P. S.; Han, D.; Rochon, Y.; Corthals, G. L.; Lin, B.; Monson, A.; Nguyen, V.; Franza, B. R.; Plymate, S. R.; Aebersold, R.; Hood, L., Comprehensive analyses of prostate gene expression: convergence of expressed sequence tag databases, transcript profiling and proteomics. *Electrophoresis* **2000**, 21, (9), 1823-31.

45. Huddleston, M. J.; Bean, M. F.; Carr, S. A., Collisional Fragmentation Of Glycopeptides By Electrospray Ionization Lc Ms And Lc Ms Ms - Methods For Selective Detection Of Glycopeptides In Protein Digests. *Analytical Chemistry* **1993**, 65, (7), 877-884.

46. Johnson, R. S.; Martin, S. A.; Biemann, K., Collision-Induced Fragmentation Of (M+H)⁺Ions Of Peptides - Side-Chain Specific Sequence Ions. *International Journal Of Mass Spectrometry And Ion Processes* **1988**, 86, 137-154.

47. Hakansson, K.; Chalmers, M. J.; Quinn, J. P.; McFarland, M. A.; Hendrickson, C. L.; Marshall, A. G., Combined electron capture and infrared multiphoton dissociation for multistage MS/MS in a Fourier transform ion cyclotron

- resonance mass spectrometer. *Analytical Chemistry* **2003**, 75, (13), 3256-3262.
48. Ge, Y.; Lawhorn, B. G.; ElNaggar, M.; Strauss, E.; Park, J. H.; Begley, T. P.; McLafferty, F. W., Top down characterization of larger proteins (45 kDa) by electron capture dissociation mass spectrometry. *Journal Of The American Chemical Society* **2002**, 124, (4), 672-678.
49. Angerer, P.; Nowak, D., Working in permanent hypoxia for fire protection-impact on health. *Int Arch Occup Environ Health* **2003**, 76, (2), 87-102.
50. Zubarev, R. A.; Horn, D. M.; Fridriksson, E. K.; Kelleher, N. L.; Kruger, N. A.; Lewis, M. A.; Carpenter, B. K.; McLafferty, F. W., Electron capture dissociation for structural characterization of multiply charged protein cations. *Analytical Chemistry* **2000**, 72, (3), 563-573.
51. Haselmann, K. F.; Jorgensen, T. J. D.; Budnik, B. A.; Jensen, F.; Zubarev, R. A., Electron capture dissociation of weakly bound polypeptide polycationic complexes. *Rapid Communications In Mass Spectrometry* **2002**, 16, (24), 2260-2265.
52. Kjeldsen, F.; Zubarev, R., Secondary losses via gamma-lactam formation in hot electron capture dissociation: A missing link to complete de novo sequencing of proteins? *Journal Of The American Chemical Society* **2003**, 125, (22), 6628-6629.
53. Kjeldsen, F.; Haselmann, K. F.; Sorensen, E. S.; Zubarev, R. A., Distinguishing of Ile/Leu amino acid residues in the PP3 protein by (hot) electron capture dissociation in Fourier transform ion cyclotron resonance mass spectrometry. *Analytical Chemistry* **2003**, 75, (6), 1267-1274.
54. Gygi, S. P.; Rist, B.; Gerber, S. A.; Turecek, F.; Gelb, M. H.; Aebersold, R., Quantitative analysis of complex protein mixtures using isotope-coded affinity tags. *Nature Biotechnology* **1999**, 17, (10), 994-999.
55. Ross, D. C.; Preter, M.; Klein, D. F., Hematologic alterations and CO(2) hypersensitivity in male panic disorder patients and normal controls: similarities to high-altitude hypoxia and chronic lung disease. *Depress Anxiety* **2001**, 14, (2), 153-4.
56. Zhong, N.; Zhang, Y.; Zhu, H. F.; Wang, J. C.; Fang, Q. Z.; Zhou, Z. N., Myocardial capillary angiogenesis and coronary flow in ischemia tolerance rat by adaptation to intermittent high altitude hypoxia. *Acta Pharmacol Sin* **2002**, 23, (4), 305-10.
57. Forner, F.; Foster, L. J.; Toppo, S., Mass spectrometry data analysis in the proteomics era. *Current Bioinformatics* **2007**, 2, (1), 63-93.
58. Keller, A.; Nesvizhskii, A. I.; Kolker, E.; Aebersold, R., Empirical statistical model to estimate the accuracy of peptide identifications made by MS/MS and database search. *Analytical Chemistry* **2002**, 74, (20), 5383-5392.
59. Steen, H.; Mann, M., A new derivatization strategy for the analysis of phosphopeptides by precursor ion scanning in positive ion mode. *Journal Of The American Society For Mass Spectrometry* **2002**, 13, (8), 996-1003.
60. Medzihradzky, K. F.; Campbell, J. M.; Baldwin, M. A.; Falick, A. M.; Juhasz, P.; Vestal, M. L.; Burlingame, A. L., The characteristics of peptide collision-induced dissociation using a high-performance MALDI-TOF/TOF tandem mass spectrometer. *Analytical Chemistry* **2000**, 72, (3), 552-558.
61. Godl, K.; Wissing, J.; Kurtenbach, A.; Habenberger, P.; Blencke, S.; Gutbrod, H.; Salassidis, K.; Stein-Gerlach, M.; Missio, A.; Cotten, M.; Daub, H., An efficient proteomics method to identify the cellular targets of protein kinase inhibitors. *Proceedings Of The National Academy Of Sciences Of The United States Of America* **2003**, 100, (26), 15434-15439.
62. Graves, P. R.; Haystead, T. A. J., Molecular biologist's guide to proteomics. *Microbiology And Molecular Biology Reviews* **2002**, 66, (1), 39.

Chapter 2

Identification of Metabolites of 4,4'-Methylenedianiline in Vascular Smooth Muscle Cells by Liquid Chromatography-Electrospray Tandem Mass Spectrometry

Abstract

A capillary liquid chromatography-electrospray tandem mass spectrometry (LC-ES-MS/MS) method was developed for identification of metabolites of 4,4'-methylenedianiline (diaminodiphenyl methane, DAPM) derived from exposure of vascular smooth muscle cells to this compound. The use of precolumn concentration and column switching techniques prior to reversed-phase liquid chromatography coupled on-line to ES-MS enabled the separation and detection of low-level DAPM and its metabolites in the exposed cell samples. The employed LC-ES-MS method, and further LC-ES-MS/MS analysis enabled structural assignments for two DAPM metabolites from vascular smooth muscle cells: N-acetyl methylenedianiline (*N*-acetyl DAPM) and *N,N'*-diacetyl methylenedianiline (*N,N'*-diacetyl-DAPM).

Introduction

The aromatic amine 4,4'-methylenedianiline (DAPM, Figure 2.1) presents health hazards to animals and humans, especially those working in industries that manufacture polymers. In recent years, DAPM has been primarily used in the production of methylene diphenyl diisocyanate (MDI) and polymeric MDI, which are employed in rigid and semi-rigid polyurethane fabrication. DAPM is also used to construct numerous medical devices including catheters, dialysis tubing and surgical implants, and it can be released during gamma-ray or autoclave sterilization of these devices [1]. Other DAPM derivatives are used to make floor coverings, dye stuff intermediates, and a hardening agent for epoxy resins [2, 3].

Both occupational and accidental exposures to DAPM are known to cause fever, rash, toxic hepatitis and jaundice with cholestasis and cholangitis [4, 5]. Hepatotoxic and carcinogenic effects in animals [6,7] and human subjects [4,8] have also been documented, but the involved metabolic pathways and the mechanism of toxicity are not clearly understood. Studies identifying DAPM metabolites in human urine have revealed that acetylation is likely an important pathway in DAPM detoxification [9,10]. In addition, prior reports examining the metabolism of DAPM in microsomal preparations revealed that it may undergo oxidation to electrophilic azo and azoxy compounds[11]. In contrast, Kautiainen et al.[12] demonstrated that the bulk of DAPM bound to hemoglobin in the blood existed in an imine form of DAPM, likely derived from extra-hepatic sources of peroxidase enzymes. Thus, investigation of hepatic metabolism of DAPM is probably insufficient for explaining its full array of toxicological effects.

T.R. Dugas et al. [13,14], reported that chronic, low-dose exposure to DAPM caused vascular toxicity in rats that was more pronounced in females than in males. The observed wall thickening of pulmonary arteries was confined to the medial layer containing vascular smooth muscle cells (VSMC). In addition, the proliferative effects of DAPM could be reproduced in cultures of VSMC treated with DAPM [14]. Treatment of VSMC with [¹⁴C]-DAPM resulted in the disappearance of DAPM and the appearance of several DAPM metabolites that were observed using HPLC with radioisotopic detection (unpublished findings). Because direct treatment of VSMC with DAPM induced cellular proliferation, we hypothesized

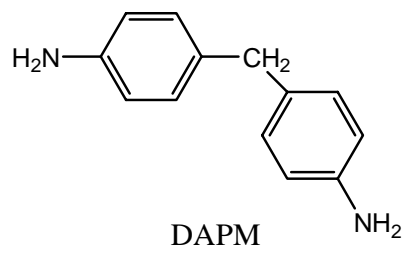


Figure 2.1 Structure of DAPM

that VSMC may be capable of metabolizing DAPM to reactive intermediates that, in turn, bind to molecular targets to promote VSMC proliferation. Importantly, no prior studies have reported on the metabolism of DAPM by extra-hepatic cells, and few studies have investigated the metabolism of xenobiotics by vascular cells. Although VSMC are known to express the cytochrome P450 enzymes CYP 1A1 and 1B1 [15] and are a rich source of the peroxidase enzyme prostaglandin H synthase, little else is known about the ability of VSMC to metabolize xenobiotics. However, because the biotransformation of DAPM by these cells is likely not as robust as that involving hepatocytes and microsomes, development of a sensitive method for separating and characterizing DAPM metabolites formed in VSMC was required and forms the basis for this paper.

Gas chromatography (GC) and liquid chromatography (LC) have been used for the separation of metabolites of DAPM in urine and blood samples [16-21]. The low volatility of DAPM and its metabolites necessitated a derivatization step [16] prior to GC separation coupled with electron capture [17], thermionic specific [18], or mass spectrometric [19] detection. Derivatization is not required for LC analyses employing ultraviolet absorbance (UV) [20], electrochemical [16] or mass spectrometric detection [21].

On-line HPLC-plasma spray mass spectrometry and off-line fast atom bombardment tandem mass spectrometry were used to study the metabolism of DAPM in rabbit hepatic microsomal incubation media, and three metabolites (4-nitroso-4'-aminodiphenylmethane, azodiphenylmethane and azoxydiphenylmethane) were identified [21]. Compared to these older techniques, capillary (300 μm ID) column LC-ES-MS can offer some performance advantages such as improved chromatographic separation and lower detection limits. However, monitoring of DAPM and its metabolites in extracts from vascular smooth muscle cells treated with low levels of DAPM can be rather challenging, and success in characterizing metabolites will require high efficiency separations coupled with high sensitivity mass spectrometric analyses.

2.3 Experimental

Chemical and reagents

4,4'-Methylenedianiline (CAS No. 101-77-9; >97% pure), formic acid and ammonium acetate (CAS No. 631-68-3 >99% pure) were purchased from Sigma Chemical Co. (St Louis, MO). HPLC-grade acetonitrile was purchased from EM Sciences (Gibbstown, NJ). Water was purified using a Milli-Q™ water system (Millipore Co, Billerica, MA). ¹⁴C-DAPM was custom synthesized by American Radiolabeled Chemicals (St. Louis, MO).

Sample Preparation and Handling

Manipulation of both DAPM and ¹⁴C-DAPM was performed in a hood using gloves and other protective equipment. When working with radiolabeled compound, every precaution was taken to contain the radioactivity. Upon completion of an experiment, all surfaces and glassware were decontaminated using Rad-Con Surface Cleaner (Fluke Biomedical, Everett, WA). Vascular smooth muscle cells were isolated from the aortas of male Sprague Dawley rats using a method described previously [14]. VSMC were cultured in Dulbecco's Modified Eagle's Medium (DMEM; Mediatech, Herndon, VA) containing 10% fetal bovine serum (FBS) and 1% antibiotic-antimycotic solution (Mediatech). For treatment with DAPM, the cells were plated into 6-well tissue culture-treated plates. Once the VSMC had reached ~70-80% confluence, the medium was aspirated, and the cells were treated for 24h with DMEM containing 10% FBS and 3.57 μM DAPM. After treatment, the cells were removed from the plate by scraping in the reaction medium, and the cell/medium mixture was homogenized using a Braun-Sonic U ultrasonicator (Allentown, PA). Cell protein was then removed from the samples using Microcon (Millipore, Bedford, MA) 10,000 M.W. cutoff centrifugal filters.

LC/MS/MS

LC analysis of DAPM and its metabolites was carried out on an "Ultimate" capillary/nano LC system (LC

Packings Inc., San Francisco, CA, USA), which includes a “Switchos” advanced microcolumn switching device. Separation was performed using a binary-gradient on a 300 μm I.D. \times 15 cm, 3 μm , peptide map C18 reversed-phase column (LC packings, Amsterdam, Netherlands) with a mobile phase of: A) 15 mM ammonium acetate buffer (pH 5.0) and B) acetonitrile, at a flow rate of 4 $\mu\text{l}/\text{min}$. The binary gradient went from 20% B hold for 8 min (including pre-column concentration 5 min), then 20 to 38% B in 10 min, then 38 to 90% B in 20 min, and finally 90% B hold for 5 min. 20 μL of the sample was injected into the loop and loaded onto a micro-precolumn (300 μm I.D. \times 5 mm, C18), with 1% aqueous acetonitrile loading mobile phase. Separation was enabled by the above-mentioned analytical column, with UV-detection at 254 nm, before the effluent was electrosprayed on-line into the mass spectrometer.

On-line HPLC-MS detection was performed with a Micromass Quattro II triple quadrupole mass spectrometer (Micromass Ltd., Cheshire, UK), equipped with an electrospray (ES) source. The electrospray voltage used was 3.0 kV; cone voltage was set at 15 V, skimmer at 2 V, and the RF lens was maintained at 0.3 V. The mass spectrometer was operated in the positive ion mode under unit-resolution conditions. All parameters were initially tuned with a DAPM standard. Tandem mass spectrometric analysis was performed with argon collision gas at a pressure of 2.0×10^{-4} mTorr (gauge external to hexapole collision cell) and a collision energy of 30 eV.

Results and Discussion

The samples studied in this work are rat aortic smooth muscle cells that have been exposed to DAPM, and a DAPM control sample that has had no cell contact. In view of the original concentration of DAPM (3.57 μM) used to initiate exposure of the cells, the concentrations of the metabolites and the remaining DAPM, of course, are expected to be lower than 3.57 μM . The challenge presented by this project is to obtain structural information concerning the bio-transformed metabolites that are present at extremely low levels.

LC/UV Chromatograms of the Sample and the Control Sample

The LC Packings Ultimate capillary HPLC features pre-column concentration and a column switching technique [22-24], which can improve the detection limits. Large amounts of sample (up to 1 mL) can be concentrated on the first 5 mm length C18 pre-column with simultaneous matrix removal (principally de-salting), followed by elution of the concentrated sample onto the analytical reversed-phase C18 column for separation (Figure 2.2). Compared to direct injection, pre-column concentration allows relatively large-volume sample injections, while maintaining narrow chromatographic peaks; sharper peaks lead to higher signal-to-noise ratios. For our experiments that employed a single injection of 20 μ L, pre-column concentration enabled an improvement of the detection limits by a factor of ~ 20 , relative to what is obtainable via direct injection with no pre-column concentration. The number of effective plates on the 15 cm length, 300 μ m i.d. C-18 analytical capillary column is approximately 30,000.

When VSMC were exposed to 14 C-labeled DAPM and the sample was extracted for analysis, there were two major metabolite peaks appearing near that of the residual DAPM starting material. Comparison of the LC/UV chromatograms obtained for DAPM exposure (Figure 2.3a) and no cell contact (control, Figure 2.3b) shows that DAPM elutes from the column at 23.0 min, just after metabolite II at 22.0 min (Figure 2.3a). The employed solvent gradient allowed baseline separation (thus minimizing the problem of ionization suppression from coeluting species) and reasonably short (~ 25 min) retention times.

A comparison of the areas of the DAPM peaks in Figures 2.3a and 2.3b (DAPM with and without vascular smooth muscle cell contact, respectively, all other experimental conditions identical) allows calculation of the fraction of DAPM converted to metabolites: $\text{DAPM fraction metabolized} = 1 - [(\text{Peak Area of DAPM in the exposed cell sample}) / (\text{Peak Area of DAPM in the control})] = 1 - (24.7/35.3) = 1 - 0.70 = 0.30$. Thus, 30% of the DAPM in the exposed VSMC sample was metabolized in 24 hr.

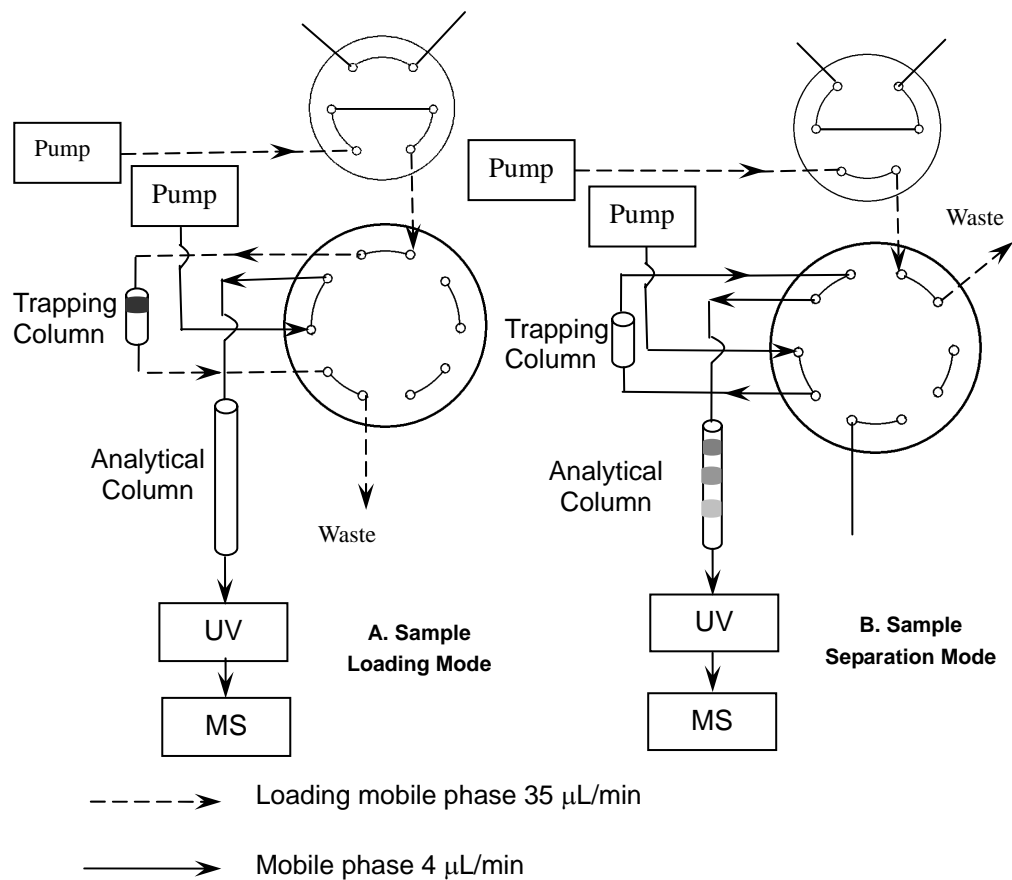


Figure 2.2 Illustration of the column switching technique for pre-column sample concentration and separation. (A) Sample is loaded from the loop onto the trapping column while the analytical column is equilibrating. (B) Sample is desorbed from the trapping column in back flush mode and delivered through the analytical column for separation while the next sample is loaded onto the loop. The LC effluent passed through the UV detector and reached the mass spectrometer for detection.

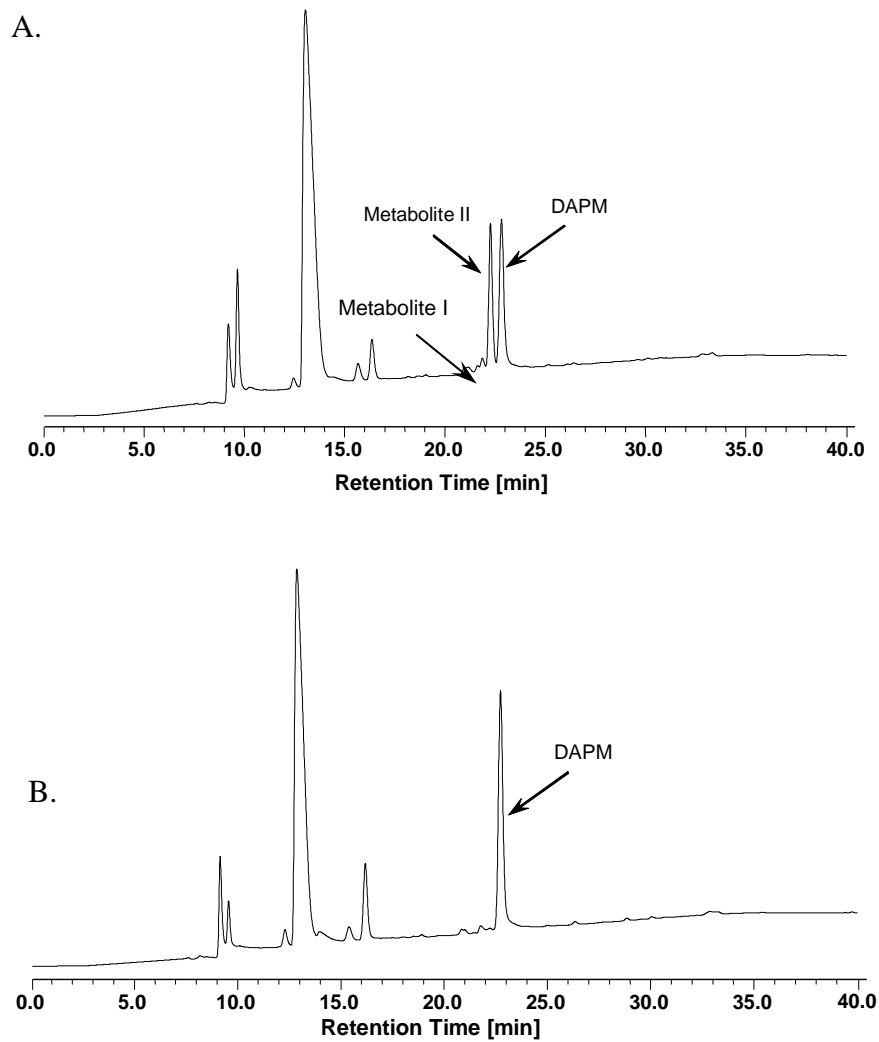


Figure 2.3 LC/UV chromatogram of (A) sample derived from vascular smooth muscle cells that have been exposed to DAPM for 24 hr and (B) the control medium (no VSMC contact).

LC/MS Chromatograms of the Sample and the Control Sample

A combination of two chromatographic detection systems resulted in the observation of many low abundance signals in the investigated samples. A UV detector provides a signal based on the response of chromophores within the compounds that absorb at the irradiation wavelength (254 nm). On-line coupling of LC with an ES mass spectrometer can allow the differentiation of each compound by m/z value; furthermore, structural information can be derived from tandem mass spectrometry (MS/MS) experiments.

In the LC/MS chromatograms of both sample and control, a peak appears at about 24.9 min representing protonated DAPM at m/z 199 (Figure 2.4c, 2.5c). Appearing only in the chromatogram of vascular smooth muscle cells that have been exposed to DAPM is another peak at 24.1 min yielding a predominant ion at m/z 241 (Figure 2.4b). Due to the conditions in our experiments, generated ions are in the form of protonated molecules, $[M+H]^+$, thus the molecular weight of the neutral molecule is 240 Da. This neutral molecule that we are naming “Metabolite II” must contain an even number of nitrogen atoms according to the nitrogen rule. The mass difference between DAPM and the heavier Metabolite II is 42 Da. The most probable modification to DAPM to account for this mass increase is to add C_2H_2O (in preference to C_3H_6 or CH_2N_2); addition of C_2H_2O implies that one new unsaturation exists within the modification. The fact that Metabolite II elutes prior to DAPM on the reversed-phase column indicates that this heavier DAPM metabolite is more polar than the DAPM parent, and quells any speculation that a saturated $-C_3H_7$ functional group could have somehow replaced a proton on DAPM.

LC-ES-MS/MS employing collision induced dissociation (CID) was performed on DAPM and Metabolite II. Figure 2.6 shows the product ion spectrum (with interpretation) of the residual DAPM starting material. Figure 2.7 shows the product ion spectrum of protonated Metabolite II (m/z 241 precursor ion) revealing a product ion at m/z 106, representative of an intact 4-methylene aniline portion within the metabolite, and a second small peak at m/z 148. The assignment of m/z 106 was supported by the appearance of an identical peak in the CID spectrum of the DAPM standard (Figure 2.6) and in other synthesized DAPM metabolites (Nitroso, Azo, Azoxy, data not shown here). Metabolite II is assigned as the acetyl derivative

of DAPM shown in Figures 2.4b and 2.7. Additional evidence for this structure is that the peak areas of the later-eluting DAPM and the early-eluting Metabolite II are nearly the same in LC/UV, but the peak area of the latter is only about one fourth of that of DAPM in LC-MS where the mass spectrometer is the detector. A reduction in the ES ionization efficiency would be expected for the new amide linkage vs. the original primary amino group, i.e., amide formation reduces ionization of the metabolite by ES. Clearly the most probable site of acetylation is the amino group, thus forming *N*-acetyl-DAPM (Metabolite II). Comparison between the LC-MS chromatogram of the sample derived from exposure of VSMC to DAPM vs the control shows that a second metabolite appearing in the exposed cell sample (Figure 2.4) is absent in the control (Figure 2.5). This metabolite, that we are naming Metabolite I, elutes at 23.5 min, but because it was present in much lower abundance than Metabolite II, informative product ion spectra could not be obtained. Metabolite I is assigned as a compound containing two acetyl groups linked to DAPM, i.e., *N,N'*-diacetyl DAPM, and it was detected in protonated form at m/z 283. The fact that Metabolite I elutes prior to Metabolite II in the reversed-phase chromatogram indicates that the former is of increased polarity relative to the latter, which is consistent with the occurrence of a second acetylation. Thus, Metabolite I is proposed to have undergone two acetylation reactions, i.e., one at each amino group of DAPM (see Fig. 4a).

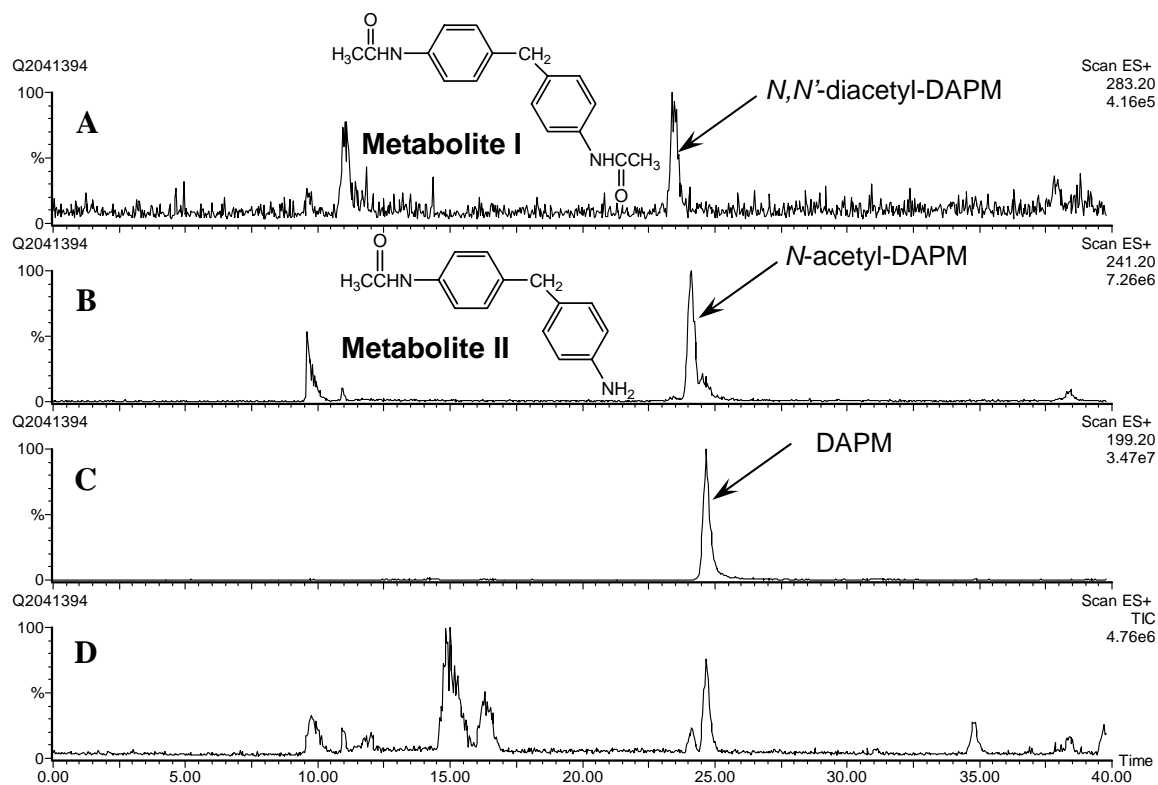


Figure 2.4 LC-ES-MS of vascular smooth muscle cells sample that has been exposed to DAPM, A) selected ion chromatogram of m/z 283; B) selected ion chromatogram of m/z 241; C) selected ion chromatogram of m/z 199; D) total ion chromatogram.

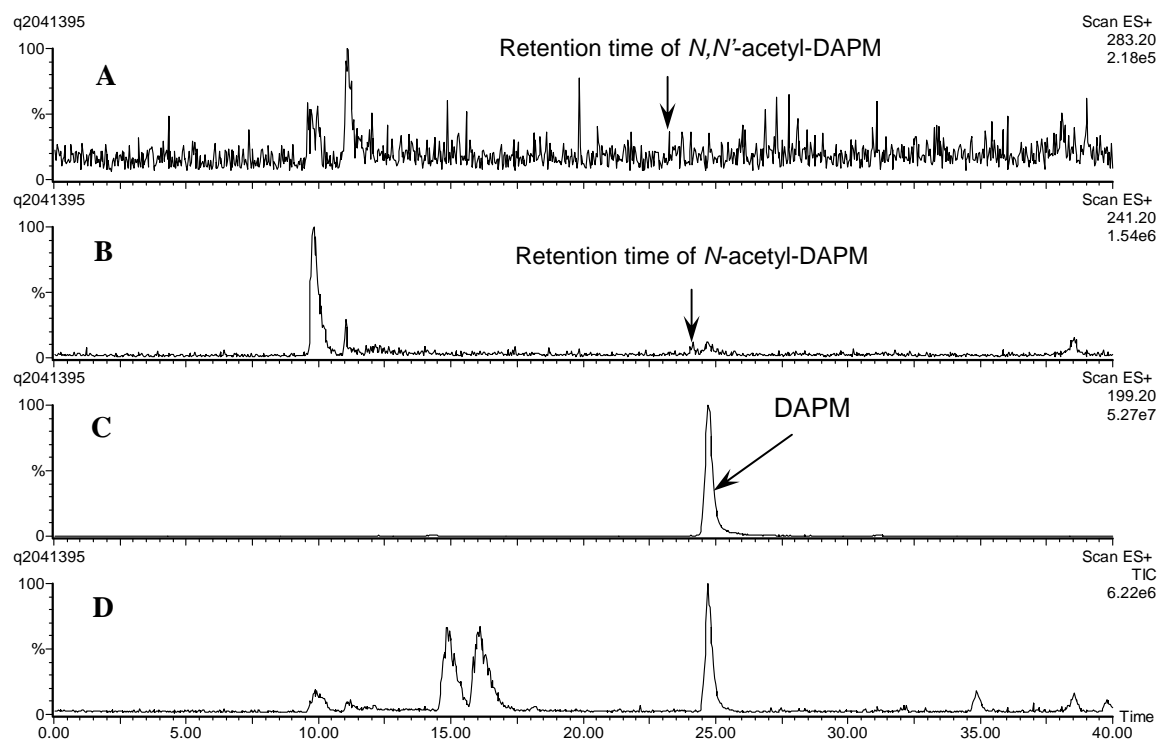


Figure 2.5 LC-ES-MS of the control sample with the same amount of DAPM (but no vascular cell contact). A) selected ion chromatogram of m/z 283; B) selected ion chromatogram of m/z 241; C) selected ion chromatogram of m/z 199; D) total ion chromatogram.

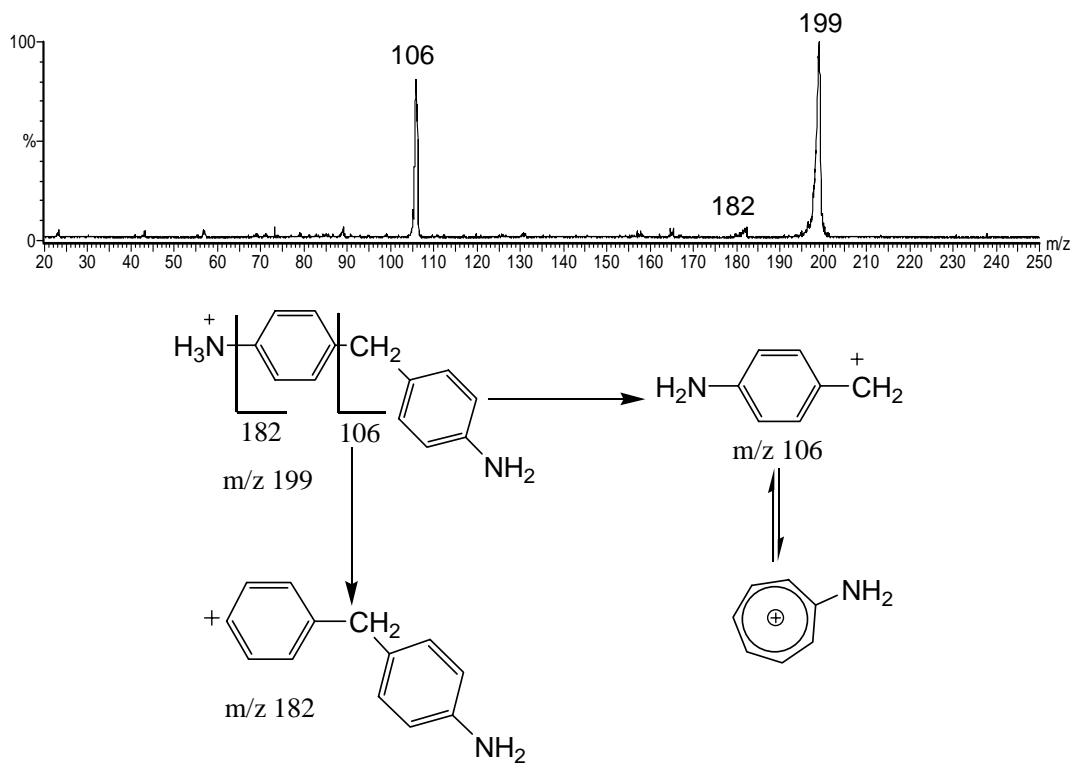


Figure 2.6 LC-ES-MS/MS product ion spectrum of protonated DAPM precursor at m/z 199.

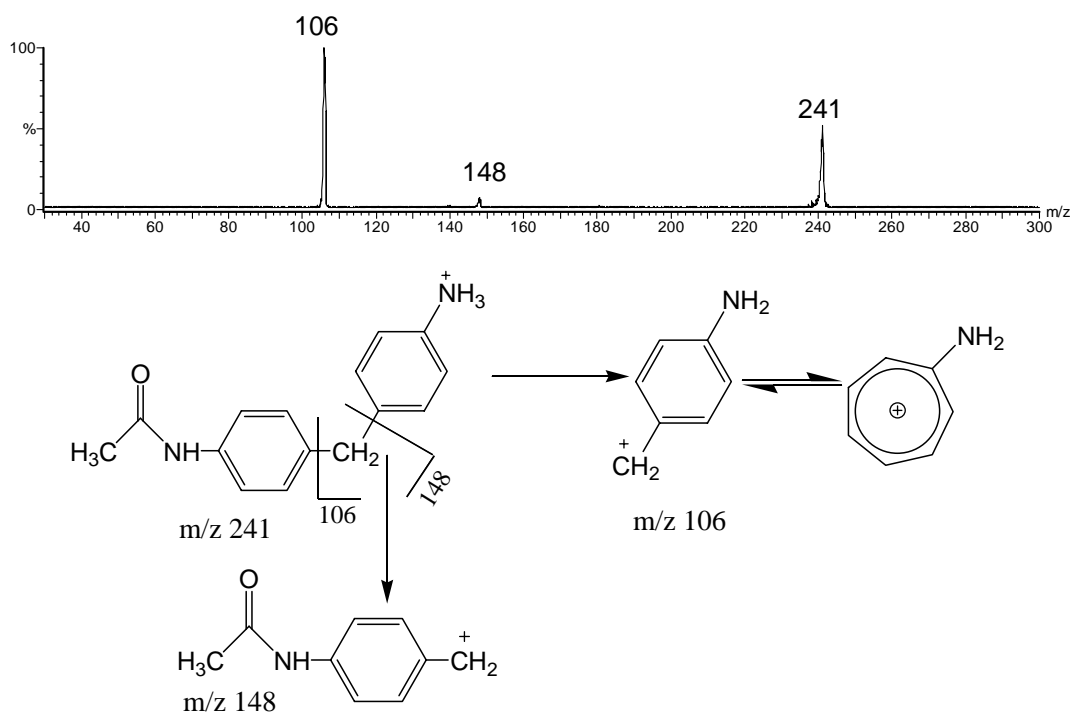


Figure 2.7 LC-ES-MS/MS product ion spectrum of m/z 241 precursor, protonated Metabolite II.

Conclusion

A simple and sensitive LC-MS method utilizing pre-column concentration has been developed to characterize low-level DAPM metabolites from vascular smooth muscle cells (detection limit, S/N = 3, of ~ 500 nM in LC/MS and 2.5 nM in LC/UV). Simultaneous de-salting and concentration utilizing column switching largely removes interferences present in the biological matrix, and thus, significantly improves the ionization efficiency of the target molecules. LC-ES-MS/MS employing CID of one metabolite (m/z 241 precursor) gave a product ion at m/z 106, representative of an intact 4-methylene-aniline portion within the metabolite. This assignment was supported by the appearance of an identical peak in the CID spectrum of the DAPM standard. Based upon a combination of evidence including m/z shifts, UV and ES responses, relative retention times, and interpretation of the product ion mass spectrum, the m/z 241 metabolite was identified as protonated *N*-acetyl-DAPM. A second metabolite, present in much lower abundance, was identified as *N,N'*-diacetyl-DAPM based upon its relative LC retention, its MS spectrum, and its relative responses to UV and ES detection. The two identifications support the notion that DAPM is unstable in the plasma of vascular smooth muscle cell, and for detoxification, is readily transformed into metabolic products. Note that prior experimentation has demonstrated that the employed dose (3.57 μ M DAPM exposure for 24h) is not cytotoxic to the cells, and the cellular response was increased proliferation and not cell death. Thus, the observed metabolism of DAPM is not an artifact due to the presence of dead and dying cells.

References of Chapter 2

1. Shintani H, Nakamura A. Analysis of a carcinogen, 4,4'-methylenedianiline, from thermosetting polyurethane during sterilization. *J. Anal. Toxicol.* 1989; **13**: 354.
2. IARC. Chemicals used in plastics and elastomers. *IARC Monogr. Eval. Carcinogen. Risk Chem. Hum.* 1986; **36**: 347.
3. Moore WM. Methylenedianiline. 3ed. In *Kirk-Othmer encyclopedia of chemical technology Methylenedianiline Vol. 2*, Mark HFDFO, Overberger CG, Seaborg GT (eds). John Wiley: New York 1978; 338.
4. Brooks LJ, Neale JM, Pieroni DR. Acute myocardiopathy following tripathway exposure to methylenedianiline. *J. Am. Med. Assoc.* 1979; **242**: 1527.
5. Kopelman H, Scheuer PJ, Williams R. The liver lesion of the Epping Jaundice. *Q. J. Med.* 1966; **35**: 553.
6. Pludro G, Karlowski K, Mankowska M, Woggon H, Udhe WJ. Toxicological and chemical studies of some epoxy resins and hardeners. I. Determination of acute and subacute toxicity of phthalic acid anhydride, 4,4'-diaminophenylmethane and of the epoxy resin: epilox EG-34. *Acta. Pol. Pharmaco.* 1969; **26**: 352.
7. Gohlke R, Schmidt P. 4,4'-Diaminodiphenyl methane, enzyme histochemical and autoradiographic investigations in acute and subacute experiments in rats with and without the additional stress of heat. *Int. Arch. Fur. Arbeitsmed.* 1974; **32**: 217.
8. Bastien PG. Occupational hepatitis caused by methylenedianiline. *Med. J. Aust.* 1984; **141**: 533.
9. Cocker J, Boobis AR, Davies DS. Determination of the N-acetyl metabolites of 4,4'-methylene dianiline and 4,4'-methylene-bis(2-chloroaniline) in urine. *Biomed. Environ. Mass Spectrom.* 1988; **17**: 161.
10. Robert A, Ducos P, Francin JM. Determination of urinary 4,4'-methylenedianiline and its acetylated metabolites by solid-phase extraction and HPLC analysis with UV and electrochemical detection. *Int. Arch. Occup. Environ. Health* 1995; **68**(1): 44.
11. Kajbaf M, Sepai O, Lamb JH, Naylor S. Identification of metabolites of 4,4'-diaminodiphenylmethane (methylene dianiline) using liquid chromatographic and mass spectrometric techniques. *J. Chromatogr.* 1992; **583**(1): 63.
12. Kautiainen A, Wachtmeister CA, Ehrenberg L. Characterization of hemoglobin adducts from a 4,4'-methylenedianiline metabolite evidently produced by peroxidative oxidation in vivo. *Chem. Res. Toxicol.* 1998; **11**(6): 614.
13. Dugas TR, Cruz VS, Liu H, Kanz MF. Evaluation of the gender differences in 4,4'-methylenedianiline toxicity, distribution, and effects of biliary parameters. *J. Toxicol. Environ. Health Part A* 2001; **62**: 467.
14. Dugas TR, Kanz MF, Hebert VY, Hennard KL, Liu H, Cruz VS, Conklin D, Boor PJ. Vascular medial hyperplasia following chronic, intermittent exposure to 4,4'- methylenedianiline. *Cardiovascular. Toxicol.* 2004; **4**: 85.
15. Zhao W, Parrish AR, Ramos KS. Constitutive and inducible expression of cytochrome P450IA1 and P450IB1 in human vascular endothelial and smooth muscle cells. *In Vitro Cell Dev. Biol. Anim.* 1998; **34**(9): 671.
16. Peterson JC, Estiva EC, Lyttle DS. High-performance liquid chromatographic determination of 4,4'-methylene dianiline in human urine. *J. Chromatogr.* 1991; **564**(1): 205.
17. Tortoreto M, Catalani P, Bianchi M. Determination of 4,4'-diaminodiphenylmethane in blood by gas-liquid chromatography with electron-capture detection. *J. Chromatogr.* 1983; **262**: 367.
18. Skarping G, Dalene M. Determination of 4,4'-methylenediphenyldianiline (MDA) and identification of isomers in technical-grade MDA in hydrolyzed plasma and urine from workers exposed to methylene diphenyldiisocyanate by gas chromatography-mass spectrometry. *J. Chromatogr. B* 1995; **63**: 209.
19. Cocker J, Boobis AR, Davies DS. Routes of activation of 4,4'-methylenebis-2-chloroaniline and 4,4'-methylenedianiline to bacterial mutagens. *Food Chem. Toxicol.* 1986; **24**(6-7): 755.
20. Brunmark P, Persson P, Skarping G. Determination of 4,4'-methylenedianiline in hydrolyzed human urine by micro liquid chromatography with ultraviolet detection. *J. Chromatogr.* 1992; **579**(2): 350.
21. Kajbaf M, Sepai O, Lamb JH. Identification of metabolites of 4,4'-diaminodiphenylmethane (methylene dianiline) using liquid chromatographic and mass spectrometric techniques. *J. Chromatogr. B* 1992; **583**(1): 63.
22. Van Soest REJ, Chervet JP, Ursem M, Suijlen JM. Analysis of fluorescence water tracers using on-line preconcentration in micro HPLC. *LC/GC International* 1996; **9**: 586.
23. Schaefer H, Chervet JP, Bunse C, Joppich C, Meyer HE, Marcus K. A peptide pre-concentration approach for nano-high-performance liquid chromatography to diminish memory effect. *Proteomics* 2004; **4**: 2541.
24. Choi SO, Um SY, Jung SH, Jung SJ, Kim JI, Lee HJ, Chung SY. Column-switching high-performance liquid chromatographic method for the determination of zaltoprofen in rat plasma. *J. Chromatogr. B* 2006; **830**(2): 301.

Chapter 3

Liquid Chromatography-Electrospray Tandem Mass Spectrometry

Investigations of Fragmentation Pathways of Biliary 4,4'-Methylenedianiline

Conjugates Produced in Rats

Abstract

4,4'-methylenedianiline (DAPM) is the main building block for production of 4,4'-methylenediphenyldiisocyanate that has been widely used in the manufacturing of polyurethane materials including medical devices. Although it was revealed that damage to biliary epithelial cells of the liver and common bile duct occurred upon acute exposure to DAPM, the exact mechanism of DAPM toxicity is not fully understood. Both phase I and II biotransformations of DAPM, some of which generate reactive intermediates, are characterized in detail by liquid chromatography electrospray tandem mass spectrometry. The two most prominent metabolites found in rat bile (M2 and M7) implicated glutathione, glucuronic acid and glycine conjugations (phase II) following hydroxylation, and N-oxidation (phase I). Their decomposition pathways, as evidenced by MSⁿ experiments, have been elucidated in detail.

Introduction

One class of xenobiotics that has attracted much attention for its potential toxicity is the aromatic amines. Reports on toxic exposure to aromatic amines date back to the early 1900s.¹ The most common threat from those compounds results from accidental occupational and incidental environmental exposure.² It has been postulated³ that reactive intermediates of the starting materials are primarily responsible for the toxicity, and that these activated forms bind with proteins critical to certain cellular functions. DAPM (also known as 4,4'-methylenedianiline or diaminodiphenylmethene), is an aromatic diamine (Figure 3.1a) of considerable industrial and commercial importance. It has been used as a chemical intermediate in several syntheses, including certain isocyanates and polyurethane polymers. It has also been employed as the cross-linking agent for epoxy resins, and as an antioxidant and curative agent in the preparation of azo dyes and rubber products.^{4,5}

DAPM is an environmental contaminant which has potentially harmful effects on human and animal health. Early documentation of DAPM hepatotoxicity was established in a study of residents of Epping (England) who had consumed DAPM-contaminated bread.⁶ Although it was revealed that biliary epithelial cells of the liver and common bile duct could be injured upon acute exposure to DAPM,^{7,8} the exact mechanism of DAPM toxicity is not fully elucidated. Other studies have shown that DAPM is an animal carcinogen, and histopathological abnormalities have been observed in the liver, kidney and lung of mice,⁹ although metabolic pathways for bioactivation of DAPM have not yet been fully described.

With the introduction of various analytical techniques such as GC, HPLC and LC/MS, investigations of the biotransformations of DAPM have grown. Acetylated metabolites were reported to be found in urine, blood and vascular smooth muscle cells.^{10, 11} However, their presence cannot explain the toxicity of DAPM. Other reactive and toxic metabolites are expected in bile, the likely route of exposure of bile duct cells to the proximate toxicant. Hemoglobin adduction with DAPM after conversion of the latter to an imine form was reported by Kautiainen and colleagues.¹² This biotransformation of DAPM into a reactive imine was speculated to be catalyzed by extrahepatic peroxidase enzyme. We recently reported the characterization of biliary metabolites of DAPM using various spectroscopic techniques¹³. DAPM was found to be converted by

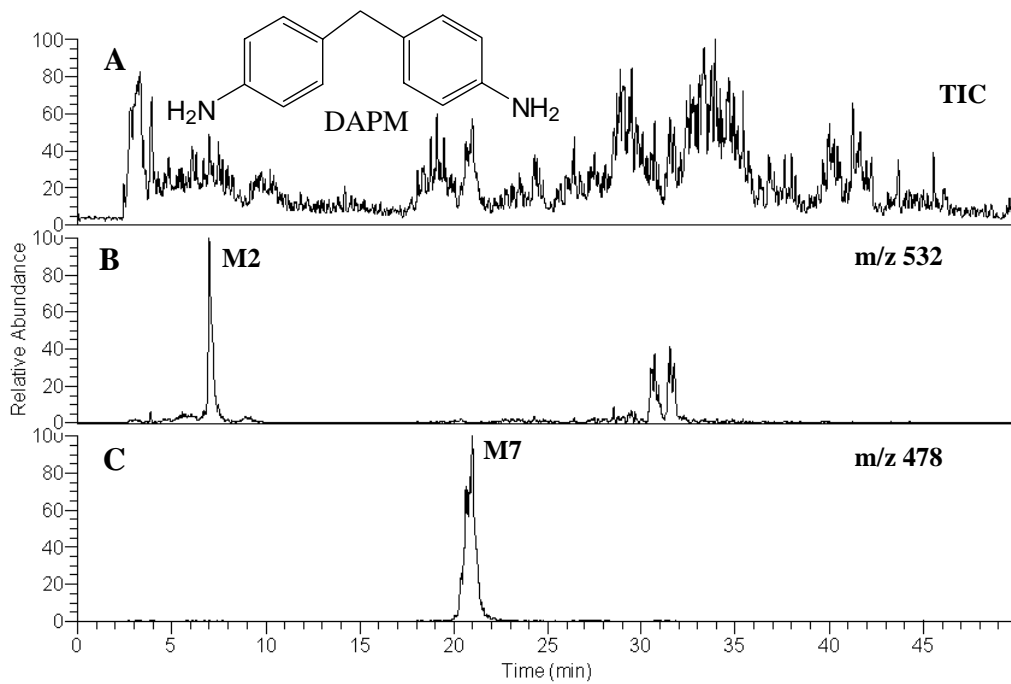


Figure 3.1 (a) LC/MS total ion chromatogram (TIC) of biliary metabolites in a rat dosed with methylenedianiline (DAPM); LC/MS reconstructed ion chromatogram of: (b) M2 at m/z 532; and (c) M7 at m/z 478

phase I and II biotransformation generating N-oxidation, hydroxylation, acetylation, glucuronic acid and glutathione conjugation products. The interesting biotransformations of these reactive and novel metabolites prompted us to decipher their fragmentation pathways observed in tandem mass spectrometry experiments under collision-induced dissociation (CID). Our assignments, and mechanistic interpretations of product ion spectra of these DAPM metabolites should prove useful in future characterizations of other aromatic amine metabolites.

Experimental Details

Animals

Bile duct-cannulated Sprague-Dawley rats were dosed with vehicle (ethanol) or 25/50 mg/kg DAPM; bile was collected for 6 hours on ice and then stored immediately at -80 °C. To remove the protein, aliquots of bile (20-50 µL) were thawed and filtered using Microcon 10,000 MW centrifugal filters (Fisher Scientific, Houston, TX). Before the samples were injected into LC/MS, they were kept on ice.

Liquid Chromatography/Mass Spectrometry

The samples were separated on a reversed-phase HPLC column (Waters XTerra-MS C18, 1 × 150 mm, 3 µm) by a gradient solvent system consisting of solvents A (10 mM ammonium acetate pH 3.5) and B (Acetonitrile). The percentage of mobile phase B was maintained at 15% for the first 2 min with the flow rate set at 50 µL/min, and then ramped linearly to 35% over the next 33 min. The proportion of B was increased to 90% over the next 15 min. Aliquots of filtered bile (20 µL) were injected onto the column and directly delivered into the electrospray LCQ Deca Xp Plus mass spectrometer (Thermo-Finnigan, San Jose, CA) that was operated in the positive ion mode. The metabolites were first detected in a LC-MS survey scan, and the most abundant ion found during each survey scan was then selected to be fragmented using the data-dependent acquisition mode. The six most abundant MS² fragments were automatically selected to acquire ensuing MS³ spectra. To cut down on redundant data acquisition, dynamic exclusion

was enabled at the following settings: repeat counts = 2, repeat duration = 0.3 min, exclusion duration = 0.4 min, and exclusion mass width = 3 Da. The temperature of the ion transfer capillary was maintained at 275 °C and the electrospray needle was operated at 3.2 kV. Tandem mass spectra were obtained with a mass window of 3 Da, relative collision energy set at 38%, and an activation time of 5-30 msec.

Results and Discussion

As described previously,¹³ biliary metabolites of DAPM have been observed using LC-radioisotope detection. Either off-line (fraction collection) or on-line LC/MS was carried out with mass spectrometric characterization of the metabolites. M1-M9 appeared at m/z 375, 532, 403, 475, 24, 417, 478, 574 and 517 Da, respectively. Of the nine metabolites, M2 and M7 are the most intriguing and complicated metabolites. Both involve N-oxidation and hydroxylation of the parent DAPM compound, along with glutathione conjugation on M2, or glucuronic acid and glycine adduction on M7. Although structural characterizations were accomplished on both metabolites via various spectroscopic techniques,¹³ their detailed fragmentation mechanisms based upon MSⁿ data are presented here for the first time.

Metabolite M2

During LC-MS analysis, M2 is observed as a protonated molecule [M+H]⁺ at m/z 532 with a retention time of 7 min (Figure 3.1b). The product ion spectrum of M2 is shown in Figure 3.2a. Major product ions of the protonated M2 precursor correspond to loss of the pyroglutamate moiety (-129) leading to the base peak at m/z 403, or loss of the glycine moiety (-75), thereby generating a fragment ion at m/z 457. Those neutral losses are characteristic of glutathione adducts during CID experiments. Two additional fragments at m/z 308 and 179 correspond to protonated glutathione (thiol form) and protonated cysteinyl-glycine, respectively. The appearance of these four characteristic fragment ions allowed the identification of M2 as a GSH adduct. In addition, fragment ions at m/z 385, 439 and 514 were formed via H₂O loss from m/z 403, 457 and 532, respectively. Glutathione conjugation is proposed to occur at the imine nitrogen atom

based on the absence of an N-H proton and the presence of a full complement of aromatic ring protons (i.e., 8) in the $^1\text{H-NMR}$ spectrum. Assignment of the hydroxylated form of the DAPM methylene bridging carbon resulting from phase I metabolism of the M2 precursor was deduced¹³ from $^1\text{H-NMR}$ and TOCSY spectra, and the predicted chemical shift of the hydroxyl proton calculated using Chemoffice Ultra 2004 software (Cambridgesoft Corporation, Cambridge, UK).

Even though solid evidence of glutathione conjugation was readily derived from LC-MS/MS, little information about the xenobiotic moiety was directly obtainable from MS^2 spectra because cleavages occurred primarily at or on the GSH moiety. To enhance the amount of structurally-informative fragmentation, the data dependent MS^3 data acquisition method was employed on mass spectral peaks appearing in the low m/z range (m/z 200-400) which represent fragments with charge retention on the xenobiotic moiety. These informative fragments appeared at m/z 199, 225, 257, 283 and 300 in the MS/MS spectrum (Figure 3.2a), and they were subjected to further fragmentation. The MH^+ -232 fragment at m/z 300 (Figure 3.2c) was formed via successive eliminations of pyroglutamic acid, glycine residues and CO from protonated M2.¹⁴ A further elimination of NH_3 led to the fragment ion at m/z 283 (Figure 3.2b). The fragment ions at 199, 225 and 257 were produced from the ion m/z 283 ion formed by the cleavage of m/z 300 (Figure 3.2b); proposed fragmentation pathways are shown in the Figure 3.2c. Additional fragments at m/z 132 and 197 were derived from MS^3 decompositions of m/z 225 (Figure 3.3a), and the corresponding cleavage mechanisms are shown in the Figure 3.3c. The formation of m/z 197 is proposed to occur via rearrangement and elimination of CO (28 Da) with the driving force being production of a highly resonance-stabilized ion shown in Figure 3.3c. The MS/MS spectrum of m/z 199 gave a fragment at m/z 106 (Figure 3.3b), representing the 4-nitrosophenyl moiety and thus presenting evidence of N-oxidation at one amino group of DAPM. The above interpretation leaves the other (non-nitroso) nitrogen as the only remaining site on M2 available for GSH adduction.

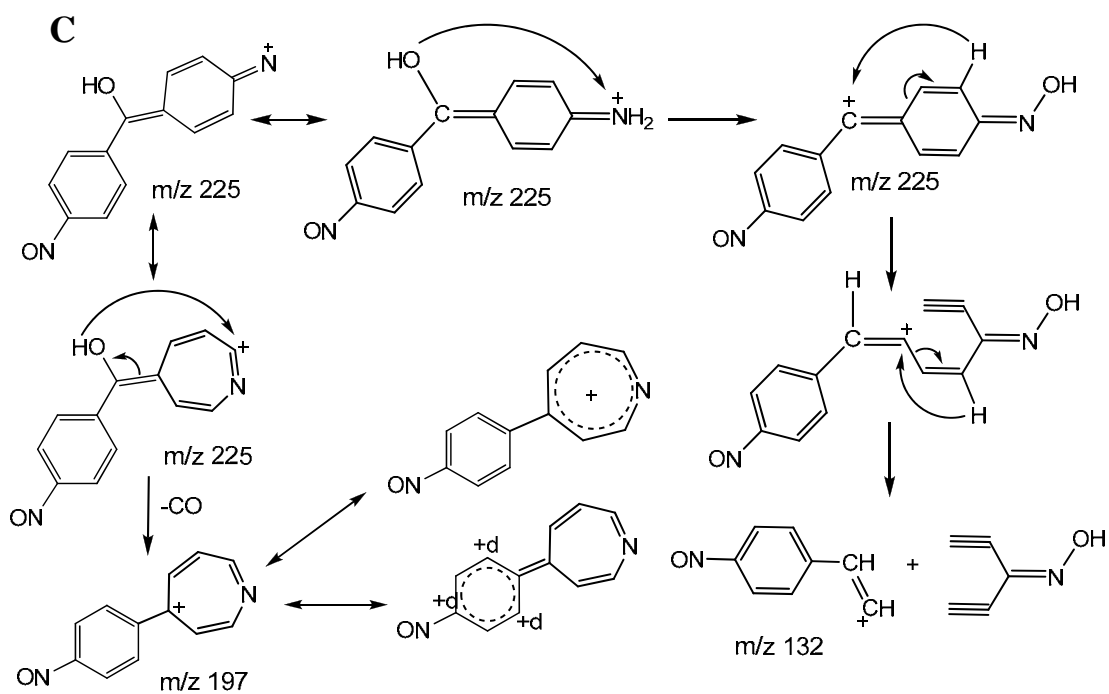
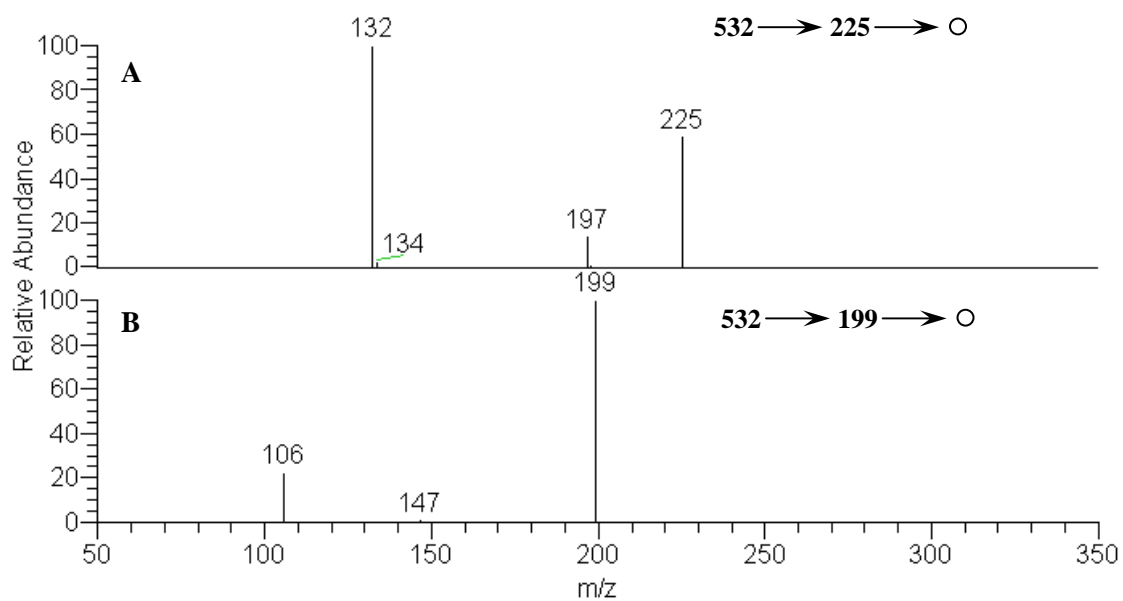


Figure 3.3 MS³ spectra of the precursor ions at: (a) m/z 225; and (b) m/z 199 derived from protonated M2 present in bile of a rat dosed with DAPM; (c) corresponding fragmentation pathways

Metabolite M7

M7, eluting at an LC-MS retention time of 21 min (Figure 3.1c), appeared as the protonated molecule $[M+H]^+$ at m/z 478. In the MS/MS spectrum (Figure 3.4a), the protonated M7 precursor underwent a 176 Da (-anhydroglucuronic acid) loss characteristic of a glucuronide to generate the product ion at m/z 302. H_2O losses to form the fragment ions at m/z 460 ($-H_2O$) and 442 ($-2H_2O$) (Figure 3.4a) were also visible. The MS^3 spectrum of m/z 302 gave a product ion at m/z 285 corresponding to NH_3 loss (Figure 3.5a). The above mentioned characteristic glucuronide loss (-176 Da) could also occur in conjunction with NH_3 loss (-17 Da) from the m/z 478 precursor to give m/z 285 (Figure 3.4a), and the corresponding mechanisms are proposed in Figure 3.4b. The MS^3 spectrum of m/z 285 (Figure 3.5b) yielded: m/z 106, 136, 148, 150, 241 and 267. The fragmentation pathways leading to m/z 136 and 150 are shown in Figure 3.5e.

The monoisotopic mass of M7 appears at an even m/z value, indicating that it contains an odd number of nitrogen atoms based on the “nitrogen rule”. The possibility of amino acid conjugation with one of the free amines of DAPM can account for both the mass increase, and the addition of a third nitrogen. There are two well-established metabolic pathways of amino acid conjugation with xenobiotics containing primary aromatic amine functional groups. One is through reaction of the amino acid carboxylic acid group with a free amine on the xenobiotic to form an amide bond, such is exemplified by glutamic acid conjugation with acetaminophen metabolites.¹⁵ Secondly, xenobiotics containing a hydroxylamine group may conjugate with the carboxylic acid group of amino acids such as proline or serine.¹⁶ This is accomplished when aminoacyl-tRNA synthetase activates the amino acid and then conjugates it with hydroxylamine to form an N-ester that can be degraded into an electrophilic nitrenium ion.¹⁷ The MS^3 loss of 44 Da from the precursor ion at m/z 285 gave the product ion at m/z 241 (Figure 3.5b), that we have assigned as CO_2 loss. Observation of this prominent CO_2 loss indicates that an N-ester (-N-O-C(O)-) had been formed rather than an amide (-N-C(O)-) bond (Figure 3.6). In our search of the literature, we were unable to find previous examples of this type of glycine conjugation to aromatic hydroxyl amines

(with glycyl- t-RNA synthetase participation). MS⁴ of m/z 241 gave the product ions at m/z 106 and 148 (Figure 3.5c), representing 4-nitrosobenzyl and its precursor (Figure 3.6). The appearance of m/z 106 indicated N-oxidation at the other free amine group of DAPM. The fragment ion at m/z 148 suggested hydroxylation on the methylene bridging carbon of DAPM (Figure 3.6). Under CID, m/z 285 also underwent H₂O loss to form a fragment ion at m/z 267 (Figure 3.5b), corroborating the postulation that hydroxylation had occurred on the methylene carbon. The MS⁴ spectrum of m/z 267 showed a fragment ion at m/z 132 (Figure 3.5d), and the corresponding pathway is shown in Figure 3.6. Because both amine groups of DAPM have been metabolized, the only reasonable site for glucuronic acid conjugation is with the hydroxyl oxygen on the bridging carbon. Thus the structure of M7 can be confidently identified.

Conclusion

The structural assignments of these metabolites from rat bile are mainly based on LC-tandem mass spectrometry data. MSⁿ spectra up to MS⁴ were acquired for the thorough structural elucidation that forms the basis for this paper. Detailed interpretation of MSⁿ spectra is essential to eliminating ambiguity in deducing metabolite structures. A combination of metabolic processes was involved in transforming DAPM into the M2 and M7 metabolites found in rat bile. These biotransformations include glutathione, glycine and glucuronic acid conjugation (phase II) of DAPM that had previously undergone hydroxylation and N-oxidation (phase I). They demonstrate that DAPM is susceptible to (phase I) conversion to electrophilic species that can be trapped by phase II metabolism. The existence of phase I reactive metabolites of DAPM supports the postulation that reactive intermediates are involved in the toxicity of DAPM, possibly implicating covalent protein adducts that were also found in rat bile.¹³ Further studies are in progress to characterize those DAPM modified proteins.

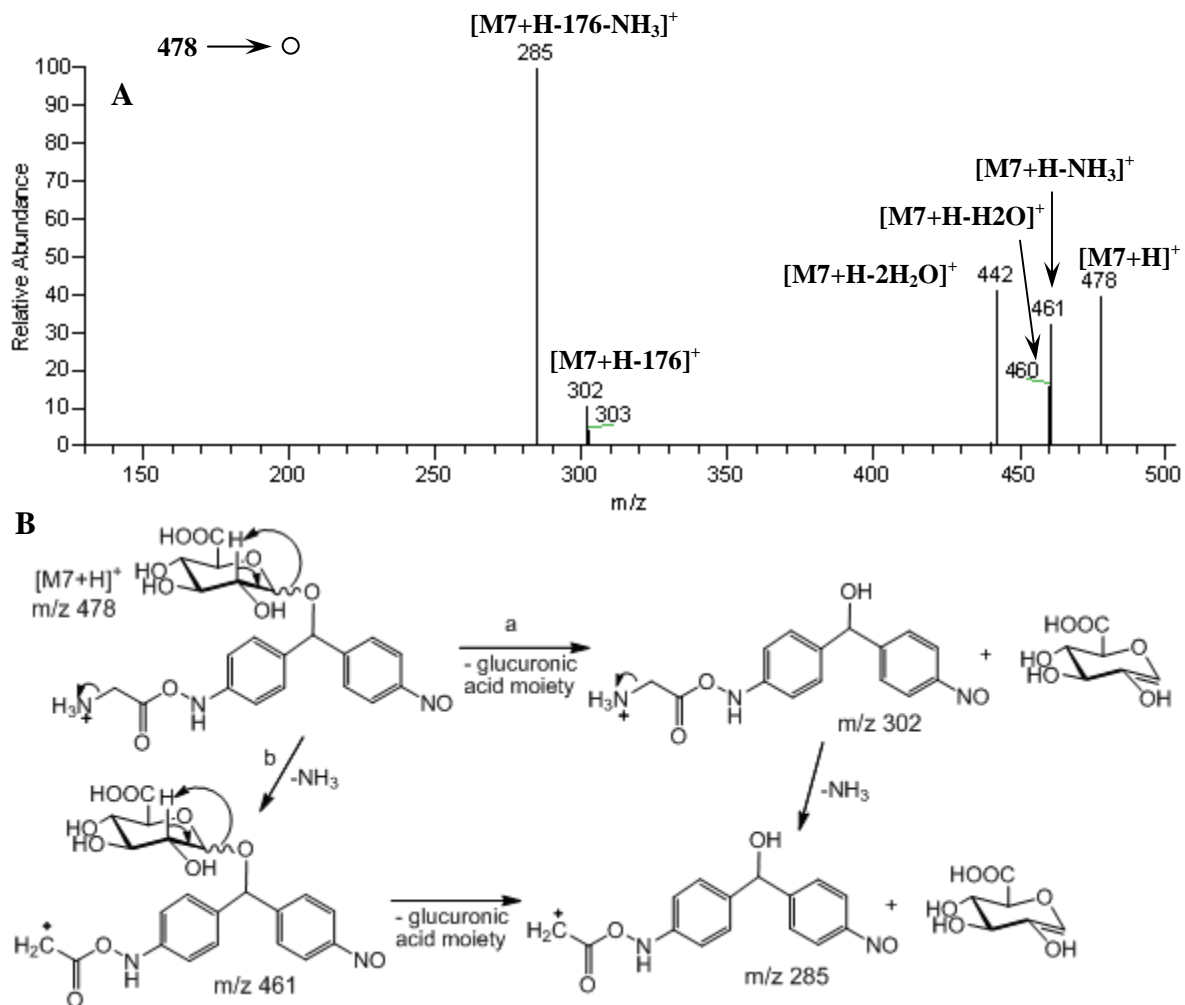


Figure 3.4 MS³ spectra of the precursor ions at: (a) m/z 225; and (b) m/z 199 derived from protonated M2 present in bile of a rat dosed with DAPM; (c) corresponding fragmentation pathways

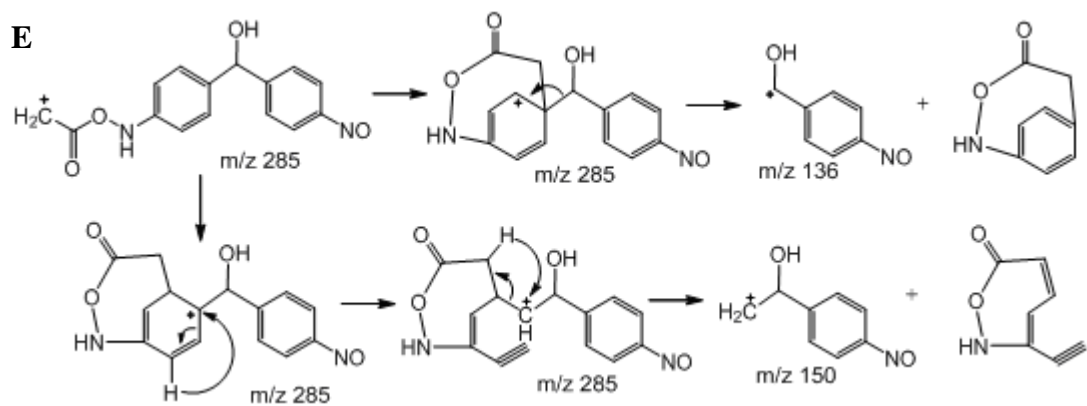
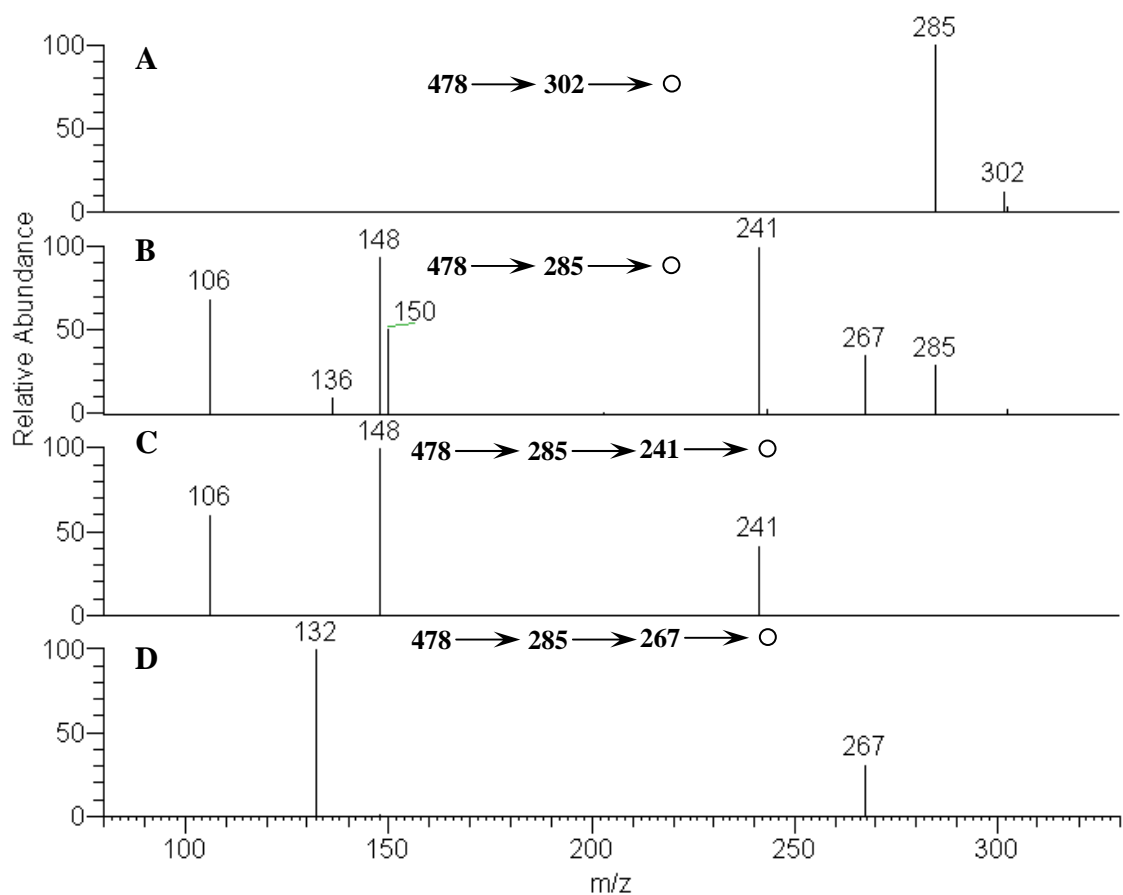


Figure 3.5. MS³ spectra of: (a) m/z 302 and (b) m/z 285; MS⁴ spectra of: (c) m/z 241; and (d) m/z 267; (e) proposed fragmentation pathways of m/z 285 leading to the fragment ions at m/z 136 and 150

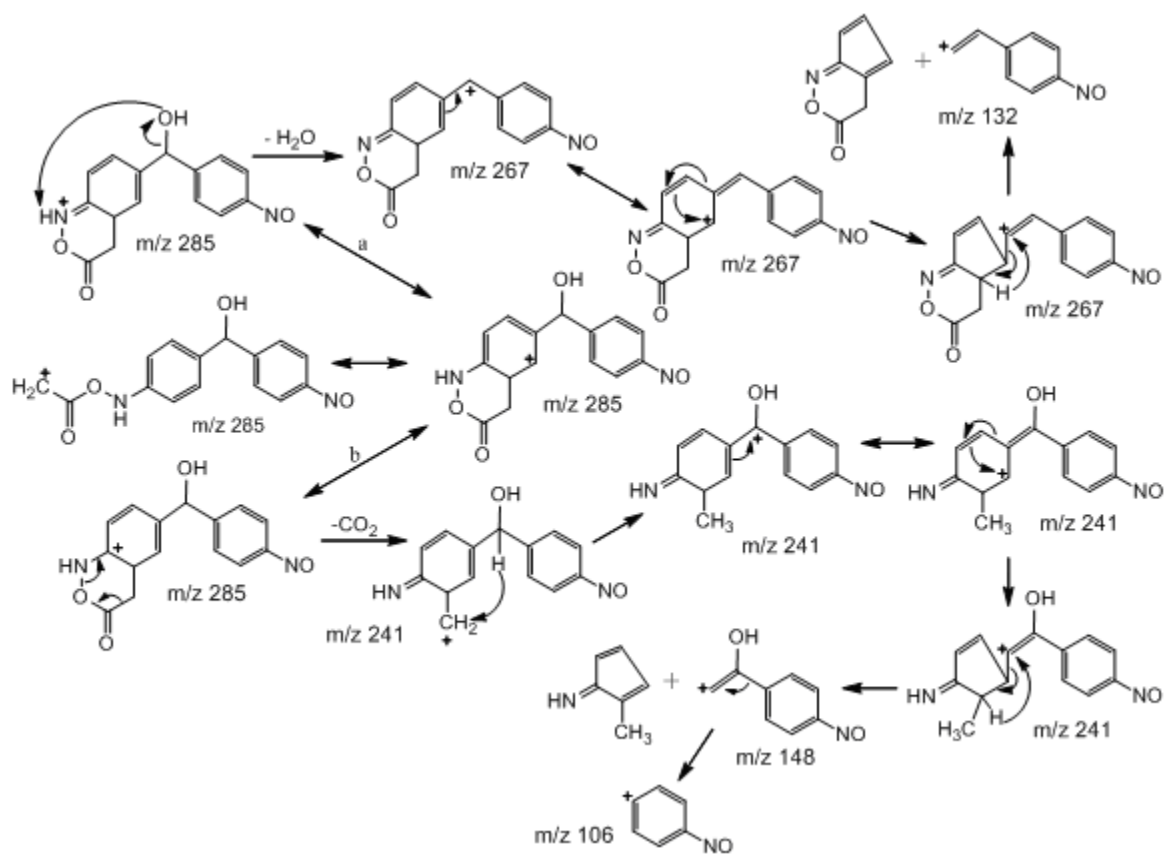


Figure 3.6 Proposed fragmentation pathways leading to the MS³ product ions at m/z 241 and 267, and the MS⁴ product ions at m/z 106, 132 and 148

References of Chapter 3

1. Loeppky, J. A.; Scotto, P.; Charlton, G. C.; Gates, L.; Icenogle, M.; Roach, R. C., Ventilation is greater in women than men, but the increase during acute altitude hypoxia is the same. *Respir Physiol* **2001**, 125, (3), 225-37.
2. Radomski, J. L., The Primary Aromatic Amines: Their Biological Properties and Structure-Activity Relationships. *Annual Review of Pharmacology and Toxicology* **1979**, 19, 129-157.
3. Hanzlik, R. P.; Koen, Y. M.; Theertham, B.; Dong, Y.; Fang, J., The reactive metabolite target protein database (TPDB) – a web-accessible resource. *BMC Bioinformatics* **2007**, 8, 95-100.
4. Kouris, C. S., p,p'-Methylenedianiline. *Dyestuffs* **1963**, 44, 287-299.
5. Braun, B.; Rock, P. B.; Zamudio, S.; Wolfel, G. E.; Mazzeo, R. S.; Muza, S. R.; Fulco, C. S.; Moore, L. G.; Butterfield, G. E., Women at altitude: short-term exposure to hypoxia and/or alpha(1)-adrenergic blockade reduces insulin sensitivity. *J Appl Physiol* **2001**, 91, (2), 623-31.
6. Kopelman, H.; Robertson, M. H.; Sanders, P. G.; Ash, I., The Epping jaundice. *Br Med J* **1966**, 1, 514-516.
7. Kanz, M. F.; Kaphalia, L.; Kaphalia, B. S.; Bomagnoli, E.; G.A., A., Methylene dianiline: acute toxicity and effects on biliary function. *Toxicol Appl Pharmacol.* **1992**, 117, (1), 88-97.
8. Kanz, M. F.; Wang, A.; Campbell, G. A., Infusion of bile from methylene dianiline-treated rats into the common bile duct injures biliary epithelial cells of recipient rats. *Toxicol Lett* **1995**, 78, (2), 165-171.
9. Schmidt, P.; Burck, D.; Weigmann, H.-J., Acute toxicity of some for plastic processing industry important amines. *Z Gesamte Hyg* **1974**, 20, (7), 393-8.
10. Zhu, W. Z.; Xie, Y.; Chen, L.; Yang, H. T.; Zhou, Z. N., Intermittent high altitude hypoxia inhibits opening of mitochondrial permeability transition pores against reperfusion injury. *J Mol Cell Cardiol* **2006**, 40, (1), 96-106.
11. Cocker, J.; Boobis, A. R.; Davies, D. S., Determination of the N-acetyl metabolites of 4,4'-methylene dianiline and 4,4'-methylene-bis(2-chloroaniline) in urine. *Biomed Environ Mass Spectrom* **1988**, 17, (3), 161-167.
12. Kautiainen, A.; Wachtmeister, C. A.; Ehrenberg, L., Characterization of hemoglobin adducts from a 4,4'-methylenedianiline metabolite evidently produced by peroxidative oxidation in vivo. *Chem Res Toxicol* **1998**, 11, (6), 614-21.
13. Chen, K.; Cole, R. B.; Cruz, V. S.; Blakeney, E. W.; Kanz, M. F.; Dugas, T. R., Characterization of Biliary Conjugates of 4,4'-Methylenedianiline in Male versus Female Rats.
14. Baillie, T. A.; Davis, M. R., Mass spectrometry in the analysis of glutathione conjugates. *Biol Mass Spectrom* **1993**, 22, (6), 319-325.
15. Mutlib, A. E.; Shockcor, J.; Espina, R.; Graciani, N.; Du, A.; Gan, L., Disposition of glutathione conjugates in rats by a novel glutamic acid pathway: Characterization of unique peptide conjugates by liquid chromatography/mass spectrometry and liquid chromatography/NMR. *J Pharmacol Exp Ther* **2000**, 294, 735-745.
16. Klaassen, C. D., *Casarett & Doull's Toxicology: The Basic Science of Poisons* 6th ed.; McGraw-Hill Professional: 2001.
17. Kato, R.; Yamazoe, Y., Metabolic activation of N-hydroxylated metabolites of carcinogenic and mutagenic arylamines and arylamides by esterification. *Drug Metab Rev* **1994**, 26, (1-2), 413-429.

Chapter 4

Unusual odd-electron fragments from even-electron protonated prodiginine precursors using positive ion electrospray tandem mass spectrometry

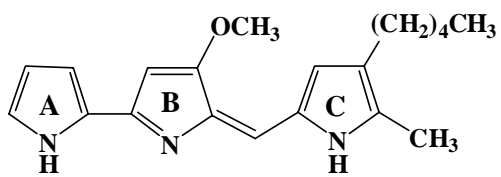
Abstract

Reports of anti-cancer and immunosuppressive properties have spurred recent interest in the bacterially produced prodiginines. We use electrospray tandem mass spectrometry (ES-MS/MS) to investigate prodigiosin, undecylprodiginine and streptorubin B (butyl-*meta*-cycloheptylprodiginine), and explore their fragmentation pathways to explain the unusual methyl radical loss and consecutive fragment ions that dominate low-energy collision induced dissociation (CID) mass spectra. Structures of the fragment ions are proposed and explanations are given for the competition between the formation of even-electron ions and radical ions. Theoretical calculations have been used to optimize the structures and calculate the energies of both reactants and products using the GAUSSIAN 03 program. Results indicate that protonation occurs on the nitrogen atom that initially held no hydrogen, thus allowing formation of a pseudo-seven-membered ring that constitutes the most stable ground state $[M+H]^+$ structure. From this precursor, experimental data show that methyl radical loss has the lowest apparent threshold, but alternatively, even-electron fragment ions can be formed by loss of a methanol molecule. Computational modeling indicates that methyl radical loss is the more endothermic process in this competition, but the lower apparent threshold associated with methyl radical loss points to a lower kinetic barrier. Additionally, this characteristic and unusual loss of methyl radical (in combination with weaker methanol loss) from each prodiginine is useful for performing constant neutral loss scans to quickly and more efficiently identify all prodiginines in a complex biological mixture without any clean-up or purification. The feasibility of this approach has been proven through the identification of a new, low abundance prodigiosin analog arising from *Hahella chejuensis*.

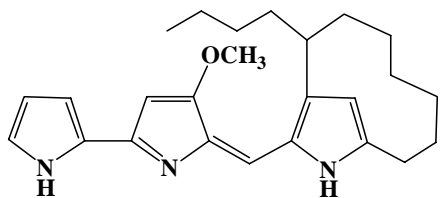
Introduction

Prodiginine analogs belong to a family of naturally occurring red-pigment antibiotics that are secondary metabolites biosynthesized by many strains of Gram-positive and Gram-negative bacteria.¹ These compounds are characterized by a common pyrrolydipyrrolylmethene backbone and a methoxy function on the B-ring (Scheme 4.1). The chemical composition of prodigiosin, a representative member of the prodiginine family, was established half a century ago by chemical synthesis.^{2, 3} Other close analogs, bearing the same skeleton but different alkyl substituents, have been reported, such as undecylprodiginine⁴, streptorubin B⁵, methylcyclodecylprodiginine⁶ and cycloprodigiosin⁷.

By virtue of their brilliant red color, these compounds were used as ink for a short time period prior to the appearance of synthetic dyes⁸. The prodiginines are also antibiotics that have a broad range of activities against bacteria, pathogenic fungi and protozoa, but they have not been widely employed in clinical trials because of their toxicity.^{9, 10} Some studies have shown that their common skeletal features, e.g., the presence of the B-ring C6-methoxy group (Scheme 4.1), are related to the cytotoxicity of prodigiosin; the A-ring also plays an important role in nuclease activity and cytotoxic effects.¹¹ The toxic effects were speculated to arise from intercalation with DNA, leading to oxidative DNA cleavages in the presence of O₂ and Cu(II).^{12, 13} Although the exact cytotoxic mechanism was not completely clarified, some recent findings have shown that prodiginine-type compounds are potent immunosuppressants at lower, non-toxic levels, and slightly higher dosages can efficiently induce apoptosis of cancer cells with little toxic effects on normal cell lines *in vivo* and *in vitro*.^{14, 15}

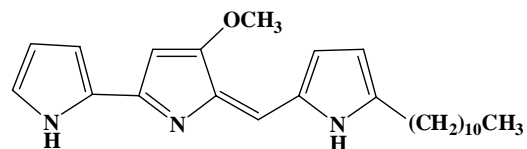


Prodigiosin



Streptorubin B

(Butyl-*meta*-cycloheptylprodiginine)



Undecylprodiginine

Scheme 4.1 Traditional structural representation of three investigated prodiginines: prodigiosin, streptorubin B, and undecylprodiginine.

Recent findings concerning their anti-cancer^{11, 16} and immunosuppressive properties^{14, 17, 18} have led to the expansion of prodiginine studies. Intrigued by their pharmaceutical prospects, the total synthesis of prodiginine-type compounds has been reported.¹⁹ Moreover, synthetic analogue named GX15-070 has been used in phase I/II clinical trials for cancer treatment.²⁰ However, other analogs anticipated to have even more anti-tumor activity, such as streptorubin B (butyl-*meta*-cycloheptylprodiginine, Scheme 1), were difficult to synthesize in the lab. Thus, a biosynthetic pathway might be a good alternative to achieving rapid and cost-effective production of prodiginine-type drugs. To improve the understanding of the biosynthesis of prodiginine antibiotics, studies have been completed to elucidate pathways in *Streptomyces coelicolor* leading to key intermediates including 4-methoxy-2,2'-bipyrrole-5-carboxaldehyde (MBC)²¹ and 2-undecylpyrrole (UP)²².

Prodiginines show a characteristic brilliant red color and they readily absorb visible region light which has been exploited for liquid chromatographic detection. Structural characterization has almost exclusively relied upon NMR spectroscopy that requires relatively large sample quantities, as well as labor-intensive purification steps. New developments in mass spectrometry over the last two decades have earned it the reputation for offering high sensitivity, a wealth of structural information with the use of complementary fragmentation techniques, and the ability to deal with complex mixtures. Up until now, however, mass spectrometry has mainly provided molecular weight confirmation in prodiginine identifications.

Understanding the major fragmentation pathways for prodiginines can help in the structural elucidation of synthetic prodiginine analogs and novel prodiginines generated by biosynthetic processes. Generally, all the prodiginine analogs are readily detected in the positive ion mode owing to available basic nitrogen atoms, which enables one to gain important structural information without further purification, especially if there are low abundance prodiginine analogs in a complex mixture. Our study investigates all the major fragmentation mechanisms using multi-stage tandem mass spectrometry as well as theoretical calculations.

Experimental

Chemicals and Sample Preparation

Undecylprodiginine and streptorubin B were purified from *Streptomyces coelicolor* strains. Undecylprodiginine was isolated from mycelia of *S. coelicolor* W31 which is unable to make streptorubin B.²³ Streptorubin B was isolated from *S. coelicolor* M511 which produces a mixture of undecylprodiginine and streptorubin B. Mycelia were extracted with acetonitrile/methanol (50:50), acidified with 2 N HCl (1%) and vortexed for 30 sec. One volume of chloroform and one volume of 1 N HCl were then added to each volume of prepared extracts; and the chloroform fractions, which contained prodiginine hydrochlorides, were recovered. The fraction originating from *S. coelicolor* W31 was washed with 1 N NaOH to afford undecylprodiginine as a free base which was purified by flash chromatography on basic alumina using 100% ethyl acetate as eluent. Undecylprodiginine appeared as a yellow pigment in ethyl acetate. The chloroform fraction originating from *S. coelicolor* M511 was evaporated to dryness and streptorubin B hydrochloride was purified by semi-preparative HPLC using an Agilent 1100 instrument equipped with a quaternary pump and variable wavelength detector set at 533 nm. Extracts that were resuspended in acetonitrile/methanol (50:50) were injected onto an Agilent C18 column (100 x 21 mm, 5 μ m) using the gradient elution profile: water (adjusted to pH 3 with HCl)/acetonitrile 30:70 to 20:80 in 20 minutes at a flow rate of 5 μ L/min; pure streptorubin B eluted after 8.2 min.

In separate experiments, prodigiosin and its analog were extracted from *Hahella chejuensis* culture with a solvent of methanol containing 0.1 N HCl on a shaker for 2 hrs at 4 °C. The resultant mixture was centrifuged at 4000 \times g for 30 min, and then the supernatant was collected.

Mass spectrometry

ES-CID-MSⁿ experiments were performed on a linear trapping quadrupole (LTQ) instrument (ThermoFinnigan, San Jose, CA) equipped with a positive ion nanospray ionization source and New Objective (Woburn, MA) nanospray silica tips. Samples were diluted in 50% aqueous methanol

containing 0.1% formic acid, and infusion loaded into the LTQ at a flow rate of 1 $\mu\text{L}/\text{min}$. The instrument was operated at a spray voltage of 2 kV and a capillary temperature of 180 $^{\circ}\text{C}$. Tandem mass spectra were acquired at a setting of 30% “normalized collision energy” of the precursor ions at $m/z = 324.2$, 392.3 and 394.3 corresponding to the three protonated prodiginines with an isolation width of 2.5 Da. Each MS and MSⁿ spectrum was acquired and averaged within 1 min.

All neutral loss (NL) scans, and also all mass spectra appearing in Supplementary Data, were performed on an Applied Biosystems/MDS SCIEX (Foster City, CA) 3200 QTRAP hybrid quadrupole/linear ion trap mass spectrometer with direct infusion of each prodiginine sample in aqueous methanol (50/50) spiked with 0.1% formic acid at a flow rate of 4 $\mu\text{L}/\text{min}$. Positive ion mode ES-MS was used for the analysis, with the Turbo VTM source settings for prodiginines optimized as follows: ionspray voltage 5.5 kV, declustering potential 60 V, source temperature 120 $^{\circ}\text{C}$, GS1 40 and curtain gas 10. Ultrahigh grade (99.999%) nitrogen was utilized as nebulizing gas and collision gas. To maximize resolution of ionizable species in the complex sample, MS spectra were acquired using Q3 in the linear ion trapping (LIT) mode. For the activation energy comparison using the 3200 QTRAP mass spectrometer, single collision conditions ensured well-controlled energy deposition on the target ions during the ion activation event with parent beam transmission $\geq 90\%$. The ion abundances of the fragments from competing pathways were monitored as the collision energy was ramped from 5 to 80 eV. Each data point shown in the breakdown curve represents an average of five consecutive runs, and error bars (showing +/- standard deviation) were calculated from the five experiments.

Computational methods

All computational calculations were performed using the Gaussian 03 (revision B.03) program.²⁴ The density functional B3PW91/6-31G* procedure (which combines the Becke three-parameter hybrid²⁵ and the Perdew-Wang correlation functionals²⁶) was used to optimize geometries and these obtained structures were then used to find energy minima at 0 K (B3PW91/6-311+G(2d,2p)) with zero-point

correction. When calculating transition states, opt=QST2 and opt=QST3 features were used with the relevant optimized reactants and products.

Results and Discussion

In positive ion electrospray mass spectra, the ions observed are generally “molecular ions” representing intact forms of the analyte molecules; those created by proton attachment are denoted as $[M+H]^+$. These ions are even-electron (EE^+) species that are generally much more stable than odd-electron ions (OE^+) formed, for example, by electron ionization. Even-electron ions such as protonated molecules formed by ES rarely decompose under low-energy collisions by homolytic cleavage involving loss of a radical to form $OE^+ + \cdot n$ (radical neutral) because the barrier to this type of process is almost always higher than those of competing processes. Rather, heterolytic bond cleavages, often involving rearrangement(s) (especially proton transfer(s)) reign. Thus, radical losses from EE^+ species are considered to be forbidden, which is a statement of the “even-electron rule”.²⁷ Certain exceptions to this “rule” have been reported where odd-electron ions were formed through the fragmentation of even-electron ions formed during electron ionization or chemical ionization or electrospray ionization²⁸⁻³². These exceptions to the “even-electron rule” were proposed to involve radical eliminations leading to odd-electron fragment ions of exceptional stability.³³

The goal of the current study is to obtain a comprehensive view of the common fragmentation pathways of prodiginines, while mainly focusing on the odd-electron fragments observed in ES-tandem mass spectra. Even though three investigated prodiginine analogs share a common skeleton (Scheme 1), differences in the behavior of the protonated molecules following ion activation were seen due to the varying alkyl chain substituents on the C-ring.

Interpretation of the Detailed Fragmentation Pathways of Prodigiosin

Although the collision induced dissociation (CID) mass spectra of some prodiginines have been

reported,³⁴ to our knowledge there has been no detailed description of mass spectra, nor interpretation of their fragmentation mechanisms in the literature. In our CID mass spectra of three prodiginine analogs, similarities in the fragmentation patterns were readily discernable. In each case, a stable OE⁺ fragment ion is initially formed through the loss of a 15 Da neutral, which we deduce can only be a methyl radical. Methyl radical loss was also observed during the fragmentation of ES-generated protonated flavanones.³¹ Because this 15 Da loss is common to MS/MS spectra of all three prodiginines, we conclude that it must correspond to loss of the methyl moiety of the methoxy group on the B-ring (m/z 324 → 309, m/z 394 → 379, m/z 392 → 377 in Figures 4.1, 4.2, and 4.3 respectively). Even though prodigiosin has another methyl substituent in the C-ring, neither of the other two prodiginines have a second methyl group, hence, C-ring methyl loss is eliminated as the source of 15 Da loss. The fully conjugated skeletons provide much resonance stabilization for both the charge and the unpaired electron; when the latter is associated with the C-ring it can initiate cleavages on the substituent alkyl chains. To aid in the interpretation of the fragmentation mechanisms, CID-MS³ experiments were performed on the OE⁺ ions of particular interest (i.e., m/z 309, 379 and 377 in Figures 4.1, 4.2 and 4.3, respectively). From these latter ions, obtained MS³ spectra could readily rationalize consecutive cleavages that appeared in the MS² spectra. For example, it can be seen that alkyl chain cleavages yield the predominant fragment ions at m/z 238 and 252 observed in the CID spectra of all three prodiginine analogs.

As a competing pathway, EE⁺ fragments are derived from the loss of methanol (m/z 324 → 292, m/z 394 → 362, m/z 392 → 360 in Figures 4.1, 4.2 and 4.3, respectively). The ion abundance of this EE⁺ product is substantially lower than those of the OE⁺ fragments (m/z 309, 379 and 377, respectively) observed in the tandem mass spectra, but it is clear that the methoxy group is involved, carrying a proton in tow in each case of methanol loss. Other OE⁺ fragments were also observed in the CID spectra of prodigiosin and its two analogs. Additional information to aid in elucidating the structure was gained using a third stage of tandem mass spectrometry. The OE⁺ products (m/z 324 → 149 (Figure 4.1), m/z 392 → 295 (Figure 4.3)) were further fragmented using on-resonance CID in the linear ion trap, giving major EE⁺

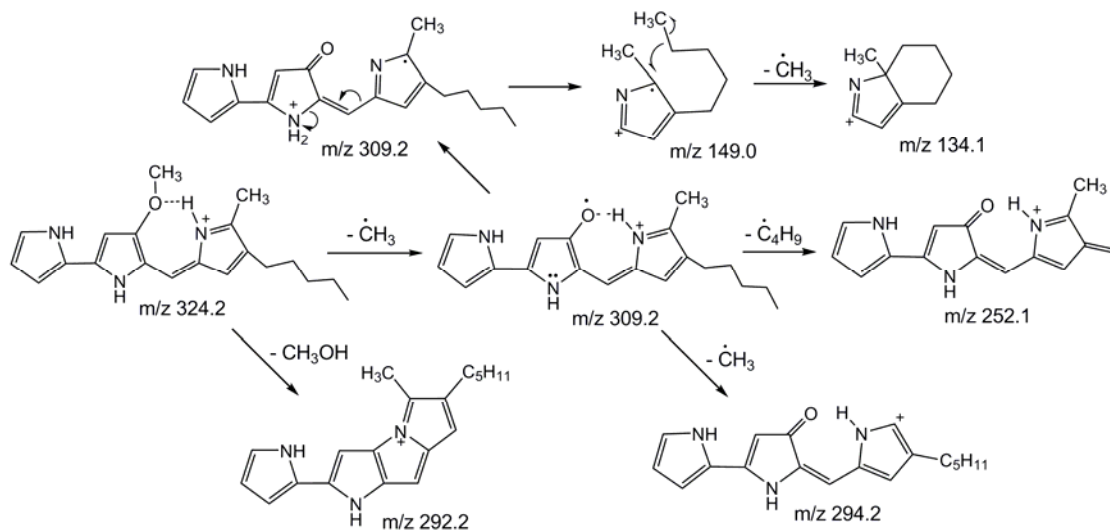
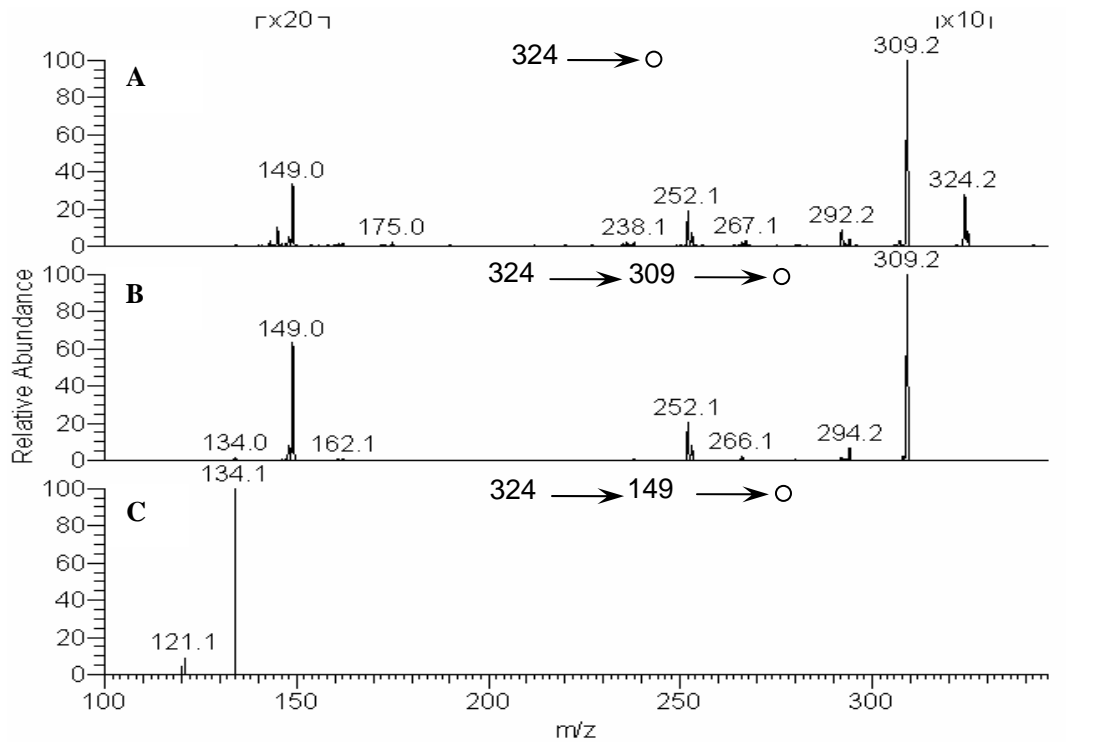


Figure 4.1 ES-CID-MSⁿ spectra for prodigiosin and the proposed major fragmentation pathways: (A) MS/MS spectrum of [M+H]⁺ precursor at m/z 324; (B) MS³ spectrum of m/z 309 (324→309); (C) MS³ spectrum of m/z 149 (324→149)

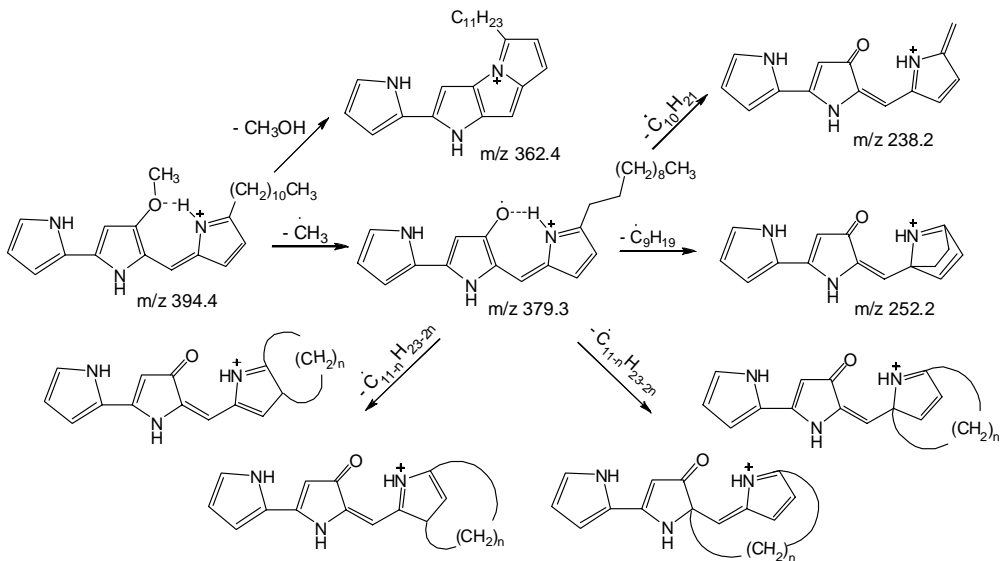
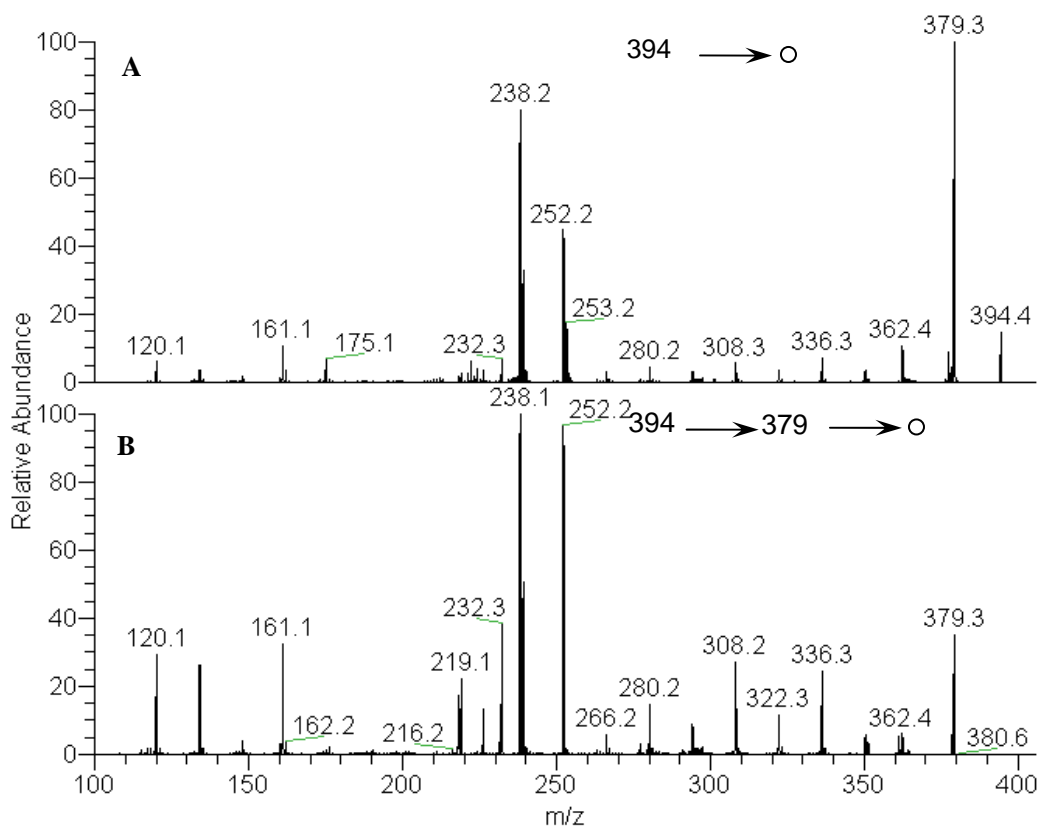


Figure 4.2 ES-CID-MSⁿ spectra for undecylprodiginine and the proposed principal fragmentation pathways: (A) MS/MS spectrum of [M+H]⁺ precursor at m/z 394; (B) MS³ spectrum of m/z 377 (394→379)

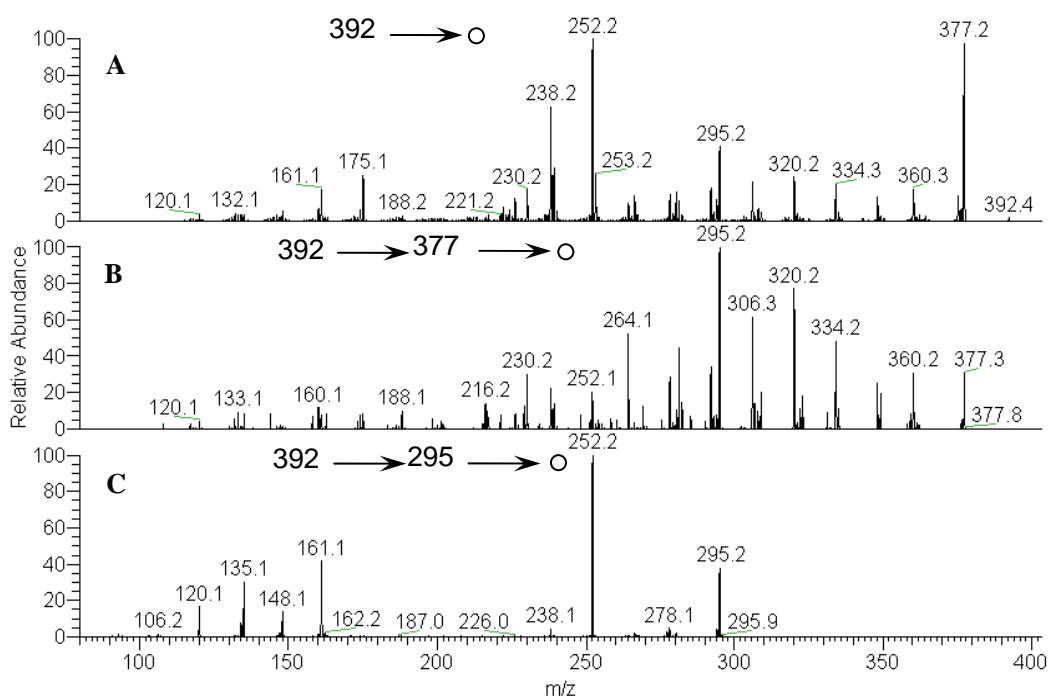


Figure 4.3 ES-CID-MSⁿ spectra for streptorubin B and the proposed major fragmentation pathways: (A) MS/MS spectrum of [M+H]⁺ precursor at m/z 392; (B) MS³ spectrum of m/z 377 (392→377); (C) MS³ spectrum of m/z 295 (392→295)

fragments (m/z 134 and 252, respectively) after C_nH_{2n+1} radical ($n = 1$ and 3) elimination. The detailed mechanisms proposed for the fragmentations of the three investigated compounds are illustrated in Figures 4.1- 3.

Additional evidence supporting these proposed mechanisms was obtained by repeating tandem mass spectrometry measurements, except that this time, a stable isotope labeled [^{13}C -methoxy-undecylprodiginine + H] $^+$ m/z 395 precursor was used (see supplemental data). All product ions appeared at exactly the same m/z values as those derived from the unlabeled [undecylprodiginine + H] $^+$ m/z 394 precursor. This unambiguously implicates the methoxy function in both methyl radical and methanol losses, and establishes that all other product ions arise from consecutive decompositions following one of these initial losses.

Computational Studies of the Fragmentation Pathways of Prodiginine

To investigate the underlying basis for the fragmentation pattern of protonated prodiginines, theoretical calculations were employed to gain additional information concerning the competition between methyl radical and methanol losses. Density functional theory (DFT) calculations were performed to obtain the structures of the precursor ion and its decomposition products, transition states and their associated energies. Due to the large numbers of atoms in the molecules of interest, it is time consuming to computationally minimize the energies of the structures using DFT, especially when a long alkyl chain with many approximately isoenergetic conformers is present. To reduce this difficulty, in all calculations, we employed an ethyl analog of the undecylprodiginine system, i.e., C_2H_5 substitution on the C-ring instead of $C_{11}H_{23}$. Traditionally, the structures of prodiginines have been drawn with the three nitrogen atoms of the tripyrrole skeleton oriented on the same side of the molecule (Scheme 1). However, theoretical calculations find that the A- and C-rings in Figure 4.1 are rotated about 180° such that the molecules are still nearly planar, but nitrogen lone pairs are located as far apart as possible to minimize the electronic repulsion, and hence, the system achieves the highest stability. Figure 4.4(a) I shows the energy optimized geometry obtained at the B3PW91/6-31G* level of theory, 4(a) II shows the chemical

structure, while 4(a) III shows the electron density map. Electron density mapping provides insight into the electron distribution over the molecule and also allows prediction of the preferred site of proton attachment on the molecule. As can be seen in Figure 4.4a (III), the lone pair of electrons of the nitrogen atom in the B-ring exhibits the highest electron density, and thus, is clearly the preferred site of proton attachment. In view of the fully conjugated structure, the positive charge carried by the ionizing proton becomes highly delocalized over the entire ring system. In considering $[M+H]^+$ ions observed in mass spectra, and placing the ionizing proton on the nitrogen that previously holds no proton, the energies of three stable conformers were calculated at the B3PW91/6-311+G(2d,2p) level of theory; the relative stabilization energies are listed below each corresponding structure (Figure 4.4b). Very importantly, a hydrogen bond may form between the C-ring proton attached to the nitrogen atom and the oxygen from the methoxy function to produce a pseudo-seven-membered ring (Scheme 2) which represents the most stable ground state conformation.

With the proton held (chelated) between the C-ring nitrogen and the methoxy oxygen ($O\cdots H$ distance = 1.397 Å), two facile decomposition pathways are possible. The first pathway is the expected loss of a methanol molecule that, afterwards, according to energy minimization studies, undergoes ring closure to form a new fused five-membered ring structure (Scheme 2). The second pathway is homolytic cleavage between the oxygen and carbon atoms of the methoxy group to produce loss of $\cdot CH_3$ which was experimentally observed to be surprisingly facile and favored.

Geometry optimization and vibrational frequency analysis for the reactant and the two products were carried out at the B3PW91/6-31G* level. These structures were then used to perform single point energy calculations at the B3PW91/6-311+G(2d,2p) level with zero-point energy correction. The calculated relative energies of the two endothermic products are 121.6 (EE⁺ product) and 226.8 (OE⁺ product) kJ/mol (Scheme 2) rendering methyl loss more endothermic by 105.2 kJ/mol. Thus, the preference for methyl radical loss over methanol loss cannot be explained by the energy difference between the reactant and the respective products.

Comparison of Apparent Thresholds and Activation Energies for the Two Competing Mechanisms

To obtain more insight into the competing processes of methyl radical loss vs methanol loss from protonated prodigine, a profiling of the fragment ion populations from each pathway as a function of increasing energy under single collision conditions was undertaken in the low-energy regime. Figure 4.5A presents the breakdown curve of the protonated prodigiosin precursor (m/z 324), plus the appearance of the fragments associated with methyl radical loss (m/z 309 and 252) and methanol loss (m/z 292). Most notably, methyl radical loss has the lowest apparent threshold ($E_{\text{lab}} \approx 5$ eV) and its consecutive fragmentation pathway (giving m/z 252, Figure 4.1) appears instantaneously thereafter.

Methanol loss exhibits a higher apparent threshold ($E_{\text{lab}} \approx 12.5$ eV) compared to the former loss. Surprisingly, Figure 4.5A shows that, regardless of collision energy, the abundances of m/z 309 and 252 are always more than 10 times higher than that of m/z 292. MS/MS spectra that were acquired at collision energies of 5 and 12.5 eV (E_{lab}) are shown in Figure 4.5B.

Methyl radical loss thus has a lower apparent threshold, but it is also a more endothermic pathway than methanol loss. This implies that OE^+ production is favored because methyl radical loss presents the lowest available kinetic barrier. Computational studies were used in an attempt to calculate activation energies, and a transition state structure for loss of methanol from protonated prodigine with only one imaginary frequency was successfully obtained. The activation energy for loss of methanol from protonated prodigine was calculated to pass through a transition state that was found to be 373.3 kJ/mol higher in energy than the ground state reactant. Unfortunately, our attempt to obtain a transition state for methyl radical loss from protonated prodigine was unsuccessful, but nonetheless, the experimental data in Figure 4.5 proves that the energy barrier for this latter process is significantly lower than that of methanol loss.

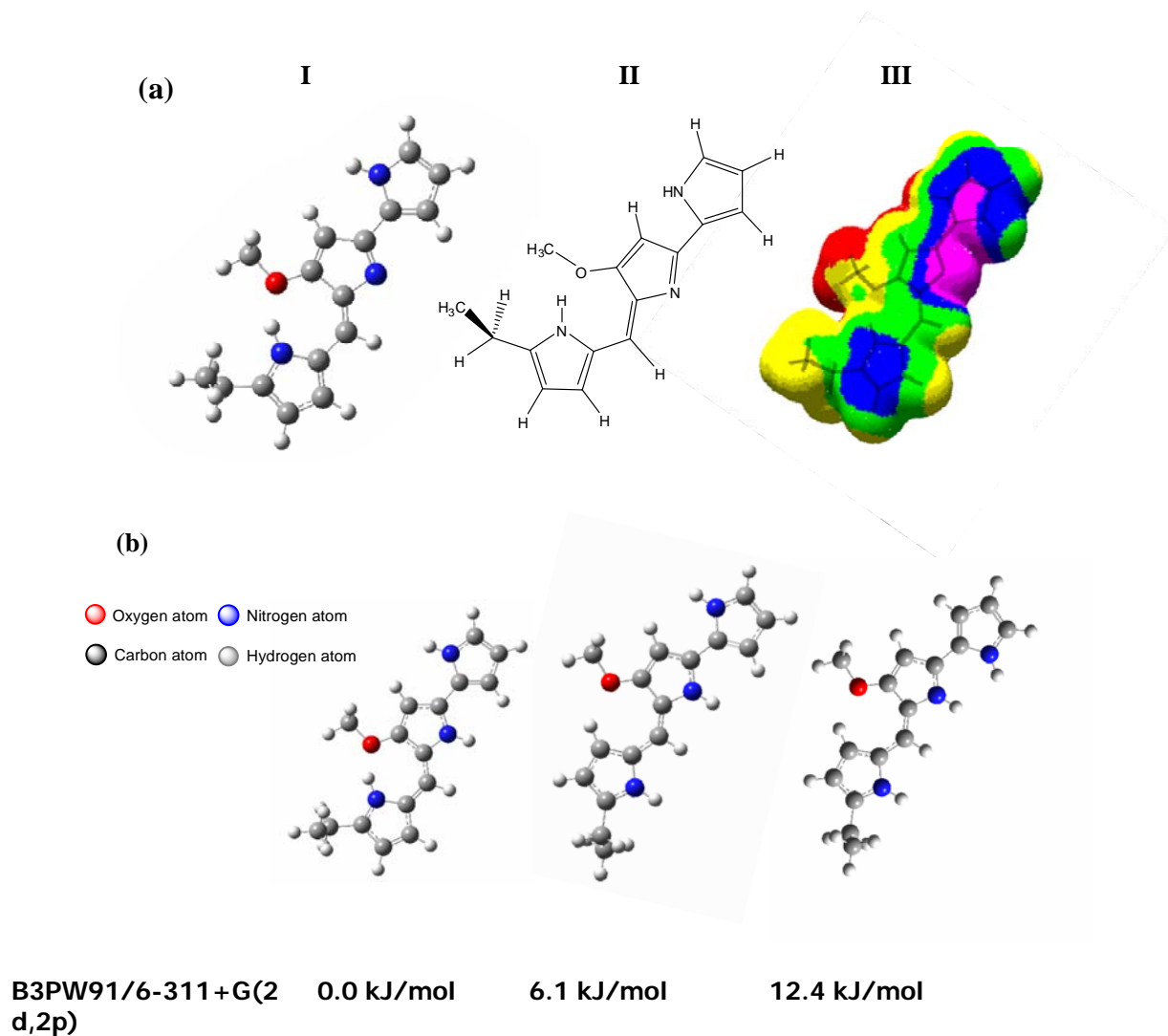
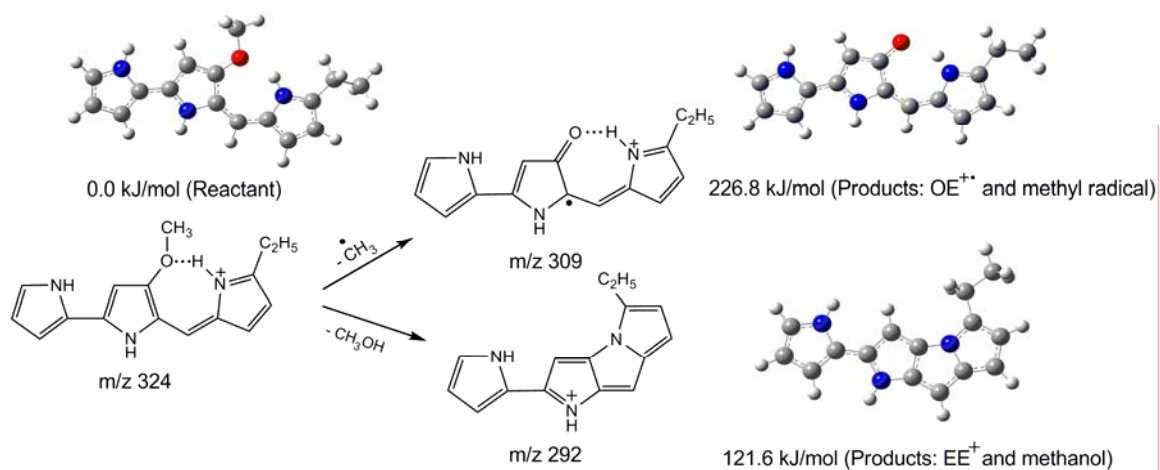


Figure 4.4 (a) Structures of neutral prodiginine model system showing the preferred site for the proton attachment during electrospray ionization process. (I) the energetically optimized geometry at the B3PW91/6-31G* level; (II) chemical structure; (III) electron density map (sequence of electron density listed as followings: purple > blue > green > yellow > red) indicating highest electron density at the central nitrogen bearing no proton. (b) The optimized prodiginine conformations and the relative energies calculated by density function theory (DFT).



Scheme 4.2 Two competing fragmentation pathways of the protonated prodiginine model system leading either to OE^+ after homolytic cleavage to lose a methyl radical, or to EE^+ after heterolytic bond dissociation to lose a methanol molecule.

New Strategy for Prodiginine Identification

Because of the distinct and unusual nature of the fragments resulting from the competing losses of either methyl radical or methanol, we decided to make an attempt to analytically exploit this uniqueness, and use the combination of the two losses as a characteristic marker for prodiginine-type compounds. The instrument design of the QTRAP mass spectrometer enables neutral loss (or gain) scans of all ions generated in the ion source, thus enabling a quick screening of all the analytes present in a crude mixture that undergo a specific type of decomposition. Neutral loss scans of 15 Da (representing a methyl radical) and 32 Da (representing a methanol molecule) were performed using the crude sample extract from *H. chejuensis* in which prodigiosin was previously identified using preparative LC separation and NMR spectroscopy³⁴. The 15 Da neutral loss scan detected not only prodigiosin, but also a new, low abundance prodigiosin analog from the crude mixture (no purification step). A subsequent 32 Da neutral loss scan confirmed the presence of this prodigiosin analog. These results are summarized schematically in Figure 4.6. The ES mass spectrum (Figure 4.6A) reveals protonated prodigiosin as the base peak at m/z 324. Figures 4.6B and 4.6C show the neutral loss mass spectra corresponding to methyl radical and methanol losses, respectively, in which both prodigiosin (m/z 324) and its analog (m/z 352) appeared.

The characterization of the analog at m/z 352 is based on its tandem mass spectra (Figures 4.6D and 4.6E). Like the other prodiginines, it shows fragments resulting from various alkyl chain cleavages. The pathways leading to the observed fragments are proposed at the bottom of Figure 4.6. In the fragmentation mechanism of prodigiosin (Figure 4.1), we proposed that the product ion at m/z 252 was generated from cleavage of the alkyl chain on the C-ring. The proposed pathway to form the same fragment at m/z 252 (in Figures 4.6D and 4.6E) indicates that the analog shares the same backbone as prodigiosin (including the methyl group on the C-ring) but differs in the nature of the second alkyl chain. The presence of a (second) methyl loss (in Figure 4.6E) leading to m/z 322 further supports the notion that, similar to prodigiosin, a second methyl group exists on the C-ring. Thus, the evidence suggests that the mass difference of 28 Da between the two compounds reflects the extension of the longer alkyl chain on the C-ring of prodigiosin by two $-CH_2-$ units. Additional evidence is provided by the fragment ion at

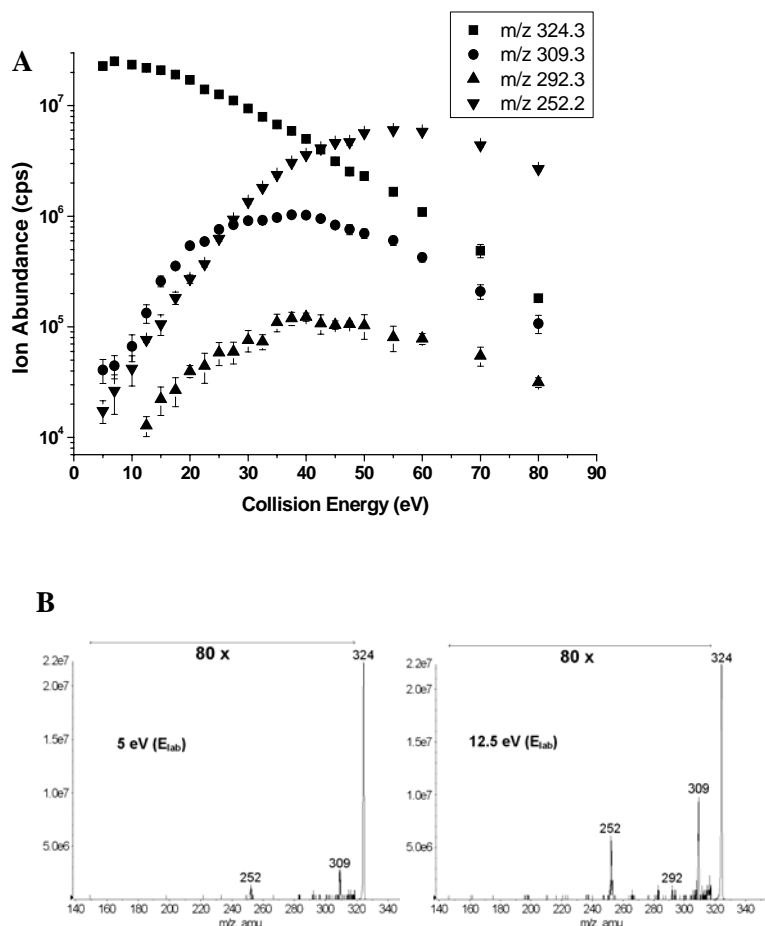


Figure 4.5 (A) Breakdown curves showing ion abundance vs. collision energy for MS/MS of prodigiosin. The plots show the evolution of precursor and fragment ions representing two competing pathways (m/z 324 = precursor; m/z 309 and 252 represent the formation of OE^+ by methyl radical loss and methyl radical loss plus consecutive butyl radical loss, respectively; m/z 292 represents the formation of EE^+ after the loss of methanol) (B) The MS/MS spectra of the m/z 324 prodigiosin precursor with collision energies of 5, 10 and 12.5 eV performed under single collision conditions

m/z 177 derived from the precursor at m/z 337 (Figure 4.6E) that was generated from the same pathway as the fragment at m/z 149 in the tandem mass spectrum of prodigiosin (Figure 4.1). This mass difference of 28 Da between these two fragments confirms the extension of the alkyl chain substitution on the C-ring. However, one cannot determine by mass spectrometry alone whether the alkyl chain is branched or not. Thus, we identified the analog as containing a C₇H₁₅ saturated alkyl chain on the C-ring instead of C₅H₁₁ in prodigiosin.³⁴ Because prodigiosin and undecylprodiginine both contain n-alkyl chains, we assign the new analog as also being unbranched.

The studies described herein have thus proven that our approach of using a combination of constant neutral loss scans (15 Da and 32 Da) is selective for the detection of unknown and low abundance prodiginine compounds; the strategy is built upon the ease of loss of methyl radicals from their common backbone structure. Without labor-intensive purification steps, the workload for identification and characterization of prodiginines can thus dramatically decrease using our approach. Owing to the excellent sensitivity of mass spectrometry, the sample quantity requirements could also decrease from milligrams (for NMR) to less than micrograms (for mass spectrometry) of a crude mixture.

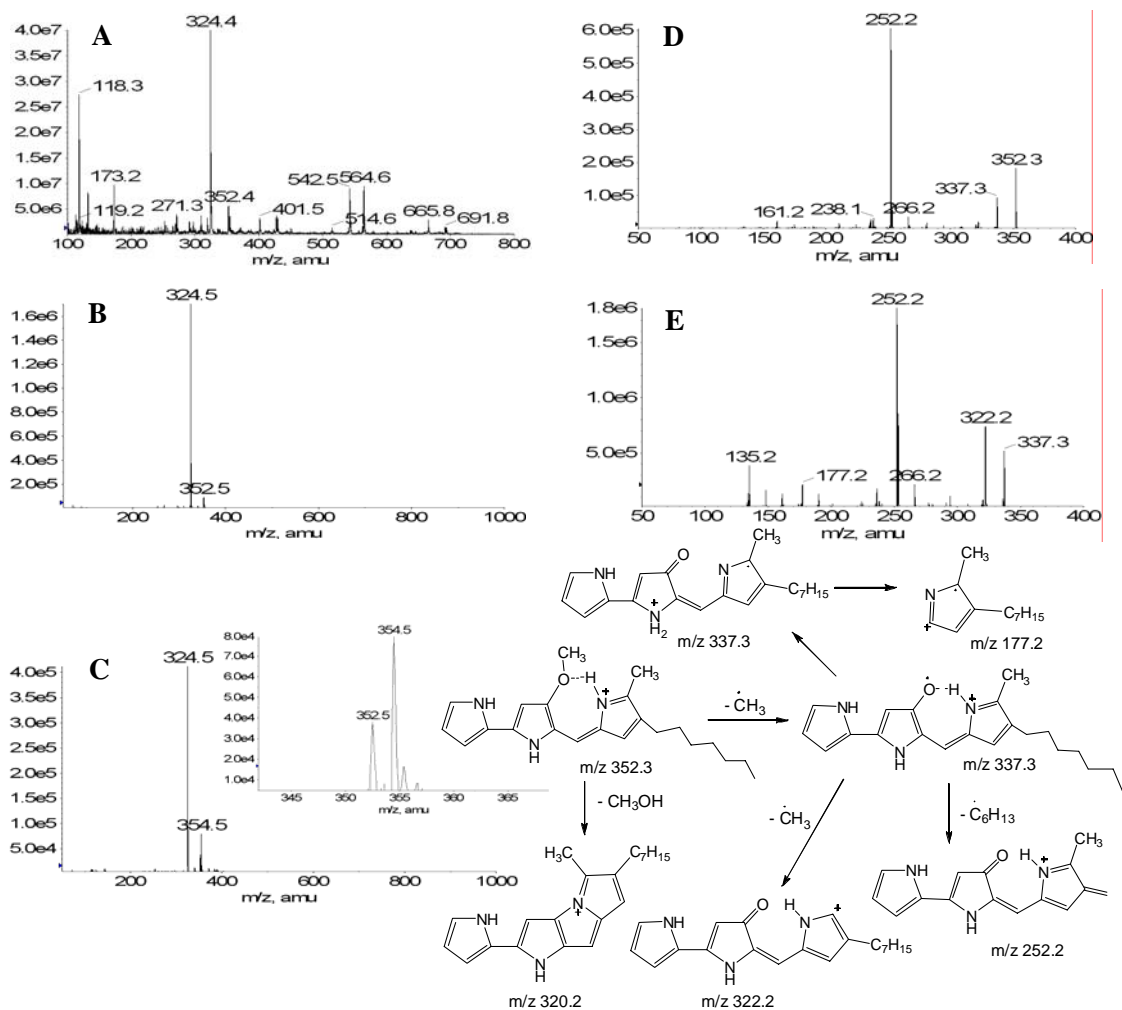


Figure 4.6 (A) Positive ion ES-MS spectrum of the extract from *H. chejuensis* showing $[M+H]^+$ of m/z 324 from prodigiosin, and m/z 352 from the analog; (B) positive ion neutral loss (15 Da) spectrum, showing both prodigiosin and its analog at m/z 324 and 352, respectively; (C) positive ion neutral loss spectrum of 32 Da mass loss, showing both prodigiosin and its analog at m/z 324 and 352; (D) Positive ion ES-MS/MS spectrum of protonated prodigiosin analog at m/z 352; and (E) MS^3 spectrum of m/z 337; the proposed fragmentation pathways of protonated prodigiosin analog at m/z 352

Conclusion

The fragmentation behavior in positive mode electrospray mass spectrometry of three representative members of prodiginines which share the same pyrrolydipyrrolylmethene skeleton has been investigated. Two competing fragmentation pathways were the loss of either methyl radical or methanol and, in violation of the even electron rule, the CID spectra were dominated by the former pathway to yield OE^+ products which may undergo consecutive fragmentations. Upon structural optimization of reactant MH^+ precursors using a Gaussian 03 computational program, results indicate that the nitrogen atom at the C-ring and the B-ring methoxy function could effectively chelate a proton to form a relatively stable H-bonded pseudo-seven-membered ring. From this precursor, methyl radical loss is the most facile decomposition pathway as evidenced by its dominance in low-energy tandem mass spectra. In a competitive pathway, the loss of a methanol molecule involving the same methoxy site on the precursor to produce an EE^+ fragment was heavily disfavored. The apparent threshold of the former pathway has been shown to be much lower than the latter by profiling the ion population of the major fragments of protonated prodigiosin against collision energy under single collision conditions. Thus, the fragmentation of prodiginines was kinetically dominated by methyl loss over methanol loss as a first step. Moreover, the characteristic and unusual loss of methyl radical from each prodiginine, in favorable competition with methanol loss, is useful for rapid identification and structural elucidation of novel prodiginines by performing constant neutral loss scans ($\cdot CH_3$, 15 Da and CH_3OH , 32 Da) to identify all prodiginines present in a mixture.

Using analytical methodology built on this strategy, we report a new and low abundance prodigiosin analog from *H. chejuensis*. Because methyl radical loss rarely occurs in the fragmentation of most ES-generated compounds (EE^+ species), the selectivity of the method will permit high sensitivity identifications of prodiginines from crude extracts of different bacterial species.

References of Chapter 4

1. Williams, R. P., Biosynthesis of Prodigiosin, a Secondary Metabolite of *Serratia marcescens*. *Appl Microbiol.* **1973**, 25, (3), 7102-7109.
2. Wasserman, H. H.; McKeon, J. E.; Smith, L., Prodigiosin. Structure and partial synthesis. *J Am Chem Soc* **1960**, 82, 506-507.
3. Rapoport, H.; Holden, K. G., The synthesis of prodigiosin. *J Am Chem Soc* **1962**, 82, 5510-5511.
4. Gerber, N. N., Prodigiosin-like pigments. *CRC Crit. Rev. Microbiol.* **1975**, 3, 469-485.
5. Wasserman, H. H.; Rodgers, G. C.; Keith, D. D., Metacycloprodigiosin, a tripyrrole pigment from *Streptomyces longisporusruber*. *J Am Chem Soc* **1969**, 91, 1263-1264.
6. Gerber, N. N., Prodigiosin-like pigments from *Actinomadura (Nocardia) pelletieri*. *J. Antibiot.* **1971**, 24, 636-640.
7. Kawachi, K.; Shibutani, K.; Yagisawa, H.; Kamata, H.; Nakatsuji, S.; Anzai, H.; Yokoyama, Y.; Ikegami, Y.; Moriyama, Y.; Hirata, H., A possible immunosuppressant, cycloprodigiosin hydrochloride, obtained from *Pseudoalteromonas denitrificans*. *Biochem. Biophys. Res. Commun.* **1997**, 237, (3), 543-547.
8. Bennett, J. W.; Bentley, R., Seeing red: the story of prodigiosin. *Adv Appl Microbiol* **2000**, 47, 1-32.
9. Furstner, A., Chemistry and biology of roseophilin and the prodigiosin alkaloids: a survey of the last 2500 years. *Angew Chem Int Ed Engl* **2003**, 42, (31), 3582-603.
10. Cerdeno, A. M.; Bibb, M. J.; Challis, G. L., Analysis of the prodiginine biosynthesis gene cluster of *Streptomyces coelicolor* A3(2): new mechanisms for chain initiation and termination in modular multienzymes. *Chem Biol* **2001**, 8, (8), 817-29.
11. Llagostera, E.; Soto-Cerrato, V.; Montaner, B.; Perez-Tomas, R., Prodigiosin induces apoptosis by acting on mitochondria in human lung cancer cells. *Ann NY Acad Sci* **2003**, 1010, 178-81.
12. Manderville, R. A., Synthesis, proton-affinity and anti-cancer properties of the prodigiosin-group natural products. *Curr Med Chem Anticancer Agents* **2001**, 1, (2), 195-218.
13. Montaner, B.; Castillo-Avila, W.; Martinell, M.; Ollinger, R.; Aymami, J.; Giralt, E.; Perez-Tomas, R., DNA interaction and dual topoisomerase I and II inhibition properties of the anti-tumor drug prodigiosin. *Toxicol Sci* **2005**, 85, (2), 870-9.
14. Perez-Tomas, R.; Montaner, B.; Llagostera, E.; Soto-Cerrato, V., The prodigiosins, proapoptotic drugs with anticancer properties. *Biochem Pharmacol* **2003**, 66, (8), 1447-52.
15. Montaner, B.; Perez-Tomas, R., The prodigiosins: a new family of anticancer drugs. *Curr Cancer Drug Targets* **2003**, 3, (1), 57-65.
16. Soto-Cerrato, V.; Llagostera, E.; Montaner, B.; Scheffer, G. L.; Perez-Tomas, R., Mitochondria-mediated apoptosis operating irrespective of multidrug resistance in breast cancer cells by the anticancer agent prodigiosin. *Biochem Pharmacol* **2004**, 68, (7), 1345-52.
17. Stepkowski, S. M.; Nagy, Z. S.; Wang, M. E.; Behbod, F.; Erwin-Cohen, R.; Kahan, B. D.; Kirken, R. A., PNU156804 inhibits Jak3 tyrosine kinase and rat heart allograft rejection. *Transplant Proc* **2001**, 33, (7-8), 3272-3.
18. Mortellaro, A.; Songia, S.; Gnocchi, P.; Ferrari, M.; Fornasiero, C.; D'Alessio, R.; Isetta, A.; Colotta, F.; Golay, J., New immunosuppressive drug PNU156804 blocks IL-2-dependent proliferation and NF-kappa B and AP-1 activation. *Journal Of Immunology* **1999**, 162, (12), 7102-7109.
19. Furstner, A.; Grabowski, J.; Lehmann, C. W., Total Synthesis and Structural Refinement of the Cyclic Tripyrrole Pigment Nonylprodigiosin. *J Org Chem* **1999**, 64, (22), 8275-8280.
20. Dairi, K.; Tripathy, S.; Attardo, G.; Lavallee, J. F., Two step synthesis of the bipyrrole precursor of prodigiosins. *Tetrahedron Lett.* **2006**, 47, 2605-2606.
21. Stanley, A. E.; Walton, L. J.; Kourdi Zerikly, M.; Corre, C.; Challis, G. L., Elucidation of the *Streptomyces coelicolor* pathway to 4-methoxy-2,2'-bipyrrole-5-carboxaldehyde, an intermediate in prodiginine biosynthesis. *Chem Commun (Camb)* **2006**, (38), 3981-3.
22. Mo, S. J.; Sydor, P. K.; Corre, C.; Alhamadsheh, M. M.; Stanley, A. E.; Haynes, S. W.; Song, L.; Reynolds, K. A.; Challis, G. L., Elucidation of the *Streptomyces coelicolor* pathway to 2-undecylpyrrole, a key intermediate in undecylprodiginine and streptorubin B biosynthesis. *Chem Biol* **2008**, 15.
23. Odulate, O.; Barona-Gomez, F.; Corre, C.; Challis, G. L.
24. Frisch, M. J.; Trucks, G. W.; Schlegel, H. B.; Scuseria, G. E.; Robb, M. A.; Cheeseman, J. R.; Montgomery, J. A. J.; Vreven, T.; Kudin, K. N.; Burant, J. C.; Millam, J. M.; Iyengar, S. S.; Tomasi, J.; Barone, V.; Mennucci, B.; Cossi, M.; Scalmani, G.; Rega, N.; Petersson, G. A.; Nakatsuji, H.; Hada, M.; Ehara, M.; Toyota, K.; Fukuda, R.; Hasegawa, J.; Ishida, M.; Nakajima, T.; Honda, Y.; Kitao, O.; Nakai, H.; Klene, M.; Li, X.; Knox, J. E.; Hratchian, H. P.; Cross, J. B.; Bakken, V.; Adamo, C.; Jaramillo, J.; Gomperts, R.; Stratmann, R. E.; Yazyev, O.; Austin, A. J.; Cammi, R.;

- Pomelli, C.; Ochterski, J. W.; Ayala, P. Y.; Morokuma, K.; Voth, G. A.; Salvador, P.; Dannenberg, J. J.; Zakrzewski, V. G.; Dapprich, S.; Daniels, A. D.; Strain, M. C.; Farkas, O.; Malick, D. K.; Rabuck, A. D.; Raghavachari, K.; Foresman, J. J. B.; Ortiz, V.; Cui, Q.; Baboul, A. G.; Clifford, S.; Cioslowski, J.; Stefanov, B. B.; Liu, G.; Liashenko, A.; Piskorz, P.; Komaromi, I.; Martin, R. L.; Fox, D. J.; Keith, T.; Al-Laham, M. A.; Peng, C. Y.; Nanayakkara, A.; Challacombe, M.; Gill, P. M. W.; Johnson, B.; Chen, M. W.; Wong, W.; Gonzalez, C.; Pople, J. A., *Gaussian 03 User's Manual*, Revision C.02; Gaussian Inc.; Wallingford CT, 2003.
25. Becke, A. D., Density-functional thermochemistry. III. The role of exact exchange. *J Chem Phys* **1993**, *98*, (7), 5648-5652.
26. Perdew, J. P.; Wang, Y., Pair-distribution function and its coupling-constant average for the spin-polarized electron gas. *Physical Review B* **1992**, *46*, (20), 12947.
27. Karni, M.; Mandelbaum, A., The 'even-electron rule'. *Org Mass Spectrom* **1980**, *15*, (2), 53-64.
28. Sigsby, M. L.; Day, R. J.; Cooks, R. G., Fragmentation of even electron ions: protonated ketones and ethers. *org. Mass Spectrom.* **1979**, *14*, 273.
29. Fenselau, C.; Brown, P.; Patterson, D. G., Fragmentation of $[M + H]^+$ to form ion radicals following chemical ionization. *Spectroscopy (Amsterdam, Netherlands)* **1983**, *2*, (4-5), 348-351.
30. Bowie, J. H.; Stringer, M. B.; Duus, F.; Lawesson, S. O.; Larsson, F. C. V.; Madsen, J. O., Fragmentations Of Organic Negative-Ions - Mercapto Acids And Esters - A Reinvestigation. *Australian Journal Of Chemistry* **1984**, *37*, (8), 1619-1624.
31. Nikolic, D.; Li, Y.; Chadwick, L. R.; Grubjesic, S.; Schwab, P.; Metz, P.; van Breemen, R. B., Metabolism of 8-prenylnaringenin, a potent phytoestrogen from hops (*Humulus lupulus*), by human liver microsomes. *Drug Metab Dispos* **2004**, *32*, (2), 272-279.
32. Levsell, K.; Schiebel, H. M.; Terlouw, J. K.; Jobst, K. J.; Elend, M.; Preib, A.; Thiele, H.; Ingendoh, A., Even-electron ions: a systematic study of the neutral species lost in the dissociation of quasi-molecular ions. *Journal of Mass Spectrometry* **2007**, *42*, (8), 1024-1044.
33. Williams, J. P.; Nibbering, N. M.; Green, B. N.; Patel, V. J.; Scrivens, J. H., Collision-induced fragmentation pathways including odd-electron ion formation from desorption electrospray ionisation generated protonated and deprotonated drugs derived from tandem accurate mass spectrometry. *J Mass Spectrom* **2006**, *41*, (10), 1277-1286.
34. Jeong, H.; Yim, J. H.; Lee, C.; Choi, S. H.; Park, Y. K.; Yoon, S. H.; Hur, C. G.; Kang, H. Y.; Kim, D.; Lee, H. H.; Park, K. H.; Park, S. H.; Park, H. S.; Lee, H. K.; Oh, T. K.; Kim, J. F., Genomic blueprint of *Hahella chejuensis*, a marine microbe producing an algicidal agent. *Nucleic Acids Res* **2005**, *33*, (22), 7066-73.

Chapter 5

Hypoxia-Induced Changes in the Zebrafish Skeletal Muscle Proteome

Abstract

Oxygen deficiency occurs under many pathological, physiological, and environmental conditions. To identify changes in protein expression patterns induced by hypoxic exposure, a quantitative proteomics technique (2D-DIGE: two-dimensional difference in-gel electrophoresis) was used to compare the zebrafish skeletal muscle protein profile *in vivo* after 48 h in hypoxia ($P_{O_2} = 1.9$ kPa) or normoxia ($P_{O_2} = 18.6$ kPa). Proteins were separated over two pH ranges in the first dimension (pH 4-7 and pH 7-11), prior to separation in the second dimension, resolving over 1000 total protein spots. Of these, 34 spots in the pH range of 4-7 and 15 in the pH 7-11 range showed statistically significant differences between the hypoxic and the normoxic groups. Twenty-three spots in the pH 4-7 range and 8 in the pH 7-11 range were identified using MALDI-TOF/TOF mass spectrometry. Spots identified as glycolytic enzymes were higher during hypoxia than in normoxia, whereas enzymes associated with mitochondrial ATP synthesis were lower during hypoxia. Interestingly, hypoxic samples exhibited higher expression of proteins identified as zebrafish hemoglobin α variants. These protein expression changes are consistent with a hypoxic response that enhances anaerobic metabolism or O_2 transport to tissues.

Introduction

Hypoxia (reduced availability of oxygen) occurs under a variety of physiological, pathological, and environmental conditions. Mountain sickness is an outcome of people unaccustomed to high altitude who experience insufficient oxygen delivery to body tissues due to decreased oxygen partial pressure at high elevation.^{1, 2} In cancer, experimental and clinical studies show that hypoxia is the consequence of functional and structural disturbances in microcirculation, and tumor hypoxia has become a central issue in cancer treatment owing to its postulated linkage with tumor progression and resistance to therapies.³⁻⁵

Aquatic hypoxia occurs naturally in many areas; however, the number and size of impacted areas and the duration of hypoxic episodes have all been increasing as a consequence of human activities.⁶ For example, the growing hypoxic zone of the northern Gulf of Mexico has reduced the size of the suitable habitat for pelagic species and caused death of bottom-dwelling species that cannot move out of the hypoxic area.⁷

Many species cope with oxygen deficiency by regulating activities at the systemic, cellular and molecular levels to ameliorate the negative effects of hypoxia. Among mammals, numerous studies demonstrate that the transcription factor, hypoxia inducible factor-1 (HIF-1)⁸⁻¹⁰, plays a central role in regulating the molecular response to low oxygen. This transcription factor consists of a constitutively expressed β subunit and an oxygen-regulated α subunit. The latter contains an oxygen-dependent degradation domain recognized by the Von-Hippel-Lindau protein (pVHL). Under conditions of oxygen sufficiency, pVHL binds HIF-1 α and directs the protein to degradation by the ubiquitin-proteasome pathway. Under hypoxia, degradation is blocked, HIF-1 α accumulates and dimerized with HIF- β , and the dimer binds regulatory regions of target genes. In this fashion, HIF-1 regulates the expression of genes involved in enhancing oxygen delivery,¹¹ glucose uptake, and glucose metabolism.¹²

Fish are the oldest and most diverse group of vertebrate animals. Bony fish comprise nearly one-half of the known species of extant vertebrates and they are found in virtually every aquatic habitat.¹³ The phylogenetic and ecological diversity of fish offers distinct advantages in studies of environmental adaptation, such as the adaptive response to hypoxia.¹⁴ Zebrafish (*Danio rerio*) is a well-characterized

species used to study development^{15, 16}, and to a lesser extent, adult physiology. Previously, cDNA microarray studies showed large-scale changes in mRNA levels in zebrafish embryos¹⁷ and adults¹⁸ exposed to low oxygen. The response to hypoxia includes changes in the expression of genes involved in glycolysis, oxidative metabolism, and protein synthesis. At the proteome level, however, Bosworth et al.¹⁹ showed more subtle effects, with a small number of low abundance proteins changing in skeletal muscle during hypoxic exposure of adult zebrafish. Those proteins were not identified due to their low amounts in two-dimensional polyacrylamide gel electrophoresis (2D-PAGE).

The development of two-dimensional difference in gel electrophoresis (2D-DIGE) improves conventional 2D-PAGE by minimizing gel-to-gel variation and broadening the linear dynamic range for protein quantification.²⁰ The use of size-matched, spectrally-distinct cyanine dyes (CyDyes) allows detection and quantification of differentially expressed proteins within a single gel. Current MALDI-TOF mass spectrometry technology provides low femtomole level detection limits and less than 10 ppm error in mass accuracy that are critical for protein identification. Thus, 2D-DIGE followed by MALDI TOF/TOF analysis allows reproducible protein expression profiling and identification in a high throughput manner. In the current study, 2D-DIGE and MALDI TOF/TOF were used to explore the proteomic response to hypoxia in the zebrafish skeletal muscle proteome.

Experimental

Chemicals and Reagents

C18 ZipTips for desalting and purifying tryptic peptides were purchased from Millipore (Bedford, MA). The 4700 Calibration Standard kit used in calibrating MS or MS/MS spectra was purchased from Applied Biosystems Inc., Foster City, CA. CyDyes, Immobiline DryStrip 24 cm gels, carrier ampholytes of different pH ranges and other reagents for the first dimension of electrophoresis were purchased from GE Healthcare (Piscataway, NJ). Second dimensional electrophoresis employed Nextgen Sciences precast 8-16% gradient gels (Ann Arbor, MI). The Zoom[®] IEF Fractionator and reagents were purchased from

Invitrogen (Carlsbad, CA). All other chemicals and reagents not listed here were either analytical or electrophoresis grade, and they were purchased from Sigma-Aldrich Chemical Co. (St Louis, MO).

Animals

Wild-type zebrafish of both sexes were purchased from a local pet store, randomly divided into two groups of 10 fish, and held in two 40 L aquaria. Prior to experimentation, zebrafish were acclimated for four weeks in well-aerated, dechlorinated tap water at room temperature (19 ± 0.3 °C). Fish were fed twice a day throughout the acclimation period. At the start of hypoxic exposure, the water in one aquarium was made hypoxic ($P_{O_2} = 1.9$ kPa) over 2 h by gassing with a mixture of 0.9 L/min nitrogen and 0.1 L/min air. Gassing was continued for 48 h, a length of exposure that adult zebrafish tolerate with minimal mortality.²¹ The control tank was maintained at normoxia ($P_{O_2} = 18.6$ kPa) by gassing with room air at approximately the same flow rate. Both aquaria were covered and fish were not fed throughout the exposure period. At 48 h, fish were rapidly netted and frozen in liquid nitrogen. Fish were kept at -80 °C until analyzed.

Preparation of Protein Extracts

White skeletal muscle was dissected while fish were maintained frozen, taking care to exclude red skeletal muscle and skin. Approximately 100 mg of tissue was pulverized under liquid nitrogen, and then homogenized using a glass-glass homogenizer in 1 mL sample buffer (SB; 7 M urea, 2M thiourea, 2% CHAPS, 1% ASB-14) with 40 mM DTT. The protein extracts were centrifuged at $30,000 \times g$ for 30 min at 8 °C. The remaining insoluble pellet was discarded, and the soluble muscle protein extracts were stored at -80 °C. The protein concentration of the resulting supernatant was measured with a GE Healthcare 2D Quant kit (Piscataway, NJ).

Two-dimensional Polyacrylamide Gel Electrophoresis

Samples were desalted with a GE Healthcare 2D cleanup kit (Piscataway, NJ) and re-dissolved in SB (see above) plus 15 mM Tris buffer at pH 8.5. Samples of 50 µg of protein from each fish were reacted with

200 pmol of either Cy 3 or Cy 5 in a final volume of 10 μ L on ice for 30 min in the dark. Labeling reactions were stopped by adding 1 μ L of 10 mM lysine. To control for potential bias in labeling efficiency of CyDyes, half of the extracts from each experimental group were labeled with Cy 3 and the other half labeled with Cy 5 (Figure 5.1). A pooled protein sample was made by combining equal amounts of protein from all the individual replicates. This pooled sample was labeled with Cy 2 and used to normalize protein abundances across different gels, thereby allowing a correction for gel-to-gel variations. Labeled samples were kept at -80 °C until use.

For DIGE analysis, each gel contained 50 μ g of one hypoxic extract labeled with either Cy3 or Cy 5, plus 50 μ g of one normoxic extract labeled with the alternative CyDye (Cy5 or Cy3, respectively), and 50 μ g of the Cy 2 labeled pooled protein sample. Mixed samples were cup-loaded on 24 cm rehydrated IPG strips, covering a pH range of either 4-7 or 7-11. For pH 4-7, non linear pH gradient IPG strips were rehydrated in sample buffer plus 20 mM DTT. For pH 7-11, IPG strips, were rehydrated in the SB containing 1.2% “destreak” reagent (GE Healthcare). Protein samples were then focused on the Ettan IPGphor IEF apparatus until 60,000 Vhr.

After the IEF separation, IPG strips were equilibrated in 50 mM Tris-HCl, pH 8.8, 6M Urea, 30% glycerol, 2% SDS containing 1% DTT for 15 min to reduce disulfide bonds. Strips were then alkylated in the same buffer with 2.5% iodoacetamide in place of DTT for another 15 min. The equilibrated strips were loaded onto Nextgen Sciences 8-16% SDS-PAGE (25 cm \times 20 cm) gradient gels in a GE Healthcare Ettan™ DALTsix system (Piscataway, NJ) and run at the constant power of 15 W and the temperature of 25 °C until the bromophenol blue tracking dye migrated to the bottom of the gel (4.5 - 6 h).

Protein Visualization and 2D-DIGE Gel Image Analysis

Images of gels were acquired with a GE Healthcare Typhoon 9400 Laser Scanner (Piscataway, NJ) using filters specific for each CyDye. Nonlinear Dynamics Progenesis Samespots software was used for image alignment, spot detection, and spot quantification. Cy 2 images were used to match the gels. Spot

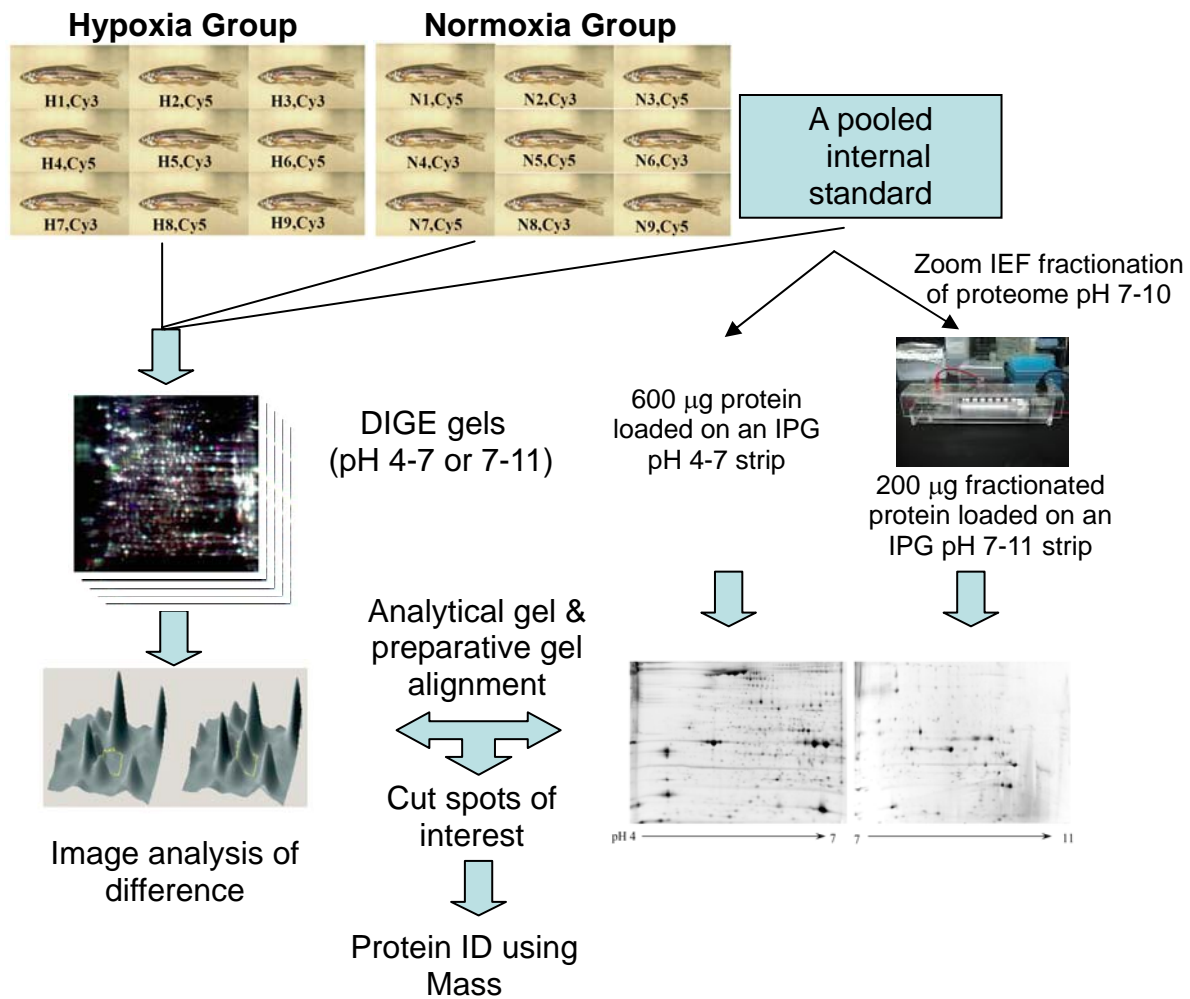


Figure 5.1 Experimental design of 2D-DIGE, preparative gel electrophoresis, and identification of zebrafish skeletal muscle proteins.

volumes for each spot in hypoxic and normoxic extracts were normalized to the Cy 2 volume for the same spot in the same gel. Analysis of variance was used to determine whether a significant difference existed between normalized spot volume of hypoxia and normoxia samples. Spots that differed significantly (ANOVA $P < 0.05$) were visually examined to determine whether they were of good quality and present in the entire image set.

Preparative 2D-PAGE and in-gel Digestion

To identify the spots of protein whose expression changed during hypoxia, two separate preparative gels were run at pH 4-7 and 7-11 intervals. In the pH 4-7 range, 600 μg of the pooled protein sample was subjected to 2D-PAGE and the resulting gel was stained with colloid coomassie blue. To enrich proteins in the pH 7-10 range, samples were first subjected to in-solution IEF using the Invitrogen Zoom[®] IEF Fractionator (Carlsbad, CA) run at 100 V for 20 min, 200 V for 80 min and 600 V for another 80 min. The fraction between pH 7 and 10 was retrieved from the electrophoresis chamber and precipitated using a 2D Cleanup kit. After protein assay, 200 μg protein was redissolved in 100 μL of the SB containing 15 mM DTT and used for 2D-PAGE as described above (pH 7-11NL IPG strip). These high pH preparative gels were stained with BioRad Flamingo fluorescent dye (Hercules, CA). Spots of interest from DIGE analysis were mapped onto images of the preparative gels and excised with a Biorad EXQuest[™] spot cutter (Hercules, CA). Gel pieces were collected in 96-well plates and digested with trypsin using a Genomic Solutions ProGest[™] (Ann Arbor, MI).

Mass Spectrometry

The tryptic digests were purified using C18 Ziptips (Millipore) and eluted in 4 μL of 50:50 acetonitrile:H₂O containing 0.1% TFA. Aliquots of 0.5 μL were dispensed on the sample support, followed by the addition of an equal volume of 10 mg/mL α -cyano-4-hydroxycinnamic acid in 50:50 acetonitrile:H₂O containing 0.1% TFA. MS and MS/MS spectra were acquired using Applied Biosystem

4800 MALDI-TOF/TOF mass spectrometer (Foster City, CA) in the positive reflectron mode. Two trypsin autolysis peaks at m/z 842 and 2211 were used as internal standards for MS calibration. Peptide mass fingerprints were acquired using 600 laser shots in a mass range between m/z 800 and 4000. The ten most intense peptide precursors were selected for MS/MS product ion acquisitions to confirm protein identifications, and the MS/MS spectra were acquired using 2500 laser shots. Data were transferred to GPS explorer software and searched against the zebrafish subset of the NCBI nr database and the zebrafish subset of the IPI FASTA sequence database with parameters: enzyme = trypsin; fixed modification = carbamidomethyl; variable modification = oxidation of methionine; max missed cleavages = 1; precursor tolerance = 100 ppm; and MS/MS fragment tolerance = 0.5 Da. Where spots were identified as unknown proteins, homology to known proteins was determined using BLAST²².

Results

Optimization of 2D-PAGE separation

2D-PAGE enables visualization and quantification of hundreds of proteins including post-translationally modified forms and related isoforms. However, great care must be taken to optimize 2D-PAGE separation conditions, which depend on sample type. For skeletal muscle, abundant proteins including actin, myosin, and tropomyosin, frequently compromise the separation and quantification of low abundance proteins on 2D-PAGE. In preliminary experiments, different forms of protein loading (active or passive rehydration, cup loading), different types and concentrations of detergents (1-4% CHAPS, 0.4-1% ASB-14), and first dimension IEF running conditions (30-80 kVhrs) were tested to achieve the best separation of zebrafish skeletal muscle proteins. The final conditions are given in the experimental section.

2D-DIGE Analysis

Of ten fish in the normoxic or hypoxic groups, nine were randomly selected for 2D-DIGE analysis. After removing gels with either severe horizontal streaking or low CyDye labeling efficiency, eight independent gels in the pH 4-7 range and seven gels in the pH 7-11 range were used to compare the zebrafish skeletal

muscle proteome between hypoxia and normoxia. These gels showed that the general pattern of zebrafish skeletal muscle protein expression under hypoxia was very similar to that under normoxia (Figure 5.2). DIGE analysis revealed that, across the entire pH range assayed (4 to 11), only 49 of 1100 spots (~ 4.4%; around 700 spots in the pH 4-7 range and 400 spots in the pH 7-11 range) showed significantly different levels of expression. Thirty-four spots in the pH range of 4-7 and 15 spots in the pH range of 7-11 showed statistically significant differences in quantity between the hypoxic and the normoxic groups (ANOVA $P < 0.05$). In the pH 4 to 7 range, 26 spots were more abundant in the hypoxic group and 8 spots were less abundant in the hypoxic group; in the pH 7-11 range, 7 spots were more abundant under hypoxia while 8 spots were less abundant.

Protein Identification

Protein spots found to be up-regulated or down-regulated during hypoxia were excised from preparative gels, digested, and subjected to MALDI-TOF/TOF mass spectrometry. Twenty three spots in the pH 4-7 range and 8 spots in the pH 7-11 range were successfully identified (see Appendix). Successful identifications were defined as those peptides achieving MASCOT scores higher than 53 ($P < 0.05$). From MS/MS experiments where fragment ions were successfully matched, MASCOT scores included these peptide ion scores. Protein identifications were performed by searching the MS data against the zebrafish subset from either NCBIInr or the IPI FASTA sequence database. Searches against the ray-finned fish subset of NCBIInr database yielded similar results.

Two spots in the pH range of 7-11 having molecular weights near 16kDa were determined as hemoglobin α variants (spot no. 0904 and 0909; Table 5.1). As shown in Figure 5.3, the expressions of both the spots are higher in the hypoxic fish than in the normoxic fish. One-way ANOVA showed that changes in protein expressions are highly statistically significant ($P < 0.002$; Table 5.1). Additionally, matches of peptide masses and fragment ions from MS/MS to variants of Hb α (Accession Nos. CAE48980 and CAE48986) were extremely significant (both $P \sim 10^{-29}$). Figure 5.4 shows the amino acid sequences of the two

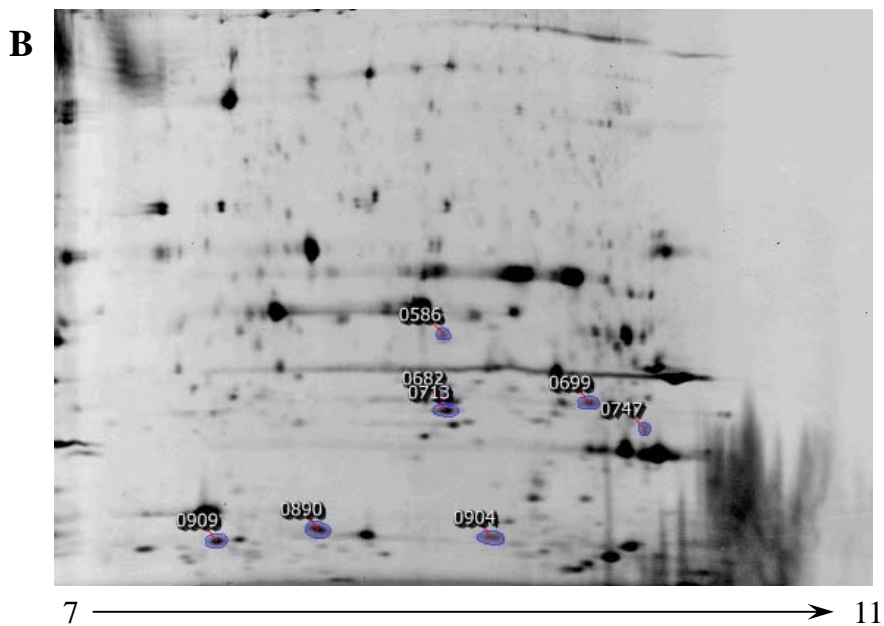
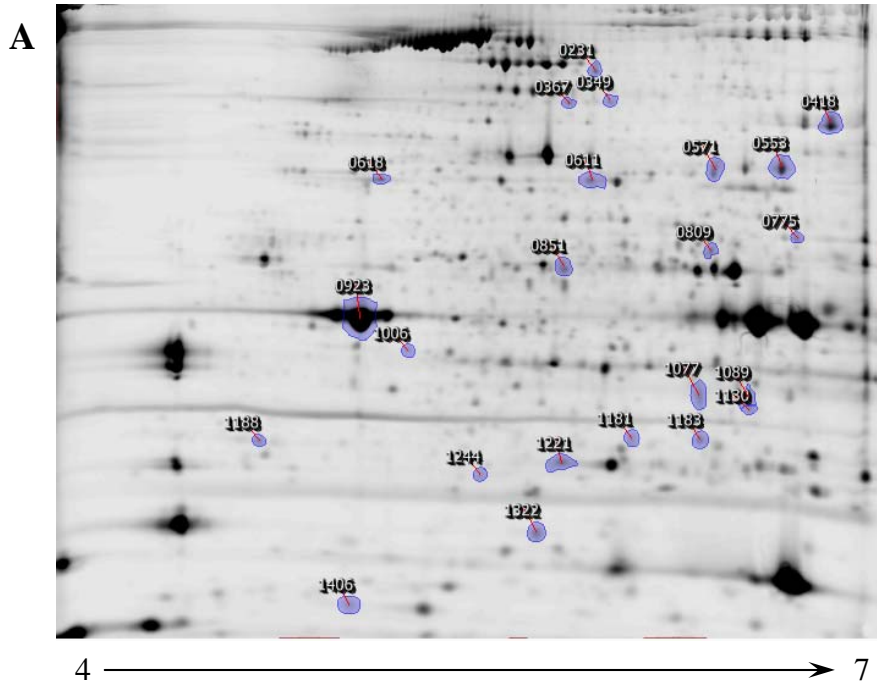


Figure 5.2 The Cy 2 images of representative 2D-DIGE gels between pH 4-7 (A) and 7-11(B) intervals. Proteins from the hypoxic or normoxic samples were labeled with either Cy 3 or Cy 5 dye. A pooled internal standard combining all extracts, labeled with Cy 2 dye, was included in all gels. Spots that differed between hypoxia and normoxia are indicated with spot number. These spots were selected for mass spectrometric analysis.

matched polypeptides with the peptides identified by MALDI-TOF/TOF shown in bold. Sequence coverage of both polypeptides was around 50%. Below these two polypeptides are other zebrafish globin protein sequences: hemoglobin α adult-1 (Hb α); hemoglobin β (Hb β), myoglobin (Mb), cytoglobin (Cyg β), neuroglobin (Nb) and globin X (gbX). Spot 0909 (CAE48986) differs from adult zebrafish Hb α adult-1 by one amino acid, whereas spot 0904 (CAE48980) differs by only two amino acids (highlighted residues). In contrast, the sequences of all Hb α variants are quite dissimilar to amino acid sequences of other zebrafish globins and the peptides determined by MALDI-TOF/TOF are not found in other globin genes. The results clearly demonstrate that spots 0904 and 0909, both up-regulated by hypoxic exposure, are variants of Hb α .

Table 5.2 shows protein spots whose molecular weight in 2D-PAGE was considerably less than predicted from their amino acid sequence. These spots likely represent fragments of the corresponding proteins. Nine spots were up-regulated while three spots were down-regulated in the pH 4-7 range; one spot was more abundant in the hypoxic group whereas one spot was less abundant in the hypoxic group in the pH 7-11 range. Most of these spots found to be more abundant during hypoxia were identified as highly expressed proteins, myosin and creatine kinase. Four other spots, less abundant in the hypoxic group, were determined as actin, mitochondrial ATP synthase, glycogen phosphorylase and isocitrate dehydrogenase. Another up-regulated spot was identified as protein arginine N-methyltransferase.

Table 5.1 Identification of differentially expressed spots corresponding to putative intact proteins

Spot No.	Expression Ratio ^a	ANOVA <i>P</i>	Protein	Mascot Score ^b	Accession Number	Coverage (%)	Matched Peptides ^c	<i>M_r</i> (kDa) obs/pred	<i>pI</i> obs/pred
pH 4-7									
1406	2.6	2.30E-03	nucleoside diphosphate kinase-Z2	386	NP_571002	59	9 (5)	16/17.2	5.0/6.75
1181	2.5	1.39E-03	triosephosphate isomerase B	200	AAK85202	53	10 (2)	28/27.1	6.2/6.45
1183	2.4	1.69E-03	triosephosphate isomerase B	153	AAK85202	39	7 (2)	28/27.1	6.5/6.45
0809	1.9	1.07E-03	Enolase 1, (alpha)	372	AAH59511	46	14 (6)	50/47.4	6.5/6.16
0851	1.9	5.22E-03	pyruvate kinase, muscle, b [zgc:92037]	910	NP_001003488	58	31 (8)	53/58.8	5.9/6.88
1244	1.8	9.69E-03	fast skeletal myosin light chain 1a	363	NP_956294	73	17 (5)	28/21.0	5.5/4.63
0231	1.7	1.25E-02	fast muscle-specific myosin heavy chain	143	AAK73348	17	15 (3)	95/95.0	6.1/5.22
0923	-1.3	7.70E-03	Actin, alpha1, skeletal muscle	595	NP_571666	49	15 (7)	42/42.2	5.0/5.23
1006	-1.6	6.09E-04	Pyruvate dehydrogenase (lipoamide) beta	211	AAH53233	43	13 (4)	39/39.7	5.1/5.78
0418	-1.8	7.47E-03	phosphorylase, glycogen; brain	152	NP_997974	10	9 (3)	95/97.7	6.7/6.11
pH 7-11									
0713	3.7	2.36E-02	phosphoglycerate mutase 2 (muscle)	561	NP_957318	63	18 (6)	30/29.0	9.0/8.83
0909	2.5	1.81E-03	novel protein similar to zebrafish hemoglobin alpha-adult 1 (hbaa1)	194	CAE48986	53	6 (2)	15/15.5	8.0/7.98
0904	2.3	2.24E-04	novel protein similar to zebrafish hemoglobin alpha-adult 1 (hbaa1)	326	CAE48980	47	6 (4)	15/15.5	9.0/8.88
0586	2.3	2.09E-03	aldolase A fructose-bisphosphate,	384	NP_998380	50	17 (4)	40/40.2	9.0/8.45
0699	-1.4	7.70E-03	hydroxyacyl-Coenzyme A dehydrogenase	160	NP_001003515	35	9 (3)	32/33.4	9.5/8.66
0747	-2.5	4.00E-03	ATP synthase, H ⁺ transporting, mitochondrial F0 complex, subunit b, isoform 1	149	AAH83308	16	6 (2)	28/28.3	9.6/9.19

a. Positive expression ratios represent the ratio of the average normalized spot volume of the hypoxic to the normoxic samples (V_h/V_n). Negative values correspond to spots more abundant in normoxic samples and calculated as $-V_n/V_h$.

b. Mascot scores over 53 are considered to be statistically significant ($P < 0.05$)

c. The number of peptides matched by PMF followed by the number of peptides with significant ion score

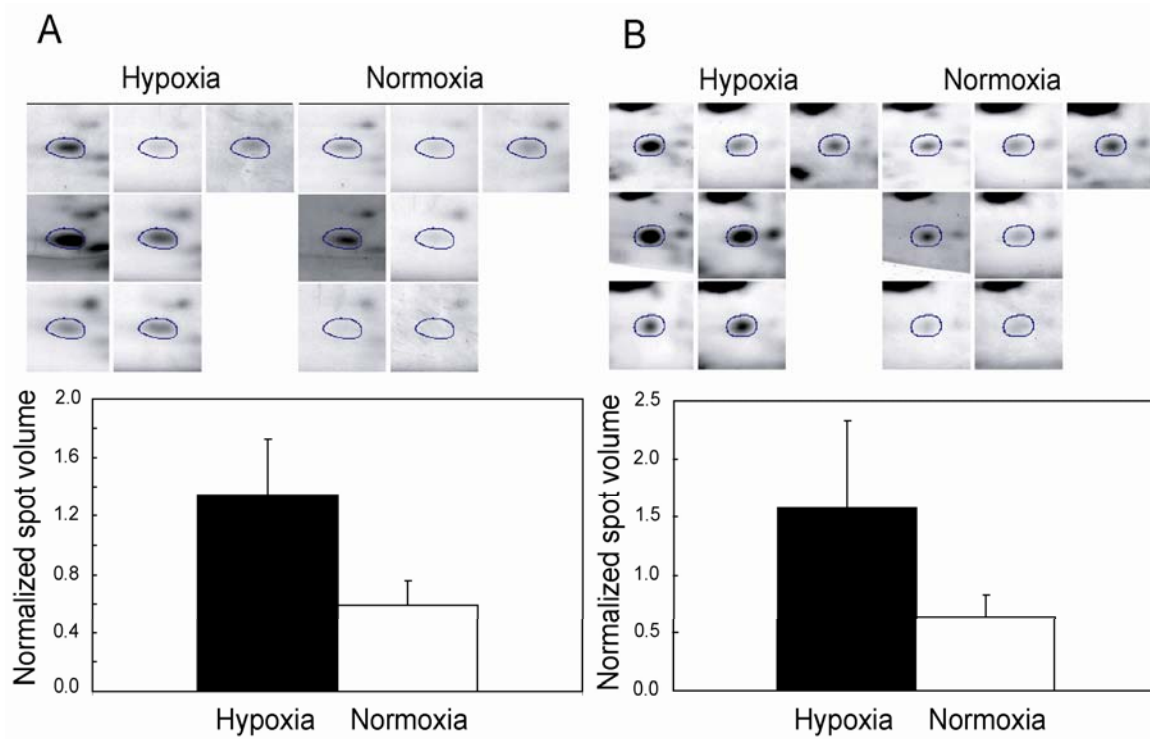


Figure 5.3 2D-DIGE gel Images showing spots identified as zebrafish hemoglobin variants (spots 0904 (A) and 0909 (B)) with quantitative comparison between hypoxia and normoxia shown below. The error bars represent the one standard deviation for $n = 7$ fish.

CAE48980	-----MSLSD K DKAVVKAIWAKISPK ADEIGAEALARMLT	Spot 0909
CAE48986	-----MSLSD T DKAVVKAIWAKISPK ADEIGAEALARMLT	Spot 0904
NP_571332	-----MSLSD T DKAVVKAIWAKISPK ADEIGAEALARMLT	Hemoglobin α
NP_571095	-----MVEWTD A ERTAILGLWGKLN--IDEIGPQALS R CLI	Hemoglobin β
NP_694484	-----MEGDGGVQLTQSPDSLTEEDVCVIQDTWKP V YAERDNAGVAVLV R FFT	Cytoglobin
NP_956880	-----MADHDLVLK C WGAVEADYAANGGEVLN R L F K	Myoglobin
NP_571928	-----MEKLSEKDKGLIRDS W ESL G KN K VPHGIVL F TRL F E	Neuroglobin
NP_001012261	MGCAISGSGLTARAPEIRAGEEET P AGLTANHIRLIK E SWRLIQEDIAK V GIIM F VRL F E	Globin X
CAE48980	VYPQTK T Y F SH W S D L S P----- G SG P V K K H G K T I M G A V G E A I SK I D D L V G G --- L A A L S E	Spot 0909
CAE48986	V Y P Q T K T Y F SH W A D L S P----- G SG P V K K H G K T I M G A V G E A I SK I D D L V G G --- L A A L S E	Spot 0904
NP_571332	VYPQTKTYF S H W A D L S P-----GSGPVKKHGKT I M G A V G E A V SK I D D L V G G ---L A A L S E	Hemoglobin α
NP_571095	VYPWTQRYFATFGN L SS P A I M G N P K V A A H G R T V M G L E R A I K N M D N V K N T---Y A A L S V	Hemoglobin β
NP_694484	N F P S A K Q Y F E H F R E L Q D P A E M Q N A Q L K K H G R V L N A L N T L V E N L R D A D K L N T I F N Q M G K	Cytoglobin
NP_956880	E Y P D T L K L F P K F S G I S Q-G D L A G S P A V A A H G A T V L K K L G E L L K A K G D H A A L---L K P L A N	Myoglobin
NP_571928	L D P A L L T L F S Y S T N C G D A P E C L S S P E F L E H V T K V M L V I D A A V S H L D D L H T L E D F L L N L G R	Neuroglobin
NP_001012261	T H P E C K D V F F L F R D V E D L E R L R L R T S R E L R A H G L R V M S F I E K S V A R L D Q L E R L E T L A L E L G K	Globin X
CAE48980	L H A F K L R V D P A N F K I L S H N V I V V I A M L F-P A D F T P E V H V S V D K F F N L A L A L S E K Y R ---	Spot 0909
CAE48986	L H A F K L R V D P A N F K I L S H N V I V V I A M L F-P A D F T P E V H V S V D K F F N L A L A L S E K Y R ---	Spot 0904
NP_571332	LHAFKLRVDPANFKILSHNVIVVIAMLF-PADFTPEVHVSVDK F F N L A L A L S E K Y R ---	Hemoglobin α
NP_571095	M H S E K L H V D P D N F R L L A D C I T V C A A M K F G Q A G F N A D V Q E A W Q K F L A V V S A L C R Q Y H ---	Hemoglobin β
NP_694484	S H A L R H K V D P V Y F K I L A G V I L V E L V E A F P Q C F S P A E V Q S S W S K L M G I L Y W Q M N R V Y A E V G	Cytoglobin
NP_956880	T H A N I H K V A L N N F R L I T E V L V K V M A E K A ---G L D A A G Q G A L R R V M D A V I G D I D G Y Y K E I G	Myoglobin
NP_571928	K H Q A V G -V N T Q S F A L V G E S L L Y M L Q S S L G P-A Y T T S L R Q A W L T M Y S I V S A M T R G W A K N G	Neuroglobin
NP_001012261	S H Y R Y N --A P P K Y Y G Y V G A E F I C A V R P I L K D R W T P E L E E A W K T L F Q Y V T S I M R E G F L E E	Globin X
CAE48980	-----	Spot 0909
CAE48986	-----	Spot 0904
NP_571332	-----	Hemoglobin α
NP_571095	-----	Hemoglobin β
NP_694484	W E N S K K -----	Cytoglobin
NP_956880	F A G-----	Myoglobin
NP_571928	E H K S N-----	Neuroglobin
NP_001012261	R N K R S N T Q T S S R E R P D K R S T A I	Globin X

Figure 5.4 CLUSTAL 2.0.8 multiple sequence alignment of the two identified hemoglobin variants (CAE48980 and CAE48986), with hemoglobin α adult-1 (NP_571332), hemoglobin β (NP_571095), cytoglobin (NP_694484), myoglobin (NP_956880), neuroglobin (NP_571928) and globin X (NP_001012261). All sequences are from zebrafish (*Danio reio*). The peptides identified by mass spectrometry are shown in bold type. The highlighted residues (in yellow) indicate the amino acid differences among the three Hb α sequences.

Table 5.2 Identification of differentially expressed spots corresponding to putative protein fragments

Spot No.	Expression Ratio ^a	ANOVA <i>P</i>	Protein	Mascot Score ^b	Accession Number	Coverage (%)	Matched Peptides ^c	Mr (kDa) obs/pred	pI obs/pred
pH 4-7									
1089	2.7	8.75E-03	creatine kinase, muscle	649	NP_571007	32	13 (8)	35/43.0	6.6/6.32
1130	2.6	2.76E-03	creatine kinase, muscle	634	NP_571007	48	18 (8)	35/43.0	6.6/6.32
1077	2.4	6.11E-03	creatine kinase, muscle	257	NP_571007	18	7 (2)	35/43.0	6.5/6.32
0611	2.2	3.98E-03	myosin heavy chain 4 [Wu:fi38g05]	491	AAH44194	19	20 (8)	80/125.2	6.0/6.21
0571	2	2.52E-03	myosin binding protein C, fast-type [Zgc:110761]	180	AAH91662	11	14 (4)	80/125.8	6.5/5.56
0367	2	4.00E-03	myosin heavy chain 4 [Wu:fi38g05]	58	AAH44194	6	8 (2)	96/125.2	6.0/6.21
0553	1.8	5.25E-03	myosin heavy chain 4 [Wu:fi38g05]	53	AAH44194	9	11 (1)	80/125.2	6.6/6.21
0349	1.6	5.10E-03	myosin, heavy polypeptide 2, fast muscle specific	68	NP_694514	7	14 (2)	96/222.8	6.1/5.55
1221	1.5	1.35E-02	protein arginine N-methyltransferase 1	54	NP_956944	29	10 (0)	30/40.0	5.9/5.47
0618	1.4	6.51E-03	fast muscle-specific myosin heavy chain	752	AAK73348	34	32 (8)	80/95.0	5.0/5.22
1188	-1.5	2.60E-02	actin, alpha 1, skeletal muscle	438	NP_571666	26	7 (5)	30/42.3	4.8/5.23
1322	-1.6	1.18E-3	mitochondrial ATP synthase	293	AAS49605	26	9 (4)	20/40.0	5.8/9.18
0775	-2	1.83E-02	phosphorylase, glycogen (muscle) b [MGC63642]	76	NP_956766	13	5 (1)	70/36.9	6.5/6.27
pH 7-11									
0890	2.3	6.35E-03	creatine kinase, muscle	351	NP_571007	32	14 (4)	30/42.3	4.8/5.23
0682	-1.7	1.32E-02	isocitrate dehydrogenase 2 (NADP+), mitochondrial	372	NP_955858	27	12 (4)	20/40.0	5.8/9.18

a. Positive expression ratios represent the ratio of the average normalized spot volume of the hypoxic to the normoxic samples (V_h/V_n). Negative values correspond to spots more abundant in normoxic samples and calculated as $-V_n/V_h$.

b. Mascot scores over 53 are considered to be statistically significant ($P < 0.05$)

c. The number of peptides matched by PMF followed by the number of peptides with significant ion score

Discussion

While the overall pattern of protein expression was similar between hypoxia and normoxia, 2D-DIGE analysis revealed that approximately 4% of the detected protein spots had statistically significant differences in expression between the hypoxic and the normoxic zebrafish. Among the proteins that were found to be up-regulated during hypoxia (Table 5.1), several were glycolytic enzymes, including phosphoglycerate mutase 2 (3.7-fold), triosephosphate isomerase B (2.4- and 2.5-fold), aldolase A fructose-biphosphate (2.3-fold), enolase-1 α (1.9-fold) and pyruvate kinase (1.9-fold). Conversely, down-regulated proteins included the enzymes of the citric acid cycle and proteins involved in aerobic ATP production, such as pyruvate dehydrogenase (lipoamide) β (1.6-fold), hydroxyacyl-coenzyme A dehydrogenase (1.4-fold), mitochondrial isocitrate dehydrogenase 2 (NADP⁺) (1.7-fold), mitochondrial ATP synthase α (1.6-fold) and ATP synthase (H⁺ transporting, mitochondrial F0 complex, subunit b, isoform 1) (2.5-fold) (Tables 5.1 and 5.2). The observation of up-regulated glycolytic enzymes and down-regulated mitochondrial enzymes is entirely consistent with measurements of metabolic enzyme activities²³ and gene expression.^{17, 18} These patterns support the view of increased capacity for glycolysis coupled with decreased capacity for aerobic ATP production during hypoxic exposure of fish.

Somewhat surprisingly, the results showed that a spot (spot no. 0418) identified as glycogen phosphorylase was down-regulated by a factor of 1.8-fold after 48 h hypoxic exposure (Table 5.1). Although database searching matched this spot against glycogen phosphorylase from brain, a hypothetical protein corresponding to muscle glycogen phosphorylase matched almost as well (NP_956766; Mascot score = 122). Glycogen phosphorylase catalyzes phosphorolytic cleavage of glycogen, releasing glucose-1-phosphate. Its activity is regulated by reversible phosphorylation/dephosphorylation to generate a more active *a* isoform or a less active *b* isoform. Intact zebrafish muscle glycogen phosphorylase has a predicted Mr of 97 kDa and a pI of 6.7 in the unphosphorylated form, which compares quite well with the pI and Mr of spot 0418 estimated by 2D-PAGE (6.7/95kDa; Figure 5.2A; Appendix Table A-1). Therefore, this spot could be the unphosphorylated less active *b* form of the glycogen phosphorylase, and its increase

suggests a reduced capacity for glycogen degradation during hypoxia. A spot corresponding to the phosphorylated more active *a* isoform, however, was not detected as being up-regulated. Therefore, the present 2D-PAGE data do not resolve whether glycogen phosphorylase phosphorylation status, and hence enzyme activity, is altered by hypoxic exposure.

Data from cDNA microarray studies suggest that expression of genes encoding major contractile proteins are down-regulation during hypoxic exposure of zebrafish.¹⁷ Consistent with that observation, the current results indicate that protein spots corresponding to intact and fragmented actin were also down-regulated by a factor of 1.3 and 1.5 fold, respectively, in skeletal muscle tissue after hypoxic exposure. Suppression of high abundance cell structural proteins indicates that this may be an energy-saving strategy for hypoxic zebrafish.¹⁷ However, some fragments of myosin respond differently to hypoxia. As shown in Table 5.1, two spots determined as fast skeletal muscle myosin light chain 1a and fast muscle-specific myosin heavy chain were more abundant in the hypoxic group than in the normoxic group. Based upon their low intensity in 2D-PAGE, however these spots appear to be minor forms of these proteins whose regulation may differ from the major forms of these contractile proteins.

I also observed an increase in the amounts of fragments of the highly abundant proteins creatine kinase and myosin (Table 5.2) in hypoxic zebrafish, compared to the normoxic group. The concentrations of these protein fragments are determined by a balance of synthesis and degradation. Changes in spot intensity corresponding to intact creatine kinase and myosin were not observed, suggesting that the expressions of these abundant proteins do not change during hypoxia. Rather, steps in the degradation of these proteins might be differentially sensitive to hypoxia. Specifically, if the initial steps of degradation occur, but the complete proteolysis to amino acids is slowed, then intermediate-sized protein fragments would be expected to accumulate during hypoxia.

In this study, I also observed that a fragment of protein arginine N-methyltransferase was up-regulated by a factor of 1.5 (Table 5.2). Protein methylation is recognized as a major modification pathway in regulation of numerous cellular events including cell proliferation, signal transduction, and protein trafficking.²⁴⁻²⁶ I also observed that nucleoside diphosphate kinase (NDP kinase) showed higher

expression by 2.6-fold during hypoxia. NDP kinase catalyzes the exchange of phosphoryl groups between nucleoside triphosphates and the corresponding diphosphates. The up-regulation of NDP kinase is not well understood currently and its role in hypoxia warrants further study.

In this analysis, one of most significant findings was that Hb α variants increased in skeletal muscle after 2 days of severe hypoxic exposure ($P_{O_2} = 1.9$ kPa). Typically, hemoglobin is found in erythrocytes where it is responsible for binding oxygen at the respiratory surface and delivering it to tissues for aerobic metabolism. During hypoxia, changes in hemoglobin concentration and oxygen affinity may help to maintain oxygen delivery to tissues.²⁷ However, Roesner et al. recently showed that mRNA of both Hb α and β subunits were down-regulated after 48 h hypoxic exposure of adult zebrafish ($P_{O_2} = 4.1$ kPa).²⁷ Ton et al. also showed similar changes of Hb mRNA levels in zebrafish embryos using cDNA microarray technology.¹⁷ The discrepancy between my results and those of previous studies could be due to differences in strain, developmental stage, or tissue sampled, or other experimental conditions, such as severity and duration of hypoxic exposure. Another possibility is that for Hb α , transcript abundance and protein levels are poorly correlated, as documented for a number of proteins and cell types.²⁸ Perhaps mRNA and protein levels are temporally uncoupled, in which an early increase in hemoglobin mRNA during hypoxia (prior to initial samples in previous studies) results in a sustained increase in protein levels, even after the transcript levels dropped below normoxic values.

Regardless of reasons for the discrepancy between Hb mRNA and protein levels, the present results demonstrate strong up-regulation of Hb α protein variants in skeletal muscle from hypoxic zebrafish. At present, the mechanism underlying this observation is not known. One possibility is that an increase in the perfusion of muscle microcirculation during hypoxia introduced more blood (thus more Hb) into the samples, despite taking care to exclude blood, red muscle, and skin during dissection. A second possibility is that there were no changes in muscle perfusion, but that the small amounts of blood in the samples had higher hemoglobin content or a different hemoglobin composition during hypoxia. Changes in hemoglobin concentration and type are both argued to be adaptive responses to hypoxia in a variety of

animals, including fish.²⁹⁻³² These scenarios are not mutually exclusive and both would yield altered hemoglobin composition in samples of skeletal muscle as a result of circulatory responses to hypoxia. A third explanation for elevated expression of Hb α variants is that these proteins are expressed *in* the skeletal muscle during hypoxia. That is, one or both of these novel Hb α subunits could be muscle-specific proteins that increase oxygen transport *intracellularly*. Although this role is generally ascribed to myoglobin, recent discovery of other intracellular globins (cytoglobin²⁷, neuroglobin³³ and globin X³⁴) demonstrates considerable diversity with regard to structure, tissue specificity, and function among members of the globin gene family. Because the tissue localization of the two Hb α variants identified here has not been previously described, the possibility that these are muscle-specific forms of Hb α cannot be ruled out.

Conclusion

Zebrafish adjust to hypoxia *via* physiological and biochemical responses. Switching from aerobic to anaerobic energy metabolism under reduced oxygen tension in our study agrees with the cDNA microarray data of hypoxic zebrafish embryo. Interestingly, modulation of glycogen phosphorylase and hemoglobin variants during hypoxia is different from the results reported in microarray and RT-PCR studies. Contrary to the up-regulation of Hb that was observed in our studies, these latter techniques indicated that gene expression of Hb is down-regulated. The discrepancy of the results acquired from proteomic and genomic studies reveals the importance of considering all sources of information to improve the understanding of hypoxic responses.

References of Chapter 5

- 1.Hopfl, G.; Ogunshola, O.; Gassmann, M., Hypoxia and high altitude. The molecular response. *Adv Exp Med Biol* **2003**, 543, 89-115.
- 2.Clarke, C., Acute mountain sickness: medical problems associated with acute and subacute exposure to hypobaric hypoxia. *Postgrad Med J* **2006**, 82, (973), 748-53.
- 3.Denny, W. A., Prodrug strategies in cancer therapy. *Eur J Med Chem* **2001**, 36, (7-8), 577-95.
- 4.Vaupel, P.; Mayer, A., Hypoxia in cancer: significance and impact on clinical outcome. *Cancer Metastasis Rev* **2007**, 26, (2), 225-39.
- 5.Harris, A. L., Hypoxia - A key regulatory factor in tumour growth. *Nature Reviews Cancer* **2002**, 2, (1), 38-47.
- 6.Council, N. R., *Clean Coastal Waters: Understanding and Reducing the Effects of Nutrient Pollution*. National Academic Press: New York, 1999.
- 7.Turner, R. E.; Rabalais, N. N.; Justic, D., Gulf of Mexico hypoxia: alternate states and a legacy. *Environ Sci Technol* **2008**, 42, (7), 2323-7.
- 8.Iyer, N. V.; Kotch, L. E.; Agani, F.; Leung, S. W.; Laughner, E.; Wenger, R. H.; Gassmann, M.; Gearhart, J. D.; Lawler, A. M.; Yu, A. Y.; Semenza, G. L., Cellular and developmental control of O₂ homeostasis by hypoxia-inducible factor 1 alpha. *Genes Dev* **1998**, 12, (2), 149-62.
- 9.Wang, G. L.; Semenza, G. L., General Involvement Of Hypoxia-Inducible Factor-I In Transcriptional Response To Hypoxia. *Proceedings Of The National Academy Of Sciences Of The United States Of America* **1993**, 90, (9), 4304-4308.
- 10.Howald, H.; Pette, D.; Simoneau, J. A.; Uber, A.; Hoppeler, H.; Cerretelli, P., Effects Of Chronic Hypoxia On Muscle Enzyme-Activities. *International Journal Of Sports Medicine* **1990**, 11, S10-S14.
- 11.Ratcliffe, P. J.; O'Rourke, J. F.; Maxwell, P. H.; Pugh, C. W., Oxygen sensing, hypoxia-inducible factor-1 and the regulation of mammalian gene expression. *Journal Of Experimental Biology* **1998**, 201, (8), 1153-1162.
- 12.Semenza, G. L.; Roth, P. H.; Fang, H. M.; Wang, G. L., Transcriptional regulation of genes encoding glycolytic enzymes by hypoxia-inducible factor 1. *J Biol Chem* **1994**, 269, (38), 23757-63.
- 13.Cossins, A. R.; Crawford, D. L., Fish as models for environmental genomics. *Nat Rev Genet* **2005**, 6, (4), 324-33.
- 14.Nikinmaa, M.; Rees, B. B., Oxygen-dependent gene expression in fishes. *Am J Physiol Regul Integr Comp Physiol* **2005**, 288, (5), R1079-90.
- 15.Langenau, D. M.; Zon, L. I., The zebrafish: a new model of T-cell and thymic development. *Nat Rev Immunol* **2005**, 5, (4), 307-17.
- 16.Shrivastava, K.; Shukla, D.; Bansal, A.; Sairam, M.; Banerjee, P. K.; Ilavazhagan, G., Neuroprotective effect of cobalt chloride on hypobaric hypoxia-induced oxidative stress. *Neurochem Int* **2008**, 52, (3), 368-75.
- 17.Ton, C.; Stamatiou, D.; Liew, C. C., Gene expression profile of zebrafish exposed to hypoxia during development. *Physiol Genomics* **2003**, 13, (2), 97-106.
- 18.van der Meer, D. L.; van den Thillart, G. E.; Witte, F.; de Bakker, M. A.; Besser, J.; Richardson, M. K.; Spaik, H. P.; Leito, J. T.; Bagowski, C. P., Gene expression profiling of the long-term adaptive response to hypoxia in the gills of adult zebrafish. *Am J Physiol Regul Integr Comp Physiol* **2005**, 289, (5), R1512-9.
- 19.Bosworth, C. A. t.; Chou, C. W.; Cole, R. B.; Rees, B. B., Protein expression patterns in zebrafish skeletal muscle: initial characterization and the effects of hypoxic exposure. *Proteomics* **2005**, 5, (5), 1362-71.
- 20.Unlu, M.; Morgan, M. E.; Minden, J. S., Difference gel electrophoresis: a single gel method for detecting changes in protein extracts. *Electrophoresis* **1997**, 18, (11), 2071-7.
- 21.Rees, B. B.; Sudradjat, F. A.; Love, J. W., Acclimation to hypoxia increases survival time of zebrafish, *Danio rerio*, during lethal hypoxia. *J Exp Zool* **2001**, 289, (4), 266-72.
- 22.Alschul, S. F.; Gish, W.; Miller, W.; Myers, E. W.; Lipman, D. J., Basic local alignment search tool. *J Mol Biol* **1990**, 215, (3), 403-10.
- 23.Martinez, M. L.; Landry, C.; Boehm, R.; Manning, S.; Cheek, A. O.; Rees, B. B., Effects of long-term hypoxia on enzymes of carbohydrate metabolism in the Gulf killifish, *Fundulus grandis*. *J Exp Biol* **2006**, 209, (Pt 19), 3851-61.
- 24.Liu, J.; Li, X. D.; Vaheri, A.; Voutilainen, R., DNA methylation affects cell proliferation, cortisol secretion and steroidogenic gene expression in human adrenocortical NCI-H295R cells. *J Mol Endocrinol* **2004**, 33, (3), 651-62.
- 25.Aletta, J. M.; Cimato, T. R.; Ettinger, M. J., Protein methylation: a signal event in post-translational modification. *Trends Biochem Sci* **1998**, 23, (3), 89-91.
- 26.Yadav, N.; Lee, J.; Kim, J.; Shen, J.; Hu, M. C.; Aldaz, C. M.; Bedford, M. T., Specific protein methylation defects and gene expression perturbations in coactivator-associated arginine methyltransferase 1-deficient mice.

- Proc Natl Acad Sci U S A* **2003**, 100, (11), 6464-8.
- 27.Roesner, A.; Hankeln, T.; Burmester, T., Hypoxia induces a complex response of globin expression in zebrafish (*Danio rerio*). *J Exp Biol* **2006**, 209, (Pt 11), 2129-37.
- 28.Gygi, S. P.; Rochon, Y.; Franza, B. R.; Aebersold, R., Correlation between protein and mRNA abundance in yeast. *Mol Cell Biol* **1999**, 19, (3), 1720-30.
- 29.Braunwald, E., *Hypoxia, polycythemia and cyanosis*. McGraw-Hill: New York, 1998; p 205-210.
- 30.West, J. B., *Respiration in unusual environments*. Williams & Wilkins: Baltimore, MD, 1990.
- 31.Jensen, F.; Weber, R., Respiratory properties of tench blood and hemoglobin. Adaptation to hypoxic-hypercapnic water. *Mol Physiol* **1982**, 2, 235-250.
- 32.Weber, R., *Functional Significance and Structural Basis of Multiple Hemoglobins with Specific Reference to Ectothermic Vertebrates*. Karger: Basel, 1990; Vol. 6, p 58-75.
- 33.Hankeln, T.; Ebner, B.; Fuchs, C.; Gerlach, F.; Haberkamp, M.; Laufs, T. L.; Roesner, A.; Schmidt, M.; Weich, B.; Wystub, S.; Saaler-Reinhardt, S.; Reuss, S.; Bolognesi, M.; De Sanctis, D.; Marden, M. C.; Kiger, L.; Moens, L.; Dewilde, S.; Nevo, E.; Avivi, A.; Weber, R. E.; Fago, A.; Burmester, T., Neuroglobin and cytoglobin in search of their role in the vertebrate globin family. *J Inorg Biochem* **2005**, 99, (1), 110-9.
- 34.Roesner, A.; Fuchs, C.; Hankeln, T.; Burmester, T., A globin gene of ancient evolutionary origin in lower vertebrates: evidence for two distinct globin families in animals. *Mol Biol Evol* **2005**, 22, (1), 12-20.

Appendix

Table A-1 pI, molecular weight, and the matched sequence to putative intact proteins

Spot No.	Protein Identification (Accession No.)	Mr (kDa) obs/pred	pI obs/pred	Matched Sequence (peptide ion score)
pH 4-7				
1406	nucleoside diphosphate kinase-Z2 (NP_571002)	16/17.2	5.0/6.78	K.FVQASEDLAK.Q K.QHYIDLK.D K.DQPFYAGLVK.Y (61) R.VMLGETDPFASKPGTIR.G R.VMLGETDPFASKPGTIR.G Oxidation (M) (70) R.GDFCIEVGR.N (43) R.NLIHGS DSEK.S K.SAATEVSLWFKPEELVSYR.S (120) R.SCAQEWIYE.- (27)
1181	triosephosphate isomerase B (AAK65202)	28/27.1	6.2/6.45	K.FFVGGNWK.M K.LNPDTEVVC GAPTIIYLDYAR.S (96) K.VAKGAFTGEISPAMIK.D K.GAFTGEISPAMIK.D Oxidation (M) R.RHVFGESDELIGQK.V K.VAHALENGLGVIACIGEK.L K.FIADNVK.D K.VVLAYEPVWAIGTGK.T K.TNVSEAVANSVR.I K.DLDGFLVGGASLKPEFIDIINAK.A (22)
1183	triosephosphate isomerase B (AAK85202)	28/27.1	6.5/6.45	K.SIEELANTLNSAK.L K.LNPDTEVVC GAPTIIYLDYAR.S (72) K.VAHALENGLGVIACIGEK.L K.FIADNVK.D K.TASPQQAQEVHDKLR.Q (31) K.TNVSEAVANSVR.I R.IYGGSVTGGTCK.E
0809	Enolase 1, (alpha) (AAH595511)	50/47.4	6.5/6.16	R.AAVPSGASTGIYEALRL.D (123) K.AVEHINK.T K.FGANAILGVSLAVCK.A R.HIADLAGNPEVILPVPAFNVINGGSHAGNK.L (35) K.LAMQEFMILPVGASNFK.E 2 Oxidation (M) R.IGAEVYHNLK.N (60) K.DATNVGDEGGFAPNILENK.E K.IVIGMDVAASEFYK.G Oxidation (M) K.YDLDFK.S (12) K.VNQIGSVTESLQACK.M K.MAQTNGWGVMSHR.S 2 Oxidation (M) (7) R.SGETEDTFIADLVVGLCTGQIK.T K.YNQLLR.I (34) R.FAGKNFR.K

Table A-1 Continued

Spot No.	Protein (Accession No.)	Mr (kDa) obs/pred	pI obs/pred	Matched Sequence (peptide ion score)
			pH 4-7	
0851	pyruvate kinase, muscle, b [zgc:92037] (NP_001003488)	53/58.8	5.9/6.88	R.NTGIVCTLGPAR.S (88) R.EMILSGMNVAR.L Oxidation (M) R.EMILSGMNVAR.L 2 Oxidation (M) R.LNFSHGTHEYHAETIK.S (107) R.EAIESFGAGTIDYRPVAIALDTK.G (120) K.GSGTEEVK.L K.LTLDDKFMDCDENTLWLDYK.N Oxidation (M) K.FMDCDENTLWLDYK.N Oxidation (M) K.VVQQGSHIYVDDGLISLK.V (130) K.EIGSDFLNCEIENGMLGSK.K Oxidation (M) K.KGVNLPGANVDLPVASEK.D K.GVNLPGANVDLPVASEK.D K.DLQFGVEQGVDMVFASFIR.K K.DLQFGVEQGVDMVFASFIR.K Oxidation (M) (48) K.AADVHAVR.K K.AADVHAVR.K.V K.LENHEGVR.K (44) R.KFDEILEASDGIMVAR.G R.KFDEILEASDGIMVAR.G Oxidation (M) (19) K.FDEILEASDGIMVAR.G Oxidation (M) R.GDLGIEIPTK.V R.IGKPIICATQMLESNIK.K 2 Oxidation (M) R.AESSDVANAVLDGADCIMLSGETAK.G Oxidation (M) K.GEYPIESVLTQHILIAR.E (123) R.EAEAAMFHR.Q R.EAEAAMFHR.Q Oxidation (M) R.QLFEELR.R R.QLFEELRR.T R.RTSHLTR.D R.DPTESVAIGAVEASFK.C
1244	fast skeletal myosin light chain 1a (NP_956294)	28/21.0	5.5/4.63	K.KAEPAPAPAPEPPK.A K.AEPAPAPAPEPPKADAVDLSGVK.L K.LDFTQDQMEDYR.E Oxidation (M) (27) K.LDFTQDQMEDYREAFLLFDR.V Oxidation (M) R.EAFLLFDR.V (62) R.VGDSKVAYNQIADIMR.A Oxidation (M) K.VAYNQIADIMR.A K.VAYNQIADIMR.A Oxidation (M) (10) R.ALGQNPTNK.E K.ILGNPTADDMVNKR.V Oxidation (M) K.RVDFEGFLPMLQVVINNPKN.A

Table A-1 Continued

Spot No.	Protein (Accession No.)	Mr (kDa) obs/pred	pI obs/pred	Matched Sequence (peptide ion score)
			pH 4-7	
1244	fast skeletal myosin light chain 1a (NP_956294)	28/21.0	5.5/4.63	K.RVDFEGFLPMLQVVINNPNK.A Oxidation (M) R.VDFEGFLPMLQVVINNPNK.A Oxidation (M) K.ATYDDYVEGLR.V (83) R.VFDKEGNGTVMGAELR.I Oxidation (M) (38) K.EGNGTVMGAELR.I Oxidation (M) R.IVLSTLGEK.M
0231	fast muscle-specific myosin heavy chain (AAK73348)	95/95.0	6.1/5.22	R.IEELEEEIEAER.A (67) R.DLEESTLQHEATAAALR.K (32) R.LQTENGEFGR.Q K.EALVSQLTR.G R.LQGEVEDLMIDVER.A Oxidation (M) K.SIHVLEK.A K.DEEMEQIKR.N R.SRNDALR.I R.NVQAQLK.D K.DAQLHLDDAVR.G R.KVAEQELVDASER.V (4) K.NLEVTVK.D K.QLQKLESR.V R.GADAVKGVK.K R.LQDLVDK.L
0923	Actin, alpha1, skeletal muscle (NP_571666)	42/42.2	5.0/5.23	K.AGFAGDDAPR.A R.AVFPISIVGRPR.H (39) R.HQGVVMVGMGQK.D Oxidation (M) K.DSYVGDEAQSQR.G K.IWHHTFYNELR.V (66) R.VAPEEHPTLLTEAPLNPK.A (77) R.TTGIVLDAGDGVTHNVPVYEGYALPH AIMR.L R.TTGIVLDAGDGVTHNVPVYEGYALPH AIMR.L Oxidation (M) R.GYSFVTTAER.E (50) K.LCYVALDFENEMATAASSSLEK.S Oxidation (M) K.SYELPDGQVITIGNER.F (111) R.KDLYANNVLSGGTTMYPGIADR.M K.DLYANNVLSGGTTMYPGIADR.M K.DLYANNVLSGGTTMYPGIADR.M Oxidation (M) (43) K.QEYDEAGPSIVHR.K (108)
1006	Pyruvate dehydrogenase (lipoamide) beta (AAH53233)	39/39.7	5.1/5.78	K.SAVSAVLR.R R.DALNQAMDEELERDER.V Oxidation (M) R.VFLLGEEVAQYDGAYK.V K.VSRGLWK.K K.TYYMSAGLQAVPIVFR.G K.TYYMSAGLQAVPIVFR.G Oxidation (M) K.VLSPWNSEDAR.G (29)

Table A-1 Continued

Spot No.	Protein (Accession No.)	Mr (kDa) obs/pred	pI obs/pred	Matched Sequence (peptide ion score)
pH 4-7				
1006	Pyruvate dehydrogenase (lipoamide) beta (AAH53233)	39/39.7	5.1/5.78	K.DFVIPIGK.A K.EGIECEVINLR.S (54) R.SIRPLDADTIETSITK.T K.TNHLVTVEGGWPQFGVGAEILAR.I (24) R.IMEGPAFNLYLDAPAVR.V Oxidation (M) (17) K.DIIFSVK.K
0418	phosphorylase, glycogen; brain (NP_997974)	95/97.7	6.7/6.11	R.HLHFTLVK.D (23) R.DYYFALAHTVR.D(83) R.NLAENISR.V R.LKQEYFVVAATLQDIIR.R K.AWEITTK.T R.IHSDIVK.T K.IGEDFLTDLFQLR.K R.IHEYKR.Q K.VIFLENYR.V (28)
pH 7-11				
0713	phosphoglycerate mutase 2 (muscle) (NP_957318)	30/29.0	9.0/8.83	R.HGESSWNQENR.F (82) R.FCGWFDADLSEK.G 938) K.GLEEAKR.G K.DAGMKFDVCYTSVLK.R Oxidation (M) K.FDVCYTSVLK.R K.FDVCYTSVLKR.A K.TLWTIMEGTDQMWWVPVVR.T K.TLWTIMEGTDQMWWVPVVR.T Oxidation (M) R.HYGGLTGLNK.A (53) R.SFDIPPPMDKDHYPYHK.I Oxidation (M) K.EGELPICESLK.D K.EGELPICESLKDTIAR.A (101) K.DTIARALPFWNEVIVPEIK.A R.ALPFWNEVIVPEIK.A (36) K.NVIAAHGNSLR.G (105) K.DLKPIKPMQFLGDEETVR.K Oxidation (M) K.DLKPIKPMQFLGDEETVRK.A Oxidation (M) R.KAMEAVAAQGK.V Oxidation (M)
0909	novel protein similar to zebrafish hemoglobin alpha-adult 1 (hbaa1) (CAE48986)	15/15.5	8.0/7.98	K.ADEIGAEALAR.M K.TYFSHWSDLSPGSGPVK.K K.TYFSHWSDLSPGSGPVKK.H (70) K.IDDLVGGLAALSELHAFK.L (112) K.LRVPANFK.I K.FFNNLALALSEK.Y
0904	novel protein similar to zebrafish hemoglobin alpha-adult 1 (hbaa1) (CAE48986)	15/15.5	9.0/8.88	K.ADEIGAEALAR.M (70) K.TYFSHWSDLSPGSGPVK.K K.TYFSHWSDLSPGSGPVKK.H (83) K.IDDLVGGLAALSELHAFK.L (99) K.LRVPANFK.I K.FFNNLALALSEK.Y (19)

Table A-1 Continued

Spot No.	Protein Identification	Mr (kDa) obs/pred	pI obs/pred	Matched Sequence (peptide ion score)
pH 7-11				
0586	aldolase A fructose-bisphosphate (NP_998380)	40/40.2	9.0/8.45	-.MPHAYPFLSPDQKK.E M.PHAYPFLSPDQK.K K.ELSDIAQR.I K.ELSDIAQRIVAPGK.G R.FQSINAENTEENRR.L (46) R.QLLFTADDR.I R.IKPCIGGVILFHETLYQK.T R.GMVVGIVKVDK.G Oxidation (M) K.VDKGVVPLAGTNGETTTQGLDGLYER.C K.GVVPLAGTNGETTTQGLDGLYER.C (79) K.ITPTTPSNLAIENANVLAR.Y (110) R.YASICQMHGIVPIVEPEILPDGDHDLKR.C Oxidation (M) K.YSPQEIAMATVTALR.R K.YSPQEIAMATVTALR.R Oxidation (M) K.YSPQEIAMATVTALRR.T K.YSPQEIAMATVTALRR.T Oxidation (M) K.GDTGAAAGESLFVANHAY.- (24)
0699	hydroxyacyl-Coenzyme A dehydrogenase (NP_001003515)	32/33.4	9.5/8.66	K.SAKGIENSLK.R K.FAEKPEDGEAFVQK.V K.VAPEHTIFASNTSSLPIADIASCTAR.L (48) K.TPATSQQTFDALLEFSK.A K.DTPGFIVNR.L (38) R.LLVPYMLEAVR.L (23) R.LLVPYMLEAVR.L Oxidation (M) K.DPDNPLFAPSLLNK.L K.TGEGFYK.H
0747	ATP synthase, H ⁺ transporting, mitochondrial F ₀ complex, subunit b, isoform 1 (AAH83308)	28/28.3	9.6/9.19	R.SMLFDAK.R Oxidation (M) R.NNVAMLLEINYR.E K.RLDYQVELQNLHR.R (51) R.LDYQVELQNLHR.R (73) R.LDYQVELQNLHRR.M K.SITPQQEK.E

Table A-2 pI, molecular weight, and the matched sequence to putative protein fragments

Spot No.	Protein (Accession No)	Mr (kDa) obs/pred	pI obs/pred	Matched Sequence (peptide ion score)
pH4-7				
1089	creatine kinase, muscle (NP_571007)	35/43.0	6.6/6.32	M.PFGNTHNNFK.L K.LNYSVDEEYPDL.SK.H (70) K.DLFDPVISDR.H (43) K.TDLNFENLK.G (53) K.GGDDLDPNYVLSSR.V (112) K.GYALPPHNSR.G (50) K.LSVEALSSLDGEFK.G (108) K.GKYYPLK.S R.GIWHNENK.T K.TFLVWVNEEDHLR.V (102) K.RFCVGLQR.I R.FCVGLQR.I (38) K.FEEILTR.L
1130	creatine kinase, muscle (NP_571007)	35/43.0	6.6/6.32	M.PFGNTHNNFK.L K.LNYSVDEEYPDL.SK.H (47) K.HNNHMAK.V Oxidation (M) K.DLFDPVISDR.H (44) K.TDLNFENLK.G K.GGDDLDPNYVLSSR.V (89) K.GYALPPHNSR.G (53) K.LSVEALSSLDGEFK.G (113) K.GKYYPLK.S K.SMTDAEQEQLIADHFLFDKPVSPLLL AAGMAR.D 2 Oxidation (M) R.GIWHNENK.T K.TFLVWVNEEDHLR.V (102) K.GGNMKEVFK.R K.GGNMKEVFK.R Oxidation (M) R.FCVGLQR.I (37) R.IEEIFKK.H (27) K.FEEILTR.L K.LMVEMEK.K Oxidation (M)
1077	creatine kinase, muscle (NP_571007)	35/43.0	6.6/6.32	K.HNNHMAK.V K.GGDDLDPNYVLSSR.V (109) R.SIKGYALPPHNSR.G K.GYALPPHNSR.G K.TFLVWVNEEDHLR.V (122) K.LMVEMEK.L K.LEKGESIDSMIPAQK.- Oxidation (M)
0611	myosin heavy chain 4 [Wu:fi38g05] (AAH44194)	80/125.2	6.0/6.21	R.MEAPPHIFSVDNAYQFMLTDR.E Oxidation (M) R.MEAPPHIFSVDNAYQFMLTDR.E 2 Oxidation (M) K.RVIQYFATVAVQGGDK.K R.VIQYFATVAVQGGDK.K (106) K.MQGSLEDQIIAANPLLEAYGNAK.T Oxidation (M) (53) R.IHFGTTGK.L K.LASADIETYLLEK.S (65) R.VTFQLPDER.G (42) K.FTGAVLHHGNMK.F Oxidation (M) (41) K.VGNEFVTK.G K.GQTVQPQVYNSVSALS.K.S (68)

Table A-2 Continued

Spot No.	Protein (Accession No)	Mr (kDa) obs/pred	pI obs/pred	Matched Sequence (peptide ion score)
pH 4-7				
0611	myosin heavy chain 4 [Wu:fi38g05] (AAH91662)	80/125.2	6.0/6.21	K.MFLWMVIR.I K.MFLWMVIR.I Oxidation (M) K.MFLWMVIR.I 2 Oxidation (M) K.LQQFFNHHMFVLEQEEYKK.E Oxidation (M) (1) K.LYDQHLGK.C (39) K.AEAHFSLVHYAGTVDYNVNGWLDK. N K.NKDPLNESVVQLYQK.S R.AYLMRR.E Oxidation (M) R.KLEGDLK.L
0571	myosin binding protein C, fast-type [Zgc:110761] (AAH91662)	80/125.8	6.5/5.56	K.WMDLGSK.A K.FSEAFLR.R (12) R.RLESAYSVNK.G K.YIMEADGNIR.T Oxidation (M) K.EPPITITK.L K.LLDDYHVVVGER.V (62) K.LNFLEIK.I K.DLSCFIIEGAER.E K.FDGGAPLK.G K.GSSRWTK.L R.SPPALLGQPVTVR.E (49) K.FTAPLVDR.A (18) R.AVTIGYSTAISCAVR.A K.MIIGDDPK.F
0367	myosin heavy chain 4 [Wu:fi38g05] (AAH44194)	96/125.2	6.0/6.21	R.VIQYFATVAVQGGDK.K (22) R.VTFQLPDER.G (27) K.ISYLLGSNSAELLKALCYPR.V K.LYDQHLGK.C R.AYLMRR.E R.AYLMRR.E Oxidation (M) K.SKIQLK.L R.KLEGDLK.L
0553	myosin heavy chain 4 [Wu:fi38g05] (AAH44194)	80/125.2	6.6/6.21	R.ENQSVLITGESGAGK.T R.VIQYFATVAVQGGDK.K R.IHFGTTGK.L R.VTFQLPDER.G (43) R.ILYGDFK.Q R.AYLMRR.E Oxidation (M) K.HWPWMK.V K.CKEDLVK.A R.MDLERAK.R R.KLEGDLK.L K.LAQESIMDLENDKQQSEEK.K
0349	myosin, heavy polypeptide 2, fast muscle specific (NP_694514)	96/222.8	6.1/5.55	R.ENQSVLITGESGAGK.T R.VIQYFATVAVQGGDK.K (17) R.VTFQLPDER.G (42) K.GQTVPQVYNSVSALSLSIYER.M R.MFLWMVIR.I 2 Oxidation (M) R.AYLMRR.E Oxidation (M) K.HWPWMK.V Oxidation (M) K.LAQESIMDLENDKQQSEEK.I K.QRADLSR.E R.SRNDALR.I

Table A-2 Continued

Spot No.	Protein (Accession No)	Mr (kDa) obs/pred	pI obs/pred	Matched Sequence (peptide ion score)
pH 4-7				
0349	myosin, heavy polypeptide 2, fast muscle specific (NP_694514)	96/222.8	6.1/5.55	R.NVQAQLK.D K.DAQLHLDDAVRGQEDMK.E K.NLEVTVK.D R.LQDLVDK.L
1221	protein arginine N-methyltransferase 1 (NP_956944)	30/40.0	5.9/5.47	-.MEVSQGESSAKPAAEDMTSK.D R.NSMFHNK.H R.NSMFHNK.H Oxidation (M) R.NSMFHNKHLFR.D K.KVIGIECSSISDYAVK.I R.QYKDYK.I K.IHWWENVYGFDMSCIK.E Oxidation (M) K.NNRDLDFTVDIDFK.G R.DLDFTVDIDFKGQLCEVSK.T K.TSEYRMR.-
0618	fast muscle-specific myosin heavy chain (AAK73348)	80/95.0	5.0/5.22	K.QRADLSR.E R.EQFEEQEAK.A K.ANSEVAQWR.T (58) R.TKYETDAIQR.T R.LQEAEQEIEAVNSK.C R.LQGEVEDLMIDVER.A R.LQGEVEDLMIDVER.A Oxidation (M) (53) K.NSYEETLDQLETLK.R K.NSYEETLDQLETLKR.E (92) K.NLQQEISDLTEQLGETGK.S (104) K.AEIQTALEEAEGTLEHEESK.I R.VQLELNQVK.G R.VTEAMQSTLDSEVR.S Oxidation (M) K.MEGDLNEMEIQLSHANR.Q 2 Oxidation (M) K.MEGDLNEMEIQLSHANR.Q K.MEGDLNEMEIQLSHANR.Q 2 Oxidation (M) R.NVQAQLK.D K.DAQLHLDDAVR.G (84) R.GQEDMKEQVAMVER.R 2 Oxidation (M) R.NTLMQSEIEELR.A R.NTLMQSEIEELR.A Oxidation (M) (4) R.AALEQTER.G R.KVAEQELVDASER.V K.VAEQELVDASER.V (86) R.VGLLHSQNTSLLNTK.K (95) K.EQDTS AHLER.M K.NLEVTVK.D R.VRELESEVEAEQR.R R.ELESEVEAEQR.R R.LQDLVDK.L R.KVQHELEEAER.A K.VQHELEEAER.A

Table A-2 Continued

Spot No.	Protein (Accession No)	Mr (kDa) obs/pred	pI obs/pred	Matched Sequence (peptide ion score)
pH4-7				
1188	actin, alpha 1, skeletal muscle (NP_571666)	30/42.3	4.8/5.23	K.AGFAGDDAPR.A (53) R.AVFPSIVGRPR.H K.IWHHTFYNELR.V (68) R.VAPEEHPTLLTEAPLNPK.A (102) R.GYSFVTTAER.E (63) K.LCYVALDFENEMATAASSSSLEK.S Oxidation (M) K.SYELPDGQVITIGNER.F (115)
1322	mitochondrial ATP synthase (AAS49605)	20/40.0	5.8/9.18	R.NVQAEEMVEFSSGLK.G Oxidation (M) (52) K.GMSLNLEPDNVGVVVFGNDK.L Oxidation (M) (43) R.TGAIVDVPVGEELLGR.V (121) R.EPMQTGIK.A Oxidation (M) K.AVDSLVPPIGR.G (41) R.ELIIGDR.Q. K.TAIAIDTIINQK.R R.LTDADAMK.Y R.LTDADAMK.Y Oxidation (M)
0775	phosphorylase, glycogen (muscle) b [MGC63642] (NP_956766)	70/36.9	6.5/6.27	M.SKPLTDQEK.R K.DRNVATK.R R.DYYFALAHTVR.D (57) R.YEFGIFNQK.I R.TISQYAR.E
pH7-11				
1188	actin, alpha 1, skeletal muscle (NP_571007)	30/42.3	4.8/5.23	K.AGFAGDDAPR.A (53) R.AVFPSIVGRPR.H K.IWHHTFYNELR.V (68) R.VAPEEHPTLLTEAPLNPK.A (102) R.GYSFVTTAER.E (63) K.LCYVALDFENEMATAASSSSLEK.S Oxidation (M) K.SYELPDGQVITIGNER.F (115)
1322	mitochondrial ATP synthase (NP_955858)	20/40.0	5.8/9.18	R.NVQAEEMVEFSSGLK.G Oxidation (M) (52) K.GMSLNLEPDNVGVVVFGNDK.L Oxidation (M) (43) R.TGAIVDVPVGEELLGR.V (121) R.EPMQTGIK.A Oxidation (M) K.AVDSLVPPIGR.G (41) R.ELIIGDR.Q. K.TAIAIDTIINQK.R R.LTDADAMK.Y R.LTDADAMK.Y Oxidation (M)

VITA

Kan Chen was born on August 6th, 1974 in Nanjing, People's Republic of China. He graduated from Nanjing University of Chemical Technology and obtained his B.Eng. degree in Biochemical Engineering. He then worked as research associate in Shanghai Anhua Biotechnology Company, and then as field service engineer in Applied Biosystems to 1998. Later he obtained his M.S. degree in Pharmaceutical Chemistry at the Medical School of Shanghai Jiaotong University in 2001. In 2002, he came to the University of New Orleans to pursue his Ph.D. degree in Analytical Chemistry.